UNIVERSITÀ DEGLI STUDI DI PALERMO
Doctorate in Civil, Environmental and Materials Engineering
Program: Road, Transport and Geomatics Engineering
Department of Engineering
S.S.D. ICAR/04

INTEGRATING VEHICLE SPECIFIC POWER METHODOLOGY AND MICROSIMULATION IN ESTIMATING EMISSIONS ON URBAN ROUNDABOUTS

PH.D. CANDIDATE
FRANCESCO ACUTO

THE COORDINATOR OF THE PH.D. PROGRAM
PROF. ANTONINA PIRROTTA

SUPERVISOR
PROF. ANNA GRANA'

XXXIII CYCLE
ACADEMIC YEAR 2021

Table of contents

Premise

Transformation toward greener, healthier, and safer management of urban mobility demand is needed soon. Several smart tools are already available to assess the impact of new infrastructural projects or existing road unit facilities also from an environmental point of view. To meet the industrial challenges posed by the decarbonization of the urban transport as requested by the EU government, emerging technologies offer smart mobile devices for collecting road traffic data and monitoring emissions from road vehicles in view of a mobile crowdsensing-based system.

In 2011 the European Commission adopted specific transport policy objectives with the White Paper "Towards a competitive and resource efficient transport system", in order to combine the increase of mobility with the reduction of traffic emissions through a wide-ranging strategy and with a long-time horizon. The target is to reach a 60% reduction in greenhouse gas emissions (GHG) by 2050 compared to 1990 levels. This objective would be the contribution offered by the transport sector to the comprehensive EU objective of an 80% - 95% GHG reduction as foreseen in the Roadmap for a low carbon economy.

However, road transport sector is one of the main sources of emissions to air. Electric vehicles, already available on the market, are an interesting option compared to diesel, petrol, LPG or CNG, even if the international community is confronted with the problems concerning extraction and mining lithium to produce batteries, and the potentially highly damaging effect to the environment after their end of life. Although emissions of air pollutants from road transport have significantly recently decreased thanks to technological innovations, the adaptation of the vehicles to the emission standards of the new vehicles still proceeds based on the physiological rate of replacement of the vehicle fleet. The same average age of the vehicular fleet is quite high as the penetration rate of modern technologies is still slow.

Emission models can predict emissions at regional or national level to obtain emission inventories at these levels or they can predict the effects on emissions produced by changes in design or operation of urban transportation at local level. In literature a distinction is between the average speed approach and the instantaneous speed approach.

Estimation of exhaust pollutants emissions produced by a car engine is still an important applied research topic because of the health effects and impacts on the environment. Despite many developments on this field in the latest years, few applications concern roundabouts. If it is true that roundabouts reduce stops and delays and slow vehicles to speeds at which emissions may be higher, it is also true that roundabouts may affect the modal events of acceleration and deceleration at which emissions are correlated. Roundabouts should be also examined from an

environmental perspective when choices among design options or forms of intersection control should be done. However, further study is still needed to better characterize the spatial distribution of emissions at roundabouts.

The aim of the PhD Thesis

In this study pollutant emissions were estimated from VSP modal emission rates and the distribution of time spent in each VSP mode obtained from the speed profiles both gathered in the field and simulated in AIMSUN at a sample of urban roundabouts. The versatility of the micro-simulation model for a calibration aimed at improving accuracy of emissions estimates was tested in order to ensure that second-by-second trajectories experienced in the field by a test vehicle through the sampled roundabouts properly reflected the simulated speed profiles. Although efforts in building the models of roundabouts and managing them in a microsimulation environment, the first results which the thesis will refer, confirmed the feasibility of the smart approach that integrates the use of field-observed and simulated data to estimate emissions at urban roundabouts. It is also revealed friendly in collecting information via smartphone and in the subsequent data analysis and provided suggestions for large-scale data collection through a digital community.

Another goal of this research is to investigate about the environmental performance after a conversion of a traditional existing roundabout into a turbo-roundabout. This aspect has been considered a positive approach for a novel attitude in the performance evaluation of road networks to align the infrastructural design with the aim of sustainable and low-emission mobility.

The main finding provided from this study is referred to the positive potential of a novel attitude in the conceptualization and performance evaluation of road units in order to align urban infrastructural projects with the worldwide shared long-term ambitions for a low-emission mobility.

Organization of the thesis

The present PhD thesis is composed by six chapters which highlight the research work and study that has been investigated during the PhD course.

- Chapter 1 is a background that traces the pollutant emission models available in literature reviews, focusing on the instantaneous emission models. In particular the Vehicle Specific Power methodology will be further explained in order to underline its affordability to compute emissions from instantaneous speed profiles.
- In Chapter 2, the most important behavioral models concerning microsimulation will be presented. The AIMSUN software model will be summarized, with particular

attention to the behavioral parameters which were considered to conduct the sensitivity analysis.

- Chapter 3 describes the pilot study of urban roundabouts selected to assess pollutant emissions by means of an empirical approach using instantaneous trajectory data from a smartphone app and the VSP methodology. In particular it will be described the data collection of vehicle activity data from six roundabouts located in the City of Palermo, Italy, and the emission estimation from a light diesel vehicle used as test vehicle.
- Chapter 4 will explore the integration of the VSP methodology and the AIMSUN microsimulation model to estimate the emissions at the sampled roundabouts. The calibration allowed to have second-by-second simulated speed profiles as close as possible to the observed ones and to improve the emissions estimations.
- In Chapter 5, the first results aimed at addressing the feasibility of converting an existing roundabout into a turbo-roundabout and their impacts from an environmental perspective will be presented. An existing two-lane roundabout in Palermo, Italy, has been considered in order to quantify the emission impacts and to compare the emissions from vehicles moving through the existing roundabout and the turbo-roundabout by using the VSP modal emission rates and the distribution of time spent in each VSP mode from the speed profiles that were simulated in AIMSUN.
- At last, in Chapter 6, the cooperation with the Centre for Mechanical Technology and Automation at University of Aveiro, Portugal, which was carried out in 2019 and 2021 will be presented. The main goal of the period of study abroad was to compare different roundabouts in terms of traffic performance, pollutant emissions and noise based on an integrated empirical approach.

Chapter 1

Road vehicle emission models

Introduction

The road transport sector has been faced with changes motivated by the need to limit as much as possible the problems arising from traffic congestion, road crashes, energy consumption, and the traffic-related air pollution. In this view, the concept of sustainable mobility has provided the starting point for investing resources to minimize or eliminate these issues at a global level. In 2011 the European Commission adopted specific transport policy objectives with the White Paper "Towards a competitive and resource efficient transport system" (1), in order to match the increase of mobility and the reduction of traffic emissions through a comprehensive strategy and with a long-time horizon. The target is to achieve a 60% reduction in greenhouse gas emissions (GHG) by 2050 compared to 1990 levels in order to meet the decarbonization goal as also most recently required from Agenda 2030 ONU and the European Green Deal[1].

The vehicle traffic on road is one of the main sources of emissions into the atmosphere. Automotive companies have been working for a long time to reduce vehicles pollutant emissions. Hybrid-electric vehicles improve the air quality, but the hypothesis of high penetration of electric cars into the road traffic is an interesting future goal compared to diesel, petrol, LPG or CNG. In addition, electric vehicles have also begun to be a valid prospect regarding the performance and operating costs.

If it is true that in recent years air pollutants emissions from road transport have fallen significantly because of the technological innovation of vehicles, it also true that the adaptation of vehicle fleets to stricter emission standards follows the trend of fleet replacement. It should also be borne in mind that the average age of the vehicle fleet is quite high, as the penetration rate of modern technology is slow.

Emission models can quantify emissions at regional or national level, making it possible to collect inventoried data, or may predict the effects on emissions from different design scenarios or in the operation of urban transport systems at local level.

[1] http://euroinnovazione.eu/green-deal-europeo/

In the literature there is also a distinction between the approaches based on average speed and the approaches based on instantaneous speed; the estimation of pollutant emissions from a car engine is still an important subject of applied research due to health effects and environmental impact.

Vehicle emissions are governed by various factors including vehicle acceleration and deceleration, signals, and idle time (2) (3) (4). The monitoring of exhaust emissions from road vehicles is one of the most common aspects of sustainable policies that are used to assess air pollution levels, human exposure to traffic-related air pollution and its effects on health.

Emission models: a literature overview

The estimation of pollutant emissions from traffic consists in average speed-based models and dynamic instantaneous models. The average speed-based approach estimates emissions by using information aggregated by vehicle type as derived from driving routes (5). The core of the average speed-based models suggests that the average emission factor for a certain pollutant and a given vehicle type varies with the average speed during a run; such models are used with macroscopic traffic flow models. The most used average speed models in Europe and US employ the emissions factors of the COPERT and TRL (6) (7).

Although the average speed-based models allow emissions calculation with few input data as average speed, traffic volume, and link length, limitations are underlined by the inability to catch the speed variation in the case of acceleration, deceleration, and idling (8), and to explain the ranges of vehicle operation and emission behavior at a given average speed (9). For these reasons, the average speed-based models can underestimate emissions especially in urban field. Some researches (10) (11) presented improvements in the accuracy of average speed models when real-time data were employed, but more investigation should be still done to account for several and various vehicles and to get better the predictive performance of these models.

Dynamic instantaneous emission models or fuel consumption models estimate instantaneous vehicle fuel consumption and second-by-second vehicle emission rates based on the instantaneous speed and acceleration of individual vehicles (12). The instantaneous speed approach uses the acceleration rate and/or the product speed-acceleration as parameters in addition to speed. Emission functions can be computed by defining emission values to specific operational conditions.

Instantaneous emission models are also used with support of microscopic traffic flow models to produce accurate estimates of pollutant emissions and fuel consumption (8), but they need

big calculation efforts especially for large-scale road networks. An interesting thing is that these models are sensitive to changes in vehicle acceleration and can be used in the evaluation of operational level transportation projects such as roundabout intersections (13). CMEM (14) is a representative instantaneous emission model that predicts second-by-second fuel consumption, and exhaust emissions of CO, CO_2, HC, and NO_X based on different modal operations from in-use vehicle fleets. According to this approach, the entire fuel consumption and emissions process is broken down into components corresponding to the physical phenomena that is associated with vehicle operation and emissions production. CMEM calculates emissions by means of each vehicle's driving cycle data, but it presents practical issues about local roads because it is impossible to collect data on every vehicle in traffic (11).

Another powerful instantaneous speed approach estimates emissions by using a modelling technique focused on the real-time engine power (Vehicle Specific Power, VSP) (15). This approach is used to assess the impact of vehicle operating conditions on emissions and energy consumption; VSP estimates depend on the speed, roadway grade and acceleration/deceleration on the basis of the second-by-second activity. This model captures dependence of emissions on power, includes the impact of different levels of accelerations and speed changes on emissions, and accounts for the effect of road infrastructure on power demand (16).

GPS second-by-second data give versatility to compute vehicle emissions by using VSP under real-world conditions at any location (17). VSP has been deployed into vehicle emission models as MOVES (15) (18) (19). Yao et al. (20) applied VSP approach to examine the role of freeway grade in VSP profiling; the results demonstrated that the sample distribution of VSP gives a better fit at lower grades. This study provided only a starting reference for preparing operating mode distribution inputs for the MOVES model, but the grade-specific VSP distributions for arterials and locals roads should be studied in more depth. Song et al. (3) estimated the VSP distributions for the urban restricted access roadways; they suggested that the distribution of VSP at different speed bins follows the normal distribution.

Zhao et al. (21) also estimated that the normal distribution provides a better match where the travel speed of light duty vehicles and heavy-duty vehicles moving along freeways is lower than 90 km/h. In turn, Liao et al. (22) proposed a simulation model for a signalized intersection where light duty vehicles were equipped with a cooperative vehicle-infrastructure system; the results confirmed that the environmental benefits depended on drivers' compliance behaviors.

A further research identified three speed profiles to cover all combinations of stop and no-stop conditions for vehicles entering a single-lane roundabout; a methodology to quantify the

emission impact of the operational performance focused on stop-and-go behavior was also developed by (23). By means of the VSP approach, they identified the parameters associated with the occurrence of changes in speed cycles with influence on emissions and showed the interaction among operational parameters, geometry, and the resulting traffic emissions.

Concerning intersections, some studies showed how roundabouts located on urban corridors affected traffic performance and pollutant emissions from vehicles. According to (23), Salamati et al. (24) tried to investigate about the difference between the characteristics of pollutant emissions at multi-lane and single-lane roundabouts; emissions were estimated by using the VSP methodology. The results highlighted that differences in emission estimation between left and right lane movements needed to be redefined more in depth. In order to finalize their research and identify the hotspots along the corridors where emissions tend to be higher, Fernandes et al. (25) found no significant differences between emissions of roundabouts characterized by similar layout and fairly spaced along the corridor.

Other studies compared the emission performances of traditional and innovative roundabouts by means of VSP methodology to estimate second-by-second pollutant emissions for a mixed fleet of conventional vehicles in urban area (13) (26); however, more experimental data should be gathered and analyzed to generalize the conclusions.

Further research estimated emissions from traffic by integrating microscopic simulation models and external emissions models. In this regard, Stogios et al. (27) explored the effects of driving settings with Automated Vehicles (AVs) on Greenhouse Gas (GHG) emissions at an urban corridor by traffic microsimulation and emissions modelling. No significant impact on GHG emission reductions was obtained when driving settings included only AVs; in turn, the inclusion of vehicle powertrain technology assessed a maximum of 24% in GHG emission reduction. In the following Table 1.1 an overview of emission estimation models is shown.

Table 1.1: Vehicle emissions estimation models

Model	Scale	Basic parameters	Input	Typical application
COPERT (6) (7)	macroscopic	average speed-based	average trip speed	regional or national emission inventories, dispersion models
EMFAC (28)	macroscopic	trip-based vehicle average speed	vehicle miles travelled, emission rates	emission inventories, impact on local roadways and intersections
TREM (29)	macroscopic	link-based vehicle average speed	traffic volume, vehicle speed, vehicle distribution per categories and per classes, road length	emission inventories, regional, local and urban-level dispersion models
aaSIDRA (30)	mesoscopic	four-modal activity	vehicle parameters, speed, acceleration rate, grade, cost parameters	environmental impacts assessment, cost, energy and air quality implications of intersections design
CMEM (14)	microscopic	instantaneous speed	individual vehicle variables such as speed, acceleration, slope; fleet composition	regional inventories, emissions benefits of project-level or corridor-specific control measures, ITS implementations
MOVES (19)	microscopic	VSP, instantaneous speed	vehicle operating time, emission rates	multiple scale analysis, emission inventories
MODEM (31)	microscopic	instantaneous speed	driving pattern	temporal and spatial analysis of emissions, dispersion models

Given that the VSP methodology has few applied studies concerning roundabouts until today, the aim of this thesis started from a reflection on the gap in the current literature with regard to the assessment of pollutant emissions at existing roundabouts.

The Vehicle Specific Power methodology

Specific Power definition

According to (15), the specific power is considered a useful parameter for analysing the remote sensing data and for emission modeling because of its capacity to capture the dependence between vehicle emissions and driving conditions, and because of the possibility to calculate it from on-road measurements.

It was also demonstrated that the dependence of CO, HC, and NO_X emissions on specific power is better than the classical kinematic parameters (speed, acceleration/deceleration rates) or fuel rate (15).

In this paragraph the rigorous proof is presented to define the expression of the vehicle specific power (VSP). The VSP is defined as the instantaneous power per unit mass of the vehicle generated by the engine to overcome the rolling resistance and aerodynamic drag, and to

increase the kinetic and potential energies of the vehicle (15). According to this definition, the mathematical expression is given below:

(1.1)

$$VehicleSpecificPower = \frac{\frac{d}{dt}(KE + PE) + F_{rolling} \cdot v + F_{aerodynamic} \cdot v}{m} =$$
$$= \frac{\frac{d}{dt}\left[\frac{1}{2} m \cdot (1 + \varepsilon_i) \cdot v^2 + mgh\right] + C_R mg \cdot v + \frac{1}{2}\rho_a C_D A (v + v_w)^2 \cdot v}{m} =$$
$$= v \cdot [a \cdot (1 + \varepsilon_i) + g \cdot grade + g \cdot C_R] + \frac{1}{2}\rho_a \frac{C_D \cdot A}{m}(v + v_w)^2 \cdot v$$

where:

- v: vehicle speed
- a*:* vehicle acceleration
- ε_i*:* mass factor, the equivalent translational mass of the rotating components of the powertrain which is gear-dependent
- *h:* altitude of the vehicle
- *grade:* vertical rise/slope length
- *g:* acceleration of gravity (9.8 m/s^2)
- C_R*:* coefficient of rolling resistance (dimensionless)
- C_D*:* drag coefficient (dimensionless)
- A*:* frontal area of the vehicle
- ρ_a*:* ambient air density (1.207 kg/m^3 at 20°C=68 °F)
- v_W: headwind into the vehicle

Using the metric units (SI) and typical values for the considered parameters, the previous expression can be written in the following form[2].

(1.2)

$$SP^3\left(\frac{kW}{MetricTon} = \frac{W}{kg} = \frac{m^2}{s^3}\right) =$$
$$= v \cdot (1.1 \cdot a + 9.81 \cdot grade + 9.81 \cdot 0.0135) + \frac{1}{2} \cdot 1.207 \cdot 0.0005 \cdot (v + v_W)^2 \cdot v =$$
$$= v \cdot (1.1 \cdot a + 9.81 \cdot grade(\%) + 0.132) + 3.02 \cdot 10^{-4} \cdot (v + v_W)^2 \cdot v$$

[2] The expressions are based on average values of the rolling resistance coefficient, the aerodynamic drag term coefficient (C_D*A/m) and the value of air density at 20°C.
[3] V and V_W are in m/s respectively; acceleration is in m/s^2.

Further details can be found in (15) where the Author continued with comparisons between the vehicle specific power and vehicle carbon emissions measured by means of tailpipe sensors for several type of light vehicles. The relationship between VSP and the second-by-second CO_2, CO, HC, and NO_X showed a strong correlation, also concerning the fuel rate (15). For this reason, the Author assessed that the specific power equation can be used to detect emissions variations for slight changes in driving behavior.

VSP emissions estimation

In order to develop a modeling tool for the estimation of emissions generated by on-road and off-road mobile sources, US EPA presented a product called MOVES (Motor Vehicle Emissions Simulator) which, by means of gathered data, allows to measure on-board emissions (18) (32).

The vehicle specific power (VSP) approach was implemented in the effort of a binning methodology to estimate pollutant emissions to be deployed in MOVES (33) (34).

The VSP expression was estimated considering the vehicle speed, the acceleration/deceleration, and the slope (33) (34).

$$VSP = v \cdot [1.1 \cdot a + 9.81 \cdot \sin(\arctan(grade)) + 0.132] + 0.000302 \cdot v^3 \quad (1.3)$$

where:

- *VSP*: Vehicle Specific Power [kW/metric ton]
- *v*: instantaneous speed [m/s]
- *a*: instantaneous acceleration/deceleration [m/s^2]
- *grade*: terrain gradient [%]

This approach allowed to define a selection of VSP modes for all the pollutant considered (33) (34) (23). The interesting thing was to defining bins in order to apply the methodology for specific type of vehicles and not for mixed fleets.

The instantaneous speed and acceleration/deceleration in the equation 1.3 make this expression suitable for emission calculations starting from instantaneous speed profiles to investigate about the influence of kinematic parameters variations in pollutant emissions (13) (23) (25).

In Table 1.2 the VSP modal definitions concerning a Light Passenger Duty Vehicle (LDDV) are presented.

Table 1.2: VSP modes and average values of CO2, CO, NOx, and HC emissions rates

VSP range [Kw/ton]	VSP mode	Average modal emission rates [g/s]			
		CO_2	CO	NO_x,	HC
VSP < - 2	1	0.21	0.00003	0.0013	0.00014
- 2 ≤ VSP < 0	2	0.61	0.00007	0.0026	0.00011
0 ≤ VSP < 1	3	0.73	0.00014	0.0034	0.00011
1 ≤ VSP < 4	4	1.50	0.00025	0.0061	0.00017
4 ≤ VSP < 7	5	2.34	0.00029	0.0094	0.00020
7 ≤ VSP < 10	6	3.29	0.00069	0.0125	0.00023
10 ≤ VSP < 13	7	4.20	0.00058	0.0155	0.00024
13 ≤ VSP < 16	8	4.94	0.00064	0.0178	0.00023
16 ≤ VSP < 19	9	5.57	0.00061	0.0213	0.00024
19 ≤ VSP < 23	10	6.26	0.00101	0.0325	0.00028
23 ≤ VSP < 28	11	7.40	0.00115	0.0558	0.00037
28 ≤ VSP < 33	12	8.39	0.00096	0.0743	0.00042
33 ≤ VSP < 39	13	9.41	0.00077	0.1042	0.00040
VSP ≥ 39	14	10.48	0.00073	0.1459	0.00042

The approach to select the specific definitions of 14 VSP bins considered that each pollutant has a different sensitivity to VSP. For this reason, the contribution of any individual mode to total emissions for a given pollutant was considered as the most important criteria (34). It was also highlighted that VSP modes have a particular impact upon CO than the other pollutant emissions (34).

Focusing on a specific vehicle category, the emissions values of CO_2, CO, HC, and NO_X pollutants are estimated from the distribution of time spent in each VSP mode obtained from the instantaneous speed profiles. The expression to compute the total emission of each source pollutant is shown below (13) (23).

(1.4)

$$E_{ij} = \sum_{k=1}^{N_k} F_{jk}$$

where:

E_{ij}: total emissions for source pollutant j and speed profile i [g]

k: label for second of travel k [s]

F_{kj}: emission factor for pollutant j in label for second of travel k [g/s]

N_k: number of seconds [s]

References

1. *Roadmap to a Single European Transport Area – Towards a competitive and resource efficient transport system.* Paper, White. 2011.

2. *State-of-the-art automobile emissions models and applications in North America and Europe for sustainable transportation.* Park, S., Lee, J., Lee, C. 3, 2016, KSCE Journal of Civil Engineering, Vol. 20, p. 1053–1065.

3. *Distribution Characteristics of Vehicle-Specific Power on Urban Restricted-Access Roadways.* Song, G., Yu, L., Tu. Z. 2, 2012, Journal of Transportation Engineering, Vol. 138, p. 202-209.

4. *Emission factors related to vehicle modal activity.* Giuffre, O., Grana, A., Giuffre, T., Marino, M. 4, 2011, International Journal of Sustainable Development and Planning, Vol. 6, p. 447-458.

5. *Estimating vehicle emissions from road transport, case study: Dublin City.* Achour, H., Carton, J.G., Olabi, A.G. 2011, Applied Energy 88, p. 1957–1964.

6. *Description of new elements in COPERT 4 v10.0 (12.RE.012.V1).* Katsis, P., Ntziachristos, G. M. Thessaloniki, Greece: s.n., 2012, EMISIA SA.

7. *COPERT III: Computer program to calculate emissions from road transport – Methodology and emissions factors (version 2.1).* Ntziachristos, L., Samaras, Z. [a cura di] European Environment Agency. 2000, Technical Report 49.

8. *The effects of route choice decisions on vehicle energy consumption and emissions.* Ahn, K., Rakha, H. 3, 2008, Transportation Research Part D, Vol. 13, p. 151–167.

9. *A review of instantaneous emission models for road vehicles.* Boulter, P.G., McCrae, I.S., Barlow, T.J. 2007, Published Project Report 267. TRL.

10. *The 'Corrected Average Speed' approach in ENEA's TEE model: an innovative solution for the evaluation of the energetic and environmental impacts of urban transport policies.* Negrenti, E. 235, 1999, Science of The Total Environment, p. 411–413.

11. *Development of a corrected average speed model for calcu- lating carbon dioxide emissions per link unit on urban roads.* Ryu, B.Y. Jung, H. J., Bae, S.H. 34, 2015, Transportation Research Part D, p. 245–254.

12. *Static and dynamic instantaneous emission modelling.* Ajtay, D., Weilenmann, M. 3, 2004, International Journal of Environment and Pollution, Vol. 22, p. 226-239.

13. *Driving around turbo-roundabouts vs. conventional roundabouts: Are there advantages regarding pollutant emissions?* Fernandes, P., Pereira, S. R., Bandeira, J. M., Vasconcelos, L., Bastos Silva, A., Coelho, M.C. 9, 2016, International Journal of Sustainable Transportation, Vol. 10, p. 847-860.

14. CMEM National Academies of Sciences, Engineering, and Medicine. *Predicting Air Quality Effects of Traffic-Flow Improvements: Final Report and User's Guide.* Washington, DC: The National Academies Press, 2005.

15. *Understanding and Quantifying Motor Vehicle Emissions with Vehicle Specific Power and TILDAS Remote Sensing.* J., Jiménez-Palacios. Massachusetts Institute of Technology. Cambridge. Mass.: s.n., 1999, PhD dissertation.

16. *Environmentally conscious transportation.* Kutz, M. Wiley, New York: s.n., 2008.

17. *Fuel Use and Emissions Comparisons for Alternative Routes. Time of Day. Road Grade and Vehicles Based on In-Use Measurements.* Frey, H.C., Zhang, K., Rouphail, N.M. 7, 2008, Environmental Science & Technology, Vol. 42, p. 2483–2489.

18. *Methodology for developing modal emission rates for EPA's multiscale motor ve- hicle and equipment emission system (EPA420).* EPA, US. Ann Arbor, MI: s.n., 2002, North Carolina State University for USEPA.

19. *The MOVES from MOBILE: Preliminary Comparisons of EPA's Current and Future Mobile Emissions Models.* Sontag, D., Gao, H.O. Washington, DC: s.n., January 21-25, 2007. TRB 86th Annual Meeting.

20. *Statistical Vehicle Specific Power Profiling for Urban Freeways.* Yao, Z., Wei, H., Liu, H., Li, Z. 96, 2013, Procedia - Social and Behavioral Sciences, p. 2927 – 2938.

21. *Characteristics of VSP distribution of Light-Duty and Heavy-Duty Vehicle on Freeway.* Zhao, Q., Yu, L., Song, G. 3, 2015, Journal of Transportation Systems Engineering and Information Technology, Vol. 15, p. 196-203.

22. *Analysis of Emission Effects Related to Drivers' Compliance Rates for Cooperative Vehicle-Infrastructure System at Signalized Intersections.* Liao, R., Chen, X, Yu, L., Sun, X. 1, 2018, Int J Environ Res Public Health, Vol. 15.

23. *Effect of roundabout operations on pollutant emissions.* Coelho, M. C., Farias, T. L., Rouphail, N. M. 5, 2006, Transportation Research Part D: Transport and Environment, Vol. 11, p. 333–343.

24. *Emission Estimation at Multilane Roundabouts: Effect of Movement and Approach Lane.* Salamati, K., Coelho, M., Fernandes, P., Rouphail, N. M., Frey, H.C., Bandeira, J. 2389, 2014, Transportation Research Record, p. 12-21.

25. *Identification of emission hotspots in roundabouts corridors.* Fernandes, P., Salamati, K., Rouphail, N., Coelho, M. 37, 2015, Transportation Research Part D Transport and Environment, p. 48-64.

26. Fernandes, P, Coelho, M. Making Compact Two-Lane Roundabouts Effective for Vulnerable Road Users: An Assessment of Transport-Related Externalities. [aut. libro] E., Akçelik, R., Sierpiński, G. Macioszek. *Roundabouts as Safe and Modern Solutions in Transport Networks and Systems.* s.l. : Springer, Heidelberg, 2018, Vol. 52, p. 99-111.

27. *Determining the Effects of Automated Vehicle Driving Behavior on Vehicle Emissions and Performance of an Urban Corridor.* Stogios, C., Saleh, M., Ganji, A., Tu, R., Xu, J., Roorda, M. J., Hatzopoulou, M. Washington DC: s.n., January 7-11 2018. Transportation Research Board 97th Annual Meeting.

28. *EMFAC2014 Version 1.0.7 User Guide.* EMFAC. April 2014.

29. (TREM), Transport Emission Model for Line Sources. Methodology - Technical Report EIE/07/239/SI2.466287.[Online] https://ec.europa.eu/energy/intelligent/projects/sites/iee-projects/files/projects/documents/t.at._trem_methodol- ogy_en.pdf.

30. *Akçelik and Associates aaSIDRA User Guide, Version 2.0.* Ltd., Akcelik and Associates Pty. Melbourne, Australia: s.n., 2002.

31. *Emission and fuel consumption modelling based on continuous measurements.* Jost, P., Hassel, D., Webber F-J,. TUV Rhineland, Cologne: s.n., 1992, Sonnborn Deliverable No. 7 DRIVE Project V1053.

32. *MOVES2004 User's Guide - Fundamental Model Features.* EPA, US. Queen's University, Ontario, Canada: s.n.

33. *Methodology for Developing Modal Emission Rates for EPA's Multi-Scale Motor Vehicle and Equipment Emission System.* NCSU. Office of Transportation and Air Quality, United States Environmental Protection Agency: s.n., 2002. EPA Contract No. PR-CI-02-10493.

34. *Modeling Mobile Source Emissions Based Upon In-Use and Second-by-Second Data: Development of Conceptual Approaches for EPA's New MOVES Model.* Frey, H., Unal, A., Chen, J. and Li, S. 69577, San Diego, California, US: s.n., 2003, Proceedings of the Air and Waste Management Association 96th Annual Conference and Exhibition.

35. *Transport Emission Model for Line Sources (TREM).* Department of Environment and Planning, University of Aveiro: s.n., Methodology- Technical Report EIE/07/239/SI2.466287.

Chapter 2

Traffic microsimulation models and tools

Introduction

Microsimulation includes a category of computerized (analytical) tools which are able to perform detailed analysis of activities; in transportation engineering "activities" can be referred to traffic flowing through an intersection or roundabout. Microsimulation is also used to evaluate infrastructural interventions and their effects before their implementation and installation in the real world. A traffic microscopic simulation model as AIMSUN, VISSIM, could be also applied to assess the effectiveness of introducing or lengthening a lane at an intersection, and thus to decide on spending money or not.

In turn, ordinary simulation can be considered the process of mathematical modelling that is performed on a computer to predict the behavior of a real-world system. Thus, microsimulation is distinguished from other computer modeling in looking at the interaction of individual units (e.g. vehicles). Each unit is treated as an autonomous entity and the interaction of the units can vary depending on the model rules - as car-following rules, lane-changing rules and gap-acceptance - and randomized parameters that should be calibrated to better represent individual driving preferences and to match better the reality. By way of example, some drivers in a traffic model could be cautious and wait for a large headway before entering the intersection, while other drivers could be aggressive and accept small headways.

A microscopic model is often calibrated by comparing measured and simulated values of traffic characteristics such as travel times and delays, or saturation flows rates and so on; see (1) and (2) for further details on traffic simulation with AIMSUN and VISSIM software. Literature also refers that the parameter setting that optimizes the fit between the simulation and observed traffic characteristics could be in general not unique.

In the PhD thesis AIMSUN (1) was used to investigate the environmental performances for existing urban roundabouts. It should be noted that microsimulation allows to represent the traffic evolution for road systems in high detail and to customize each single vehicle characteristic and movement, the infrastructure's geometry, and the user's behavior. By means of microsimulation, several vehicle classes, with their specific features, can be also taken into account to better represent the phenomena observed in field.

Specifically, this microsimulation software was used to analyze the impact of roundabouts and vehicle traffic from an environmental point of view. The possibility to customize vehicle fleets and driver's behavior has enabled to extract simulated instantaneous speed profiles in order to implement second-by-second kinematic data into the VSP emission model (see the following chapters).

Traffic microsimulation

The management of road networks requires the assessment of the impacts derived from implementing different traffic management measures, which often include signal coordination, high occupancy vehicle lanes, one-way systems, different types of intersection control (e.g., priority sign, signal, or roundabout), signal priority, driver information systems, safety statistics, and so on.

Traffic models are usually classified into the following categories (1) (2).

- Macroscopic simulation: Vehicle movements are modelled as packets in a network with a time step of one or more seconds. An analytical model such as the platoon dispersion model is used to rule the movement of a vehicle platoon along a road link. A macroscopic simulation can be considered deterministic, and it is useful for extensive networks design and optimization.
- Mesoscopic simulation: this approach combines a detailed microscopic simulation of some key components of a model (e.g., intersection operations) with analytical models[1] (e.g., speed-flow relationships for traffic assignment).
- Microscopic simulation: a microscopic technique is traced through a road network over time at a small time (also less than one second). This framework is useful for a wide range of applications but requires more computational resources and efforts. Random number generators are involved, and the calibration of these models can require a certain amount of time and investment in terms of computational resources and expert knowledge to be able to optimize model parameters.

Microsimulation models can shape each single vehicle within a network. Theoretically, such models should provide the complex representation of the actual driver behavior and network

[1] Analytical modelling technique relates to traffic flow theory and it is commonly a set of equations governing driver behavior such as gap acceptance, lane changing, car– following, or platoon dispersion.

performance, particularly when the road networks are close to capacity and vehicle interactions become essential in determining the operational performance output.

The scale of application of microsimulation models depends on both the computer memory and on the computer processor power. Usually, the scale of application ranges varies from about 20 km, 50 nodes, and one thousand vehicles, to a large application of 200 nodes and many thousands of vehicles.

The calibration, validation and subsequent performance of any model are fundamental, and the parameters considered in the micro-simulation models have led to questions as to the validity of the results obtained and the degree to which confidence can be placed on modelling.

Micro simulation modeling confirmed its capacity to be useful in situations that are not so close to the traditional techniques. These often include complex intersection layouts or heavily congested arterials.

The calculation procedure takes place for *simulation step* of all kinematic quantities (e.g., positions, speeds, accelerations, etc.) related to the travelling of each single vehicle. The single steps represent a set of instructions that the software must perform cyclically at fixed amplitude time intervals. Evidently, by reducing the duration of the interval between one step and the next one, it is possible to obtain increasingly accurate representations of the real phenomenon under examination. Updates can be calculated on the basis of laws related to the vehicle motion and user behavior.

As introduced before, the behavior of each single vehicle placed on the network is constantly modelled according to several driver behavior models or model rules as car-following rules, lane-changing rules and gap-acceptance. These models constitute the mathematical laws by which the mutual influence of user behaviors in particular situations can be assessed. Although these theories were born around the middle of the last century, they are still a current research subject with the aim of producing increasingly updated versions, able to represent more and more faithfully the real phenomena each time considered (3) (4) (5) (6) (7) (8).

Car-following model

Car-following models assume that the behavior of each user belonging to a vehicle flow is influenced by the behavior of the user of the vehicle preceding it. In particular, these models consider that the *follower* vehicle tends to align its own movement to those of the previous vehicle (*leader*), with a time lag equal to the *reaction time* (5) (6). For this reason, microsimulation softwares

consider the *sampling time*, which is the amplitude of time intervals between one step and the next one, that must be sub-multiple of the reaction time considered.

AIMSUN software implements the Gipps car-following model (6) by taking some adaptations. This model considers that the speed experienced by each vehicle depends on its propensity to reach a certain limit speed value, that is its desired speed V*, and the conditioning it undergoes from the presence of the leading vehicle and from its own kinematic properties. The Gipps model considers two distinct speed values based on acceleration and deceleration.

The first values V_a represents the maximum speed that a vehicle can reach at time t due to its previous speed and its desire (and ability) to accelerate. Its mathematical formulation is expressed as follows:

$$V_a(n,t+T) = V(n,t) + 2.5 \cdot a(n) \cdot T \cdot \left[1 - \frac{V(n,t)}{V^*(n)}\right] \cdot \sqrt{0.025 + \frac{V(n,t)}{V^*(n)}} \qquad (2.1)$$

Where:

- $V(n,t)$ is the speed of the vehicle n at time t;
- $a(n)$ is the maximum acceleration for the vehicle n;
- T is the reaction time or the sampling time;
- $V^*(n)$ is the desired speed of the vehicle (n) for current position.

The maximum speed V_b that a vehicle may reach during the same time interval, (t, t + T), considering its own characteristics and the limitations imposed by the presence of the vehicle ahead is:

$$V_b(n,t+T) = d(n) \cdot T + \sqrt{d(n)^2 \cdot T^2 - d(n)\left\{2[x(n-1,t) - s(n-1) - x(n,t)] - V(n,t) \cdot T - \frac{V(n-1,t)^2}{d'(n-1)}\right\}} \qquad (2.2)$$

where:

- $d(n)$ is the maximum deceleration desired by vehicle n;
- $x(n, t)$ is the position of the vehicle n at time t;
- $x(n-1, t)$ is the position of the preceding vehicle (n−1) at time t;
- $s(n-1, t)$ is the effective length of the vehicle (n−1);
- $d(n-1)$ is an estimate of the vehicle (n−1) desired deceleration.

The speed of the vehicle (n) during time interval (t, t+T) is the minimum of the Equation 2.1 and Equation 2.2:

$$V(n, t+T) = min\{V_a(n, t+T);\ V_b(n, t+T)\} \quad (2.3)$$

Therefore, the position of the vehicle (n) inside the current lane is updated taking a constant speed into the movement equation:

$$x(n, t+T) = x(n, t) + V(n, t+T) \cdot T \quad (2.4)$$

Note that the car-following model provides a leading vehicle driving freely without any vehicle affecting its behavior, would try to drive reaching its maximum desired speed. Three parameters are usually used to calculate the maximum desired speed of a vehicle into a specific section or turning; two of these parameters are related to the vehicle and one to the section or turning:

- Maximum desired speed of the vehicle *i:* $V_{max}(i)$
- Speed acceptance (usually near 1) of the vehicle *i:* $\theta^2(i)$
- Speed limit of the section or turning *s:* $S_{limit}(s)$

The expression for the speed limit of a vehicle *i* on a section or a turning *s*, is computed by means of the following equation:

$$S_{limit}(i, s) = \theta(i) \cdot S_{limit}(s) \quad (2.5)$$

Thus, the maximum desired speed of the vehicle *I* on a section or a turning *s* is expressed:

$$V_{max}(i, s) = min[S_{limit}(i, s); V_{max}(i)\ ] \quad (2.6)$$

The previous expression of maximum desired speed V_{max} (*i*, *s*) is the of that in the Gipps' car-following model above introduced as $V*(n)$.

The Gipps car-following model is a one-dimensional model and considers only the vehicle and its leader. Its implementation of the car following model in AIMSUN also considers the influence of adjacent lanes (1). Two cases can be distinguished: the case where the lane adjacent

[2] If θ(n) < 1, the user tends not to reach the speed limit although he can; if θ(n) = 1, the user reaches the speed limit as he is able to do it; if θ(n) > 1 the user exceeds the speed limit when he is able to do it.

to the lane of the considered vehicle is an acceleration lane, and the case where the adjacent lane is any other one. In this way, the software user can set two parameters: the *Maximum Speed Difference (ΔV_{MSD})*, and the *Maximum Speed Difference On-Ramp (ΔV_{MSDR})*; they are defined as the the maximum speed difference between adjacent lanes in the two considered cases. The software also allows to customize the number of vehicles to take into account in the adjacent lane and the maximum distance within which they should be considered. These parameters permit to determine the *Mean Speed Vehicles Down (ΔV_{MSVD})*, which is the average between the speeds of the adjacent vehicles. AIMSUN also considers the influence of the gradient terrain on the maximum desired acceleration and deceleration.

This contribute appears into the expressions of the speed component of the Gipps model (1) (6) (7).

For further information the car-following implemented model in VISSIM software is reported. In the psychophysical car-following model developed by Wiedemann (9), the driving behavior of humans is considered to be normally distributed: each driver has different driving capabilities for perception, reaction, and estimation of surrounding traffic environment, safety needs, desired speed, and aggressiveness towards maximum acceleration/deceleration values (9) (10). Wiedemann defines different thresholds and regimes in the relative speed/space (DX/DV) diagram for the psychophysical follower-leader pair, including the desired distance (AX), the desired minimum following distance (ABX), the maximum following distance (SDX), the perception threshold (SDX), and the decreasing and increasing speed differences (CLDV, OPDV). The desired distance for a stationary vehicle is underlined by the threshold of "*AX*". It contains the length of the front vehicle and the desired front-to-front distance (*L*), which is defined (10) (11):

$$AX = L_{n-1} + AX_{add} + RND1_n \cdot AX_{mult} \tag{2.6}$$

where:

- *n*: subject vehicle
- *n-1*: leading vehicle
- AX_{add} AX_{mult}: calibration parameters
- $RND1_n$: normally distributed parameter for desired front-to-rear distance (it depends on the driver's safety

The desired minimum following distance at low-speed differences is denoted by the threshold of "ABX". At higher speeds, the driver would undervalue the safe distance and drive closely unlike at slower speed with safe gaps (10), which can be expressed as:

(2.7)

$$ABX = AX + BX$$

(2.8)

$$BX = (BX_{add} + BX_{mult} \cdot RND1_n) \cdot \sqrt{v}$$

where BX_{add} BX_{mult} are calibration parameters.

The speed v is defined:

(2.9)

$$v = \begin{cases} v_{n-1} \; for \; v_n > v_{n-1} \\ v_n \; for \; v_n \leq v_{n-1} \end{cases}$$

The maximum following distance is denoted by the threshold of "*SDX*". At this threshold, the driver realizes that the following distance is growing. The threshold distance ranges between 1.5 and 2.5 times the minimum following distance ("*ABX*") (10), which can be estimated as:

(2.10)

$$SDX = AX + EX \cdot BX$$

(2.11)

$$EX = EX_{add} + EX_{mult} \cdot (NRND - RND2_n$$

where:

- EX_{add} EX_{mult}: calibration parameters
- *NRDN*: independent random parameter
- $RND2_n$: expression of driver's estimation ability (normally distributed parameter)

SDV is the perception threshold for approaching a point at long distances; the driver reaches to appoint where he met with a slow-moving vehicle, therefore the driver will react by decreasing the speed of his vehicle to maintain a gap higher than the minimum desired distance (ABX) (10) as:

(2.12)

$$SDV = \left(\frac{\Delta x - L_{n-1} - AX}{CX}\right)^2$$

(2.13)

$$CX = CX_{const} \cdot [CX_{add} + CX_{mult} \cdot (RND1_n + RND2_n)]$$

in which the Wiedemann model define the range for calibration parameters CX as between 25-75 (10).

CLDV is a threshold that recognizes decreasing speed differences. This is similar to the behavior of the approaching point (SDV). In this threshold, the driver perceives small speed differences, in short, decreasing distances. In VISSIM CLDV is not considered and it is assumed to be equal to SDV (2). The OPDV is a threshold that recognizes increasing speed differences. It defines a point where the driver observes that he is moving at a slower speed than the leader as (10):

(2.14)

$$OPVD = CLDV \cdot (-OPDV_{add} - OPDV_{mult} \cdot NRND)$$

The driver of the following-vehicle falls in the four different regimes that decide the driving behavior, i.e., the value of acceleration in the longitudinal direction (9). For the following behavior, the thresholds ABX, SDX, SDV and OPDV influences the driver's following behavior. Wiedemann defines that in the following regime if the vehicle passes SDV or ABX thresholds, it is assigned a deceleration rate B_{null}. This is due to the fact that vehicle should slow down to prevent an accident. However, if the vehicle passes SDX or OPDV regime, it is assigned with an acceleration rate $+B_{null}$ (9) (11). The deceleration rate can be expressed as:

(2.15)

$$B_{null} = BNULL_{mult} \cdot (RND4_n + NRND)$$

where $BNULL_{mult}$ is a calibration parameter and $RND4_n$ represent the driver's ability to control acceleration. The maximum acceleration for a passenger car B_{max} is given as:

(2.16)

$$B_{max} = BMAX_{mult} \cdot (v_{MAX} - V \cdot FaktorV)$$

(2.17)

$$FaktorV = \frac{v_{MAX}}{v_{DES} + Faktormult \cdot (v_{MAX} - v_{DES})}$$

in which, v_{MAX} and v_{DES} are the maximum speed and the desired speed, the FaktorV is a calibration parameter. About the approaching behavior, the driver is in SDV threshold and understands that he is approaching a slower vehicle. The required deceleration to avoid the impact is:

(2.18)

$$B_n = \frac{1}{2} \cdot \frac{(\Delta v)^2}{ABX - (\Delta x - L_{n-1})} + B_{n-1}$$

in which B_{n-1} is the leader's acceleration. For the emergency breaking, the following driver experiences a sudden decrease in the front-to-rear distance as compared to *ABX* because of the leading vehicle. In such a scenario, the following driver applies a maximum deceleration B_{MIN} to avoid vehicle crash, which can be expressed (10):

(2.19)

$$B_n = \frac{1}{2} \cdot \frac{(\Delta v)^2}{AX - (\Delta x - L_{n-1})} + B_{n-1} + B_{MIN} \cdot \frac{ABX - (\Delta x - L_{n-1})}{BX}$$

(2.20)

$$B_{MIN} = -BMIN_{add} - BMIN_{mult} \cdot RND3_n = BMIN_{mult} \cdot v_n$$

in which $BMIN_{add}$ and $BMIN_{mult}$ are calibration parameters, and $RND3_n$ is a random driver parameter.

All calibration parameters reported in the previous equations are shown in Table 2.1 below.

Table 2.1: Wiedemann calibration parameters, typical values *(10) (2)*

Parameter	Description	Value
AXadd	Additive calibration parameter	1.25 (m)
AXmult	Multiplicative calibration parameter	2.5 (m)
BXadd	Additive calibration parameter	2.0 (m)
BXmult	Multiplicative calibration parameter	1.0 (m)
EXadd	Additive calibration parameter	1.5 (m)
EXmult	Multiplicative calibration parameter	0.55 (m)
OPDVadd	Additive calibration parameter	1.5
OPDVmult	Multiplicative calibration parameter	1.5
CX	Calibration Parameter	40 *
BNULLmult	Multiplicative calibration parameter	0.1 (m/s^2)
NRND	Normally distributed random number	N (0.5, 0.15) **
RND1	Normally distributed driver number	N (0.5, 0.15) **
RND2	Normally distributed driver number	N (0.5, 0.15) **
RND4	Normally distributed driver number	N (0.5, 0.15) **

* (2), ** (9), *** (9).

Lane changing model

In roads with two or more lanes, to assess the vehicle traffic, consideration must also be given to the conditions under which vehicles can change lanes. The condition for changing lanes is that the gap between the two vehicles running on the parallel current is enough to accommodate the changing vehicle. In fact, lane changing models are often considered as particular cases of gap acceptance models (7).

The lane-changing is a decision model that approximates the driver's behavior in the question if it is necessary or desirable to change lanes. This aspect depends on the distance to the next turning and the traffic conditions (such as speed and queue lengths) in the current lane.

To achieve an accurate representation of the driver's behavior in the lane-changing decision process, three different zones, each one corresponding to a different lane-changing motivation, can be considered as shown in Figure 2.1. These zones feature the distance up to the end of the section, i.e., the next point of turning (1) (12).

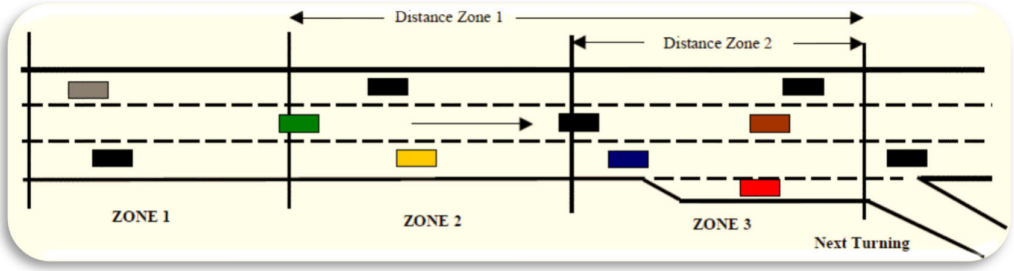

Figure2.1: Lane Changing Zones *(12)*

Figure 2.1 shows:

- *Zone 1*: The lane-changing decisions are mainly governed by the traffic conditions of the lanes involved. To measure the improvement that the driver will get from changing lanes, several parameters can be considered: The desired speed of a driver, the speed and distance of current preceding vehicle, speed, and distance of the future preceding vehicle in the destination lane. The model implemented in this zone is the overtaking maneuver model (1).
- *Zone 2*: This is the intermediate zone. Vehicles driving in the "wrong" lane (i.e., lanes where the desired turn movement cannot be made) tend to get closer to the correct side of the road from which the turn can be allowed. Vehicles looking for a gap try to adapt their speed to find gaps located either downstream or adjacent to them (1).
- *Zone 3*: Vehicles are urgently trying to reach their valid lane, looking for gaps upstream and reducing speed if necessary, even coming to a complete stop in order to make the lane change possible.

Briefly, the lane changing of each vehicle (n) at section s has five aspects (1):

- Lane Changing zone distance calculation
- Target Lanes calculation
- Vehicle behavior considering the target lanes
- Gap Acceptance model for Lane Changing
- Target Gap and Cooperation

It is also well known that the Lane changing zones are defined by two parameters, at level of turning: Distance to Zone 1 and Distance to Zone 2. These parameters are defined in time (seconds) or distance (meters), depending on the user preferences. When these parameters are defined in time, the conversion to physical distance is calculated as follows (1):

$$D_m = D_T \cdot S_{limit}(s) \tag{2.21}$$

Where:

- Dm: Distance in meters
- D_T: Distance in seconds
- S_{limit}: Speed limit of the section "s"

The perception of Distance to Zone 1 and Distance to Zone 3 for each vehicle could be varied using the Distance Zone Variability defined at level of Experiment.

The lane changing process starts by calculating the valid target lanes. The output of this process is a set of valid lanes for zone 3 and a set of valid lanes for zone 2. When the current lane of a vehicle is in a valid lane determined by zones 2 and 3, in general the behavior can be modelled as if it was in zone 1, i.e., overtaking maneuver may be initiated. However, if a leader vehicle is affected by an obstacle (e.g., turn movement, incident, lane closure, etc.), then overtaking the leader can require using a lane that can be outside of the subset of lanes given by Zone 2.

Concerning the gap acceptance model, it is consistent with the car following model to avoid artificial break down situations (7) (1):

$$V_n\,(t+T) = d_n \cdot T + \sqrt{(d_n \cdot T)^2 + d_n \cdot \left\{2 \cdot [x_1(t) - x_n(t) - s_1 - s_n] - V_n(t) \cdot T - \frac{V_1^2(t)}{d_1}\right\}} \tag{2.22}$$

$$Gap(t) = [x_1(t) - x_n(t) - s_1 - s_n] = \frac{V_1^2(t)}{2d_1} - \frac{V_n^2(t+T)}{2d_n} + [0.5 \cdot V_n(t) + V_n(t+T)] \cdot T \tag{2.23}$$

The Gipps car following model is stable, i.e., it does not require the use of decelerations above the maximum desired deceleration when (1):

$$V_n\,(t+T) \geq max[0; V_n(t) + \alpha \cdot d_n \cdot T] \tag{2.24}$$

where d_n is an estimation of vehicle leader desired deceleration, α is a parameter of aggressiveness set to 1 as a default value and takes the value defined inside the vehicle type as Sensitivity for Imprudence Lane Changing if there is an Imprudence Lane Changing.

This condition is met when:

$$Gap(t) \geq \frac{V_1^2(t)}{2d_1} + 0.5 \cdot V_n(t) \cdot T + max\left[-\frac{V_n^2(t)}{2d_n} + (1 - 0.5 \cdot \alpha) \cdot \alpha \cdot d_n \cdot T^2 + (1 - \alpha) \cdot V_n(t) \cdot T\right] \quad (2.25)$$

The Gipps car following model is crash free when the gap remains positive throughout the deceleration process (1). This gives an additional constrain:

$$Gap(t) \geq max\left\{0; \frac{V_1^2(t)}{2d_1} + 0.5 \cdot V_n(t) \cdot T + max\left[-\frac{V_n^2(t)}{2d_n} + (1 - 0.5 \cdot \alpha) \cdot \alpha \cdot d_n \cdot T^2 + (1 - \alpha) \cdot V_n(t) \cdot T\right]\right\} \quad (2.26)$$

This condition must be fulfilled to apply the Gipps car following model (6) (7) with a new leader when a vehicle changes lane (i.e., selection of possible leader and gap acceptance). It is possible to evaluate the speed and position of all vehicles at time *t+dt* if the vehicle changes lane:

- for the vehicles that are already updated, we take their current speed and position
- for the others, the speed and position are computed assuming that the vehicle changes lane at time *t+dt*

The Gap is acceptable if the physical quantities at time *t+dt* fulfill the three following requirements:

- the gaps are positive
- the computed speeds are positive
- the decelerations imposed are smaller than *a max desired acceleration*

By means of the previous equations this can be achieved with one condition at time *t* that needs to be fulfilled for both the upstream and downstream gaps (1) (7):

$$Gap_{dw}(t) \geq max\left\{0; \frac{V_{dw}^2(t)}{2d_{dw}} + 0.5 \cdot V_{lc}(t) \cdot T + max\left[0; -\frac{V_{lc}^2(t)}{2d_{lc}} + (1 - 0.5 \cdot \alpha_{lc}) \cdot \alpha_{lc} \cdot d_{lc} \cdot T^2 + (1 - \alpha_{lc}) \cdot V_{lc}(t) \cdot T\right]\right\} \quad (2.27)$$

$$Gap_{up}(t) \geq max\left\{0; \frac{V_{lc}^2(t)}{2d_{lc}} + 0.5 \cdot V_{up}(t) \cdot T + max\left[0; -\frac{V_{up}^2(t)}{2d_{up}} + (1 - 0.5 \cdot \alpha_{up}) \cdot \alpha_{up} \cdot d_{up} \cdot T^2 + (1 - \alpha_{up}) \cdot V_{up}(t) \cdot T\right]\right\} \quad (2.28)$$

It is possible modifying the acceptance of the gap in the lane changing model by defining the following parameters into AIMSUN (1):

- *Percentage for Imprudent Lane Changing Cases*: This parameter defines the probability to one vehicle apply a lane changing with a non-safe gap (reducing the gap until the length of the vehicle);
- *Sensitivity for Imprudent Lane Changing Cases*: This parameter determines the deceleration of the upstream vehicle in order to estimate the gap necessary to apply an Imprudent Lane Changing. If this parameter is greater than 1, it overestimates the deceleration of the vehicle upstream assuming a non-realistic gap.

The reader must be informed that the above is only a brief summary of the behavioral rules that govern AIMSUN; for this reason, he or she is invited to consult at least (9) where other micro simulators are also described.

Calibration and validation

Simulation, as defined above, is a sampling experiment on a dynamic real system through a computer model formally representing it (13). This kind of technique assumes that the evolution of the system's model over time well imitates the evolution of the modeled system over time. For this reason, samples of the observational variables of interest should be collected. From these samples, conclusions on system behavior can be explained by using statistical analysis techniques. The process of determining whether the simulation model is close enough to the actual system is usually achieved through the validation of the model until the accuracy is deemed acceptable. Validation of the model is an iterative process that calibrates the model parameters and compares the model to the real system behavior. The calibration process goal is to find the values of these parameters that will produce a valid model. Model parameters must be supplied with values. Calibration is the process of obtaining such values from field data in a specific setting (13).

The calibration methodology assumes that we are able of model well the input data and that the set of observed data to compare with the simulation results are "error free" (13).

Data inputs to traffic models are usually classified in two categories:

- measurements of traffic parameters affected by errors (speeds, flows, travel times, etc.) which should be filtered and processed before their using in the applications.
- data not directly observable (transport demand modeled in terms of O/D matrices.

Calibration and validation of simulation models is still a major in the case of microscopic traffic simulation models that match the high level of uncertainty of the modeled system with a big set of parameters, including behavioral aspects of the vehicle–driver system. Thus, calibration and validation has attracted the attention of many researchers in recent years to develop guidelines for calibration and validation of microscopic simulation results (13) (14) (15) (16) (17) (18). Specifically, all methodological guidelines recommend the decomposition of the main calibration problem into "sub-problems" taking into account the different nature of the parameters to be calibrated (13). This practice is usually of help in determining the likely intervals of parameter variability and constitutes a strong input for simultaneous procedures.

The FHWA guidelines structure this process into a four-steps framework (13) (19):

- Error checking: the coded transportation network and demand data are reviewed for errors.
- Capacity calibration: an initial calibration is performed to identify the values for the capacity adjustment parameters that cause the model to best reproduce observed traffic capacities in the field.
- Route choice calibration: route choice is strongly important when microsimulation model includes parallel streets. In this case, a second calibration process is performed in terms of link-specific fine-tuning.
- Performance validation: Finally, the overall model estimates of system performance in terms of travel times and queues are compared to field measurements.

Hollander and Liu, in their critical review, define the measures of goodness of fit used by the different calibration methodologies as objective functions (13) (18). Among the most used measures, if x_i and y_i are the i^{th} measured and observed value, respectively, it is possible to define the following expression:

- Root mean square error, which allows to calculate the overall error:

(2.29)

$$RMSE = \sqrt{\frac{1}{N} \cdot \sum_{i=1}^{N} (x_i - y_i)^2}$$

- Root mean squared normalized error, which gives information about the magnitude of the errors compared to the average measurements:

(2.29)

$$RMSNE = \sqrt{\frac{1}{N} \cdot \sum_{i=1}^{N} \left(\frac{x_i - y_i}{y_i}\right)^2}$$

Toledo and Koutsopoulous define two other measures of goodness of fit (20):

- Mean error:

(2.30)

$$ME = \frac{1}{N} \cdot \sum_{i=1}^{N} (x_i - y_i)$$

- Mean normalized error:

(2.31)

$$MNE = \frac{1}{N} \cdot \sum_{i=1}^{N} \left(\frac{x_i - y_i}{y_i}\right)$$

Measures 2.30 and 2.31 indicate the existence of systematic bias in terms of under or over-prediction by the simulation model (13) (20). Despite this, several analysts consider it more useful to implement measures that provide an overall view. One of the most used and accepted is the Geoffrey E. Havers's statistic GEH, that calculates the index for each counting station (13) (21):

(2.32)

$$GEH_i = \sqrt{\frac{2 \cdot (x_i - y_i)^2}{x_i + y_i}}$$

The GEH_i estimate an aggregate index by means of the following algorithm (13) (21):

(2.33)

For i = m (number of counting stations)
  If $GEH_i \leq 5$, then set $GEH_i = 1$
    Otherwise set $GEH_i = 1$
  Endif;
Endfor;
Let $GEH = \frac{1}{m}\sum_{i=1}^{m} GEH_i$
If $GEH \geq 85\%$ then accept the model
  Otherwise reject the model
Endif;

In other terms, if the deviation of the simulated data respect to the measured ones is smaller than 5% in at least the 85% of the cases, the model can be accepted (13) (21).

Other analysts propose statistical methods which account for the comparison of disaggregated time series of collected and simulated values. Theil defined indices to achieve this goal, and these indices have been used in literature for that purpose (12) (13) (20) (18) (22). The Theil indicator, called Theil's inequality coefficient, provides a normalized measure of the relative error that equalizes the impact of large errors:

(2.34)

$$U = \frac{\sqrt{\frac{1}{N}\cdot\sum_{i=1}^{N}(x_i - y_i)^2}}{\sqrt{\frac{1}{N}\cdot\sum_{i=1}^{N}(x_i)^2} + \sqrt{\frac{1}{N}\cdot\sum_{i=1}^{N}(y_i)^2}}$$

The global index U is bounded, $0 \leq U \leq 1$, with U=0 for a perfect fit and $x_i = y_i$ for i=1-N, between observed and simulated values. For $U \leq 0.2$, the simulated series can be accepted. The closer are the values to 0, the better. For U>0.2 the simulated series is rejected (13) (21).

The Theil indicator can be expressed into three proportions:

(2.35)

$$U_m = \frac{N(\bar{x} - \bar{y})^2}{\sum_{i=1}^{N}(x_i - y_i)^2}, \qquad U_s = \frac{N(\sigma_x - \sigma_y)^2}{\sum_{i=1}^{N}(x_i - y_i)^2}, \qquad U_c = \frac{2N(1-\rho)\sigma_x\sigma_y}{\sum_{i=1}^{N}(x_i - y_i)^2}$$

Where:

- $\bar{x}$ and $\bar{y}$: means of observed and simulated values

- σ_x and σ_y: standard deviations
- ρ: correlation coefficient

Equations in 2.35 satisfy the relationship Um+Us+Uc=1; the bias proportion Um measures the systematic error, and values close to 1 reveal an unacceptable bias. Us is Theil's variance proportion and it measures the goodness of simulated values to replicate the variability of the observed series. Us close to 1 means that the simulated series has strong variability. The covariance proportion, Uc, measures the unsystematic error, thus it should be close to 1 for a good fit (13) (22).

References

1. TTS - Transport Simulation System. AIMSUN Version 8.3 User's Manual . 2020.

2. VISSION, PTV. PTV VISSIM 9 User Manual. *PTV AG.* Kalsrhure, Germany : s.n., 20165.

3. *An operational analysis of traffic dynamics.* Pipes, L.A. 3, 1953, Journal of Applied Physics, Vol. 24, pp. 274–281.

4. *Vehicle movements in a platoon.* Reuschel, A. 1950, Oesterreichisches Ingenieeur-Archir, Vol. 4, pp. 193–215.

5. *Traffic dynamics: Studies in car following.* Chandler, R., Herman, R., Montroll, E. 1958, Opns. Res., Vol. 6, pp. 317–345.

6. *A behavioural car following for computer simulation.* Gipps, P. 1981, Transportation Research, Vol. B15, pp. 105–111.

7. *A model for the structure of lane-changing decisions.* Gipps, P. 1986, Transportation Research Part B, Vol. 5, pp. 403–414.

8. *A microscopic traffic simulator forevaluation of dynamic traffic management systems.* Yang Q. Koutsopoulos, H.,. 3, 1996, Transportation Research Part C: Emerging Technologies, Vol. 4, pp. 113–129.

9. *Microscopic Traffic Simulation: The Simulation System MISSION, Background and Actual State.* Wiedemann, R. and Reiter, U. Brussels, Belgium : s.n., 1992, Project ICARUS (V1052) Final Report, Vol. Vol.2, pp. 1-53.

10. *A Review of Car-Following Models and Modeling Tools for Human and Autonomous-Ready Driving Behaviors in Micro-Simulation.* Ahmed, H.U., Huang, Y. and Lu, P. 2021, Smart Cities, Vol. 4, pp. 314-335.

11. *Simulation des StraBenverkehrsflusses in Schriftenreihe des Tnstituts fir Verkehrswesen der Universitiit Karlsruhe.* Wiedemann, R. Universität Karlsruhe: Karlsruhe, Germany : s.n., 1974.

12. Barcelo, J. Casas, J. Dynamic network simulation with AIMSUN. *Simulation Approaches in Transportation Analysis.* 2005, pp. 57-98.

13. Barcelò, Jaume. International Series in Operations. *Fundamentals of traffic simulation.* s.l. : Springer, 2010, Vol. 145, 1.

14. *Standard verification process for traffic simulation model – verification manual.* T, Yoshii. Kochi University of Technology, Kochi, Japan : s.n., 1999.

15. *A framework for validation of computer models.* Bayarri MJ, Berger JO, Higdon D, Kennedy MC, Kottas A, Paulo R, Sacks J, Cafeo A, Cavendish JC, Lin CH, Tui J. 2002, NISS technical report number 128.

16. *framework for calibrating microscopic traffic simulation models.* Ciuffo B, Punzo V, Torrieri V. Washington, DC : s.n., 2007, Proceedings of the 86th TRB annual meeting.

17. *Guidelines for calibration of microsimulation models: framework and application.* Dowling R, Skabardonis A, Halkias J, McHaie G, Zammit G. 1876, Washington, DC : s.n., 2004, Journal of the Transportation Research Board.

18. *The principles of calibrating traffic microsimulation models.* Hollander Y, Ronghui L. 2008, Transportation 35, pp. 347-362.

19. FHWA. *Traffic analysis toolbox, volume II: guidelines for applying traffic microsimulation software.* US Department of Transportation. s.l. : Publication FHWA-HRT-04-040, 2004.

20. *Statistical validation of traffic simulation models.* Toledo T, Koutsopoulos H. Washington, DC : s.n., 2004. Proceedings of the 82nd annual meeting of the transportation research board.

21. Agency, Highway. *Design manual for roads and bridges, vol. 12, Traffic appraisal of road schemes, Section 2.5, Part I, Traffic appraisal in urban areas.* The Stationery Office, London : s.n., 1996.

22. *Economic forecasts and policy.* Theil, H. North Holland, Amsterdam : s.n., 1961, Publishing Company.

Chapter 3

Estimating emissions on urban roundabouts

Introduction

In this section a set of six four-legged urban roundabouts operating in the road network of Palermo City, Italy, are considered to investigate their environmental performance. Based on the speed-time profiles collected in the field by using a GPS smartphone free application installed on a light duty diesel vehicle, emissions were calculated by using the Vehicle Specific power (VSP) methodology as literature refers. It should be noted that in the next sections focus will be made on the performance evaluation of urban roundabouts starting from a pilot sample that was identified in the urban road network of Palermo City, Italy. However, before describing how the vehicle emissions were estimated according to the objectives of this study, a short background on roundabouts has been introduced only for informative purposes.

Roundabouts in brief

Among the different intersection layouts, the roundabout is an interesting design choice given its widespread in recent decades. The increasingly frequent use of roundabouts occurs after the 1980s, when new traffic rules were introduced on these intersection patterns, which have allowed to obtain many advantages in terms of functionality and safety compared to grade-level intersections. Since the 1980s, most of the research in this area has focused on the study of roundabouts both concerning traffic safety issues and regarding performance and operational aspects (1) (2).

The initial circular layout of roundabout was born in the early twentieth century in Paris, France, and then spread in other countries especially in the urban environment as a central element of furniture. The imposed circulation rules induced phenomena of self-saturation of roundabouts which, therefore, were characterized by inadequate levels of service. All these disadvantages did not favour the use of this kind of layout although the same issues did not happen in the Anglo-Saxon countries with left-hand drive.

Since 1980s, thanks to the operational improvement due to the introduction of the new rules of circulation, there has been the proliferation of new realizations or conversions of existing intersections into modern roundabouts in several European countries such as France, Germany,

the Netherlands, the Scandinavian countries, and with some delay also in Italy. Roundabouts have a fewer number of vehicular conflict points compared to conventional intersections; the potential for high-severity conflicts, (i.e. right angle, left-turn head-on crashes, and so on) is greatly reduced (3). When high volumes of traffic are detected, it may be necessary to increase the number of ring lanes by converting the roundabout layout from single-lane to multi-lane roundabout (Figure 3.1), improving the incoming capacity (3). By way of example, Figure 3.2 shows the conflict points qualification for: a) single-lane roundabout and b) multi-lane counterparts.

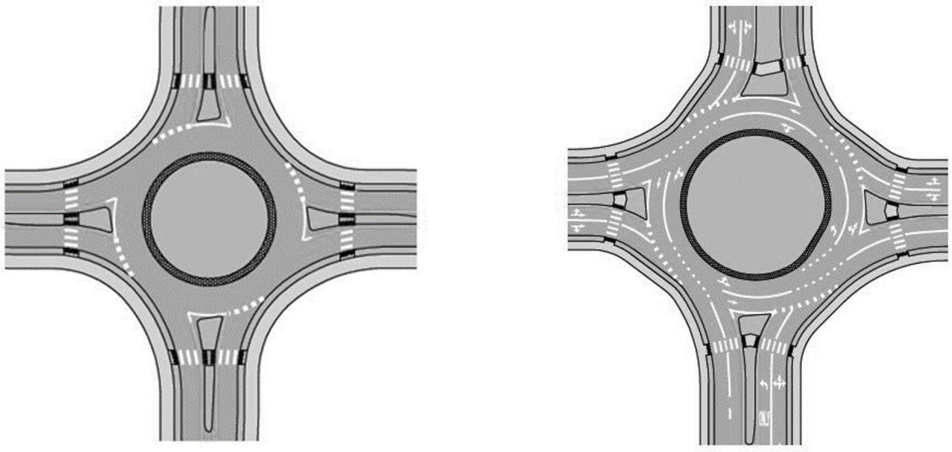

a) b)

Figure 3.1: Roundabout layouts: a) single-lane layout; b) multi-lane layout

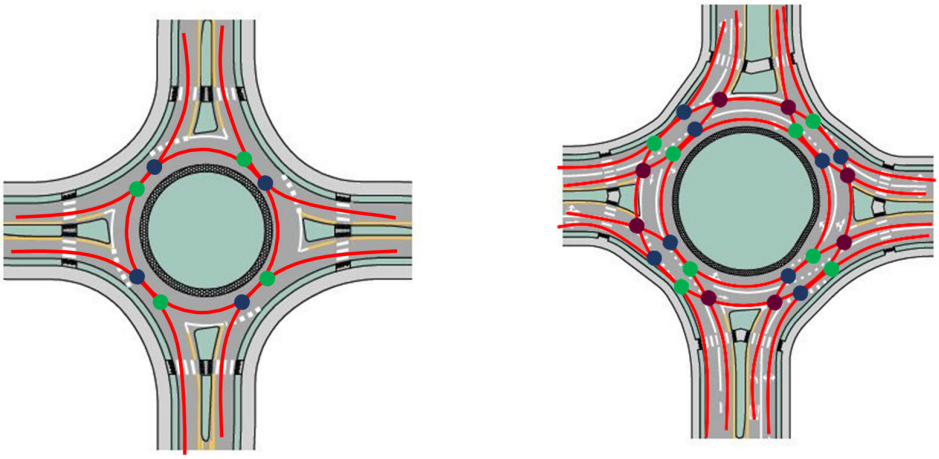

a) b)

Figure 3.2: Conflict points qualification: a) single-lane conflict points; b) multi-lane conflict points
Note: ● divergence, ● convergence, ● crossing

The operational performance of roundabouts is mostly influenced by the traffic volume desiring to enter a roundabout at a given time, the vehicle flow rate on the ring and the arrival headway distributions, as well as the layout design, vehicle and environment characteristics that reveal each individual gap acceptance behavior (4) (5).

According to The Highway Capacity Manual (HCM) model, roundabouts capacity depends on the entries capacity (6): the number of lanes at entry and the ring ones, the traffic volumes[1] per approach and per lane are the input parameters which allow to calculate the entry capacity for each leg (4) (5). The capacity model is calibrated by using the critical headway and the follow-up headway:

$$c_{pce} = Ae^{(-Bv_c)} \qquad (3.1)$$

$$A = \frac{3600}{t_f} \qquad (3.2)$$

$$B = \frac{t_c - (\frac{t_f}{2})}{3600} \qquad (3.3)$$

where:

- c_{pce} – lane capacity, adjusted for heavy vehicles (pc/h);
- v_c – conflicting flow (pc/h);
- t_c – critical headway (s);
- t_f – follow-up headway (s).

Once the entry capacity values are calculated and the flow rates are converted to vehicle per hour the Volume-to-Capacity Ratio can be computed (6):

$$x_i = \frac{v_i}{c_i} \qquad (3.4)$$

where:

- x_i – volume-to-capacity ratio of the lane i;
- v_i – demand flow rate of the lane i (veh/h);
- c_i – capacity of the lane i (veh/h).

The following equation shows the model used to estimate average control delay for each lane of roundabout approaches (6):

$$d = \frac{3600}{c} + 900T\left[x - 1 + \sqrt{(x-1)^2 + \frac{(\frac{3600}{c})x}{450T}}\right] + 5 \times min[x, 1] \qquad (3.5)$$

[1] Traffic volumes consist in conflicting, approaching and exiting flow rates.

where:

- d – average control delay (s/veh);
- x – volume-to-capacity ratio of the subject lane;
- c – capacity of the subject lane (veh/h);
- T – time (s) (T= 0,25h for a 15-min analysis).

The last step of HCM method allows to determine the Level of Service (LOS) for each approach of the roundabout; see table 3.1 as referred by (6):

Table 3.1: Level of Service (LOS) criteria for motorized vehicles in roundabout

Control Delay (s/veh)	**LOS by Volume-to-Capacity Ratio**	
	v/c ≤ 1,0	**v/c ≥ 1,0**
0-10	A	F
>10-15	B	F
>15-25	C	F
>25-35	D	F
>35-50	E	F
>50	F	F

According to TRRL formula (United Kingdom), capacity C of a generic entry is determined as a function of the leg and circle geometric parameters and of the circulating flow in the circle (Qc) in front of the entry (7). The relationship is based on experimental observation in roundabouts located in England, and it has the following expression:

(3.6)

$$C = k \cdot (F - f_c Q_c) \cdot (pcu/h)$$

Where:

- $F = 303 \cdot x_2$
- $f_c = 0.210 \cdot t_D \cdot (1 + 0.2 \cdot x_2)$
- $k = 1 - 0.00347 \cdot (\phi - 30) - 0.978 \cdot (1/r - 0.05)$
- $t_D = 1 + \frac{1}{2 \cdot [1 + \exp((D-60)/10)]}$
- $x_2 = v + \frac{(e-v)}{(1+2S)}$
- $S = 1.6(e - v)/l' = (e - v)/l$

In Table 3.2 and Figure 3.3 the geometric parameters, the symbols used in the expressions and their range are reported.

Table 3.2: Geometric parameters used by the TRRL formula (7)

Parameters	Decription	Range values
e	Entry width	3.6-15 mt
v	Lane width	1.9-12.5 mt
e'	Previous entry width	3.6-15 mt
v'	Previous lane width	2.9-12.5 mt
u	Circle width	4.9-22.7 mt
l,l'	Flare mean length	1-∞ mt
S	Sharpness of the flare	0-2-9
r	Entry bend radius	3.4-∞ mt
Φ	Entry angle	0-77°
D=Dext	Inscribed circle diameter	13.5-171.6 mt
W	Exchange section width	7.0-26.0 mt
L	Exchange section lenght	9.0-86.0 mt

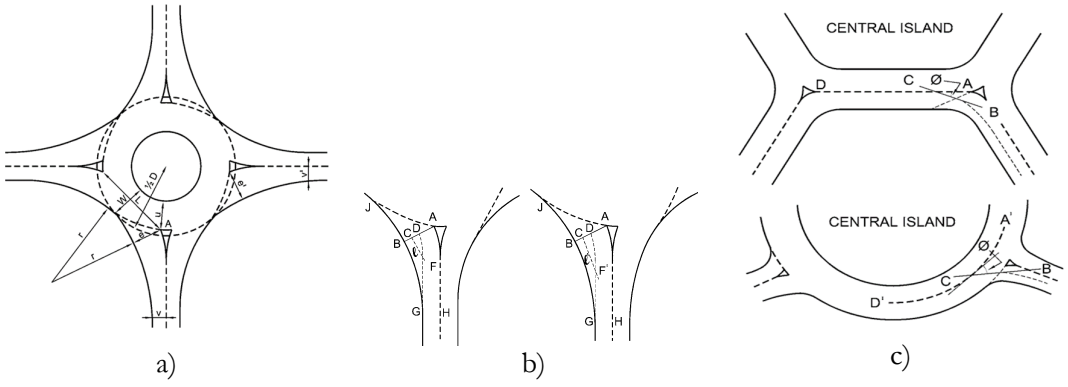

Figure 3.3: Geometric elements used in TRRL formula (a); construction and determination of f and f' (b); determination of entry angle Φ (7)

Speed profiles and instantaneous pollutant emissions

Several research have shown as the speed management is an important factor in roundabouts in terms of designing, operational, and environmental performances (8). One of the most interesting design features to control the speed is the entry deflection, which is determined by sketching the centerline radius of a vehicle that travels with the fastest path through the roundabout. According to (9) the fastest path is defined as the flattest path possible for a single vehicle, in the absence of other traffic and ignoring all lane markings, traversing through the entry, around the central island, and out the exit. For this reason, the geometric design which allows little speed variations for vehicles crossing or turning into the roundabouts may maximize the efficiency (8).

The aim of the study referred in this chapter is to assess the roundabout performances in terms of pollutant emissions produced based on characteristic speed profiles of vehicles passing through existing roundabouts in urban areas. Speed profiles are related to the length from upstream to downstream in which the drivers' speed are affected by the intersection (influence area); according to this aspect roundabouts are often employed as speed control instrument for traffic calming (10).

In chapter 1 it is showed as the instantaneous speed and acceleration profile approach from second-by-second GPS data give flexibility to characterize vehicle emission phenomenon by using instantaneous emission models to produce pollutant emission estimates and energy consumption with good accuracy (11). This kind of approach need large computation times for large-scale networks, and it is more suitable for investigate the environmental impact of road intersections such as roundabouts (12).

An application concerning roundabout describes three speed profiles covering all combinations of stop and no-stop conditions for vehicles entering a single-lane roundabout and show a methodology to quantify the emission impact of the operational performance related to stop-and-go behavior. By using the VSP approach, the parameters associated with the occurrence of changes in speed cycles with influence on emissions can be identified just like the interaction among operation variables, geometry, and the resulting traffic emissions (13).

As demonstrated by (13) (14), vehicles experience three possible trajectories as they enter a roundabout, depending on the congestion level of the approach:

- *No stop*: A vehicle starting to decelerate while approaching the roundabout, enters and negotiates the circulating area without stopping, and then accelerates back to cruise speed as it is leaving the roundabout (12) (13);
- *One stop*: A vehicle decelerates and comes to a complete stop at the yield line to enter in the circulating stream, then accelerates to cross the circulating ring and exits the roundabout (12) (13);
- *Multiple stops*: A vehicle that experiences several stops on the approach as it moves up the queue to reach the yield line, and then accelerates into the circulating ring and leaves the roundabout (12) (13).

Concerning the VSP methodology as instantaneous speed approach to estimate emissions, it depends on the speed, roadway grade and acceleration or deceleration on the basis of the second-by-second cycles. Once the speed profiles are collected it is possible to characterize the second-by-second vehicle activity by using VSP expression and to set up modal emission factors from the instantaneous emissions data (15). According to (15), Figure 3.4 shows the typical speed profiles that were experienced by the test vehicle through the roundabout sample that will be described in the next sections.

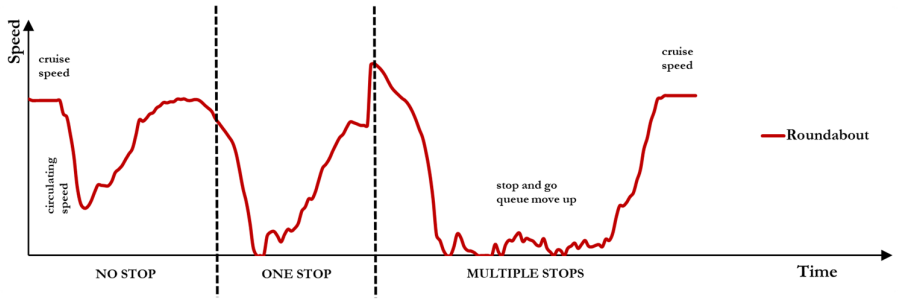

Figure 3.4: Typical speed profiles of vehicles crossing a roundabout.

Case study

A set of six roundabouts in of Palermo, Italy, was selected for this study because critical nodes of the road network. The pilot sample is distinguished by multi-lane layout (two lanes in the ring road) and four legs, apart from roundabout 6 in Pertini str which is made up of three approaches. Roundabouts characterized by great variability were considered in terms of shape and number of branches, entry and circulating speeds, traffic flows, to have a broad study base and to develop a methodological approach for the estimation of pollutant emissions from vehicular

traffic. Table 3.3 shows details on the roundabouts and descriptions of the roads approaching the roundabout; Figure 3.5 shows the roundabout location into the urban road network of Palermo, while Figure 3.6 shows each roundabout layout.

Table 3.3: Description of the roundabout sample

N	Name	Type	Roads approaching the roundabout
1	Attinelli	one-lane	Caltagirone str (Northbound), Michelangelo str (Southbound), Acireale str (Eastbound), Attinelli str (Westbound)
2	Besta	two-lane	Lanza di Scalea str (Northbound – Southbound), Besta str (Eastbound), Einaudi str (Westbound)
3	San Lorenzo	one-lane	San Lorenzo str (Northbound), Lanza di Scalea str (Southbound), San Lorenzo str (Eastbound), C. Grande str (Westbound)
4	Castelforte	two-lane (atypical shape)	Castelforte str (Northbound), Mattei str (Southbound), Olimpo str (Eastbound), Venere str (Westbound)
5	Castellana	2-lane (circular intersection)	Sarullo str (Northbound; entry with by-pass for right turners), De Mauro str (Southbound), Castellana str (Eastbound; entry with by-pass for right turners), L. da Vinci str (Westbound)
6	Pertini	2-lane (square shape)	Pertini str (Northbound), Olimpo str (Northbound – Southbound)

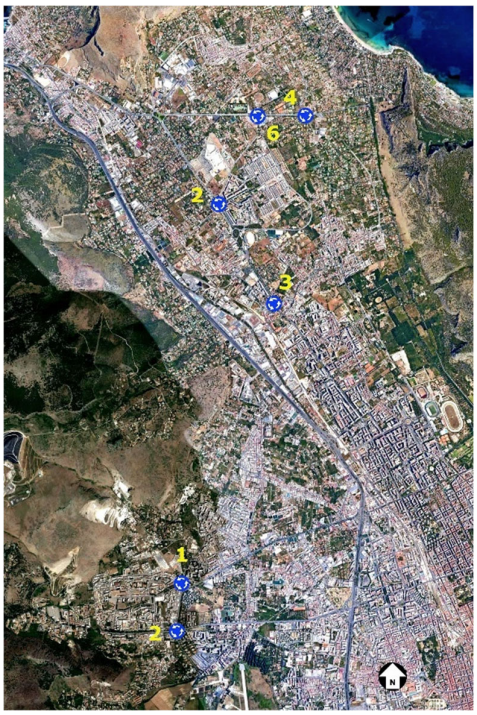

Figure 3.5: Location of roundabouts in the City of Palermo, Italy (Source: *Google Heart*)

Figure 3.6: Layouts of the surveyed roundabouts[2] (Source: *Google Heart*)

Data collection

The travel data collection by using smartphones has become more and more interesting in recent years since they are the low-cost tools (16) (17). Current smartphones are equipped with GPS sensors and triaxial accelerometers, and they provide a greater amount of information about travel experiences. Although the advantages, signal losses, degradation in high-density urban areas and cold/warm start issues are often encountered in GPS devices (16).

[2] A, B, C only denote the legs interested by through movements (A to B and B to A) and left turns.

To overcome this issues related to GPS probes, the accelerometers allow to integrate the lack of satellite signal, and their simultaneous use provides to detect transportation modes by means of positioning and kinematic data from smartphone sensors (18) (19) (20) (21).

Several Android OS or Apple IOS applications allow to extract GPS receiver information and they often retrieve information by NMEA standard protocol used by GPS sensors to record data in a comma-separated format (17); orbit information from satellites in view, position and distance using ground triangulation are thus available (17).

The goodness related to the positions estimate is affected by the number of satellites, their relative position, and other environmental factor like the weather condition or multipath interference phenomena, which are strongly connected with the typical buildings and overpasses density in urban areas (22).

Despite these aspects, researches about the use of both GPS and accelerometer sensors equipped in smartphones demonstrated that real-time probe estimates as speed, acceleration, location provide accurate output values (17) (20) (21).

In order to assess the applicability of pollutant emission models (VSP methodology) based on instantaneous speed profiles, the trajectory data were estimated from vehicle dynamics using a light passenger diesel vehicle (LPDV) conforming to Euro IV Emission Standard as the test vehicle[3]. The vehicle was equipped by the "Speedometer GPS PRO for Android smartphone", a free application that can record speed, distance, time, location, altitude at 1Hz frequency (second-by-second recording). The application allows to set other parameters such as the unit of measurement (Mph, Km/h, kn), it display the satellites sky-plot and the instantaneous position into the Google Maps environment (Figure 3.7 and Figure 3.8).

Figure 3.7: Speedometer GPS PRO display

[3] The LPDV test vehicle used for data collection is a Toyota Urban Cruiser equipped with a 1.4 lt engine (95hp).

Figure 3.8: Travel recording information available in *http://gpxscan.com*

The big advantage of using this specific Android application for data collection is the .xls output file in which second-by-second speeds, travel distances, altitudes and GPS coordinates are stored as raw data (Figure 3.9).

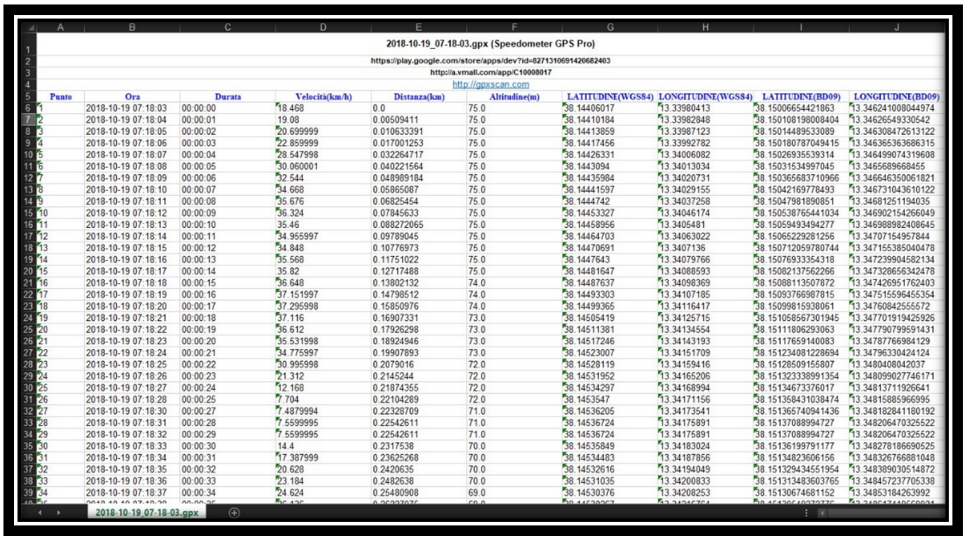

2018-10-19_07-18-03.gpx (Speedometer GPS Pro)

https://play.google.com/store/apps/dev?id=8271306914206624O3

http://a.vmall.com/app/C10008017

http://gpxscan.com

Punto	Ora	Durata	Velocità(km/h)	Distanza(km)	Altitudine(m)	LATITUDINE(WGS84)	LONGITUDINE(WGS84)	LATITUDINE(BD09)	LONGITUDINE(BD09)
1	2018-10-19 07:18:03	00:00:00	18.468	0.0	75.0	38.14406017	13.33980413	38.15006654421863	13.346241008044974
2	2018-10-19 07:18:04	00:00:01	19.08	0.00509411	75.0	38.14410184	13.33982848	38.150108198008404	13.346265493330542
3	2018-10-19 07:18:05	00:00:02	20.699999	0.010633391	75.0	38.14413859	13.33987123	38.15014489533089	13.346308472613122
4	2018-10-19 07:18:06	00:00:03	22.859999	0.017001253	75.0	38.14417456	13.33992782	38.150180787049415	13.346365363686315
5	2018-10-19 07:18:07	00:00:04	28.547998	0.03226417	75.0	38.14426331	13.34006082	38.15026935539314	13.346499074319608
6	2018-10-19 07:18:08	00:00:05	30.060001	0.040221564	75.0	38.1443094	13.34013034	38.15031534997045	13.346568668455
7	2018-10-19 07:18:09	00:00:06	32.544	0.048989184	75.0	38.14435984	13.34020731	38.150365683710966	13.346646350061821
8	2018-10-19 07:18:10	00:00:07	34.668	0.05865087	75.0	38.14441597	13.34029155	38.15042169778493	13.346731043610122
9	2018-10-19 07:18:11	00:00:08	35.676	0.06825454	75.0	38.1444742	13.34037258	38.15047981890851	13.346812511194035
10	2018-10-19 07:18:12	00:00:09	36.324	0.07845633	75.0	38.14453327	13.34046174	38.150538765441034	13.346902154266049
11	2018-10-19 07:18:13	00:00:10	35.46	0.088272065	75.0	38.14458956	13.34054481	38.15059493494277	13.346988982408645
12	2018-10-19 07:18:14	00:00:11	34.955997	0.09789045	75.0	38.14464703	13.34063022	38.15065229281256	13.347071549557844
13	2018-10-19 07:18:15	00:00:12	34.848	0.10776973	75.0	38.14470691	13.3407136	38.150712059780744	13.347155385040478
14	2018-10-19 07:18:16	00:00:13	35.568	0.11751022	75.0	38.1447643	13.34079766	38.15076933354318	13.347239904582134
15	2018-10-19 07:18:17	00:00:14	35.82	0.12717488	75.0	38.14481647	13.34088593	38.15082137562266	13.347328656342478
16	2018-10-19 07:18:18	00:00:15	36.648	0.13802132	74.0	38.14487637	13.34098369	38.15088113507872	13.347426951762403
17	2018-10-19 07:18:19	00:00:16	37.151997	0.14798512	74.0	38.14493303	13.34107185	38.150937669878715	13.347515596455354
18	2018-10-19 07:18:20	00:00:17	37.295998	0.15850976	74.0	38.14499365	13.34116417	38.15099815938061	13.347608425555572
19	2018-10-19 07:18:21	00:00:18	37.116	0.16907331	73.0	38.14505419	13.34125715	38.151058567301945	13.347701919425926
20	2018-10-19 07:18:22	00:00:19	36.612	0.17926298	73.0	38.14511381	13.34134554	38.15111806293063	13.347790799591431
21	2018-10-19 07:18:23	00:00:20	35.531998	0.18924946	73.0	38.14517246	13.34143193	38.15117659140083	13.347877669841129
22	2018-10-19 07:18:24	00:00:21	34.775997	0.19907893	73.0	38.14523007	13.34151709	38.15123408122869	13.347963304241124
23	2018-10-19 07:18:25	00:00:22	30.995998	0.2079016	72.0	38.14528119	13.34159416	38.15128509155807	13.348040804420037
24	2018-10-19 07:18:26	00:00:23	21.312	0.2145244	72.0	38.14531952	13.34165206	38.151323339991354	13.348099027746171
25	2018-10-19 07:18:27	00:00:24	12.168	0.21874355	72.0	38.14534297	13.34168994	38.15134673376017	13.34813711926641
26	2018-10-19 07:18:28	00:00:25	7.704	0.22104289	72.0	38.1453547	13.34171156	38.151358431038474	13.348158859695995
27	2018-10-19 07:18:30	00:00:27	7.487994	0.22328709	71.0	38.14536205	13.34173541	38.151365740941436	13.348182841180192
28	2018-10-19 07:18:31	00:00:28	7.5599995	0.22542611	71.0	38.14536724	13.34175891	38.15137088994727	13.348206470325522
29	2018-10-19 07:18:32	00:00:29	7.5599995	0.22542611	71.0	38.14536724	13.34175891	38.15137088994727	13.348206470325522
30	2018-10-19 07:18:33	00:00:30	14.4	0.2317538	70.0	38.14535849	13.34183024	38.15136199791177	13.348278186690525
31	2018-10-19 07:18:34	00:00:31	17.387999	0.23625268	70.0	38.14534483	13.34187856	38.15134823606156	13.348326766881048
32	2018-10-19 07:18:35	00:00:32	20.628	0.2420635	70.0	38.14532616	13.34194049	38.15132943455954	13.348389030514872
33	2018-10-19 07:18:36	00:00:33	23.184	0.2482638	70.0	38.14531035	13.34200833	38.151313483603765	13.348457237705338
34	2018-10-19 07:18:37	00:00:34	24.624	0.25480908	69.0	38.14530376	13.34208253	38.15130674681152	13.348531842639992

2018-10-19_07-18-03.gpx

Figure 3.9: Example of .xls output file with recorded data

The research team collected data at the roundabouts during the morning peak periods (7:00–8:30 a.m.) on regular weekdays (Wednesday to Thursday) in October and November of 2018. The speed limit in the surveyed networks is 50 km/h. Location, travel time, distance, grade, speed, and acceleration with 1Hz of frequency are the values extracted from the GPS and accelerometer recorded data by the smartphone probe (23). The through movements and left turns at multi-lane sites were experienced by entering from the left entry lane; from 7 to 10 runs

were done for a total of 236 GPS travel runs (188 travel runs of through movements in both directions and 48 travel runs of left turn movements).

Entry and conflicting traffic flows were videotaped in some sites. The surveyed roundabouts are located in areas different from the urbanistic point of view, and the percentage of the heavy vehicles did not overcome 10 percent during the observational time slots.

The number of runs per roundabout was deemed sufficient to obtain appropriate results from the collected data (12) (24); almost 90 km were travelled and over 15 h were gathered.

In Table 3.4 an overview is stated about geometric characteristics, averaged speeds recorded in entry, exit approaches and in the ring lanes and the total entering traffic gathered from counting. The deflection angle is roughly equal in crossing movements related to all surveyed roundabouts: for this reason, the influence of the registered kinematic parameters and the pollutant estimations with it has not been investigated. It must be noticed that although traffic volumes recorded for morning peak hours, they were far from congestion.

Table 3.4: Roundabouts' information overview

No	entry (exit)	outer diameter [m]	entry (exit) lane width [m]	ring width [m]	mean entry (exit) speed [km/h]	mean circulating speed [km/h]	total entering traffic [vph]
1	3 (4)	48.00	3.50 (3.50)	7.00	22 (30)	18.00	1577
2	4 (4)	80.00	4.50 (4.50)	8.00	26 (36)	23.00	3983
3	4 (4)	50.00	3.50 (3.50)	9.00	23 (31)	20.00	2336
4	4 (4)	60.00	4.75 (4.75)	10.00	30 (42)	25.00	1317
5	4 (4)	80.00	4.00 (5.00)	9.00	25 (35)	23.00	4052
6	3 (3)	80.00	5.00 (4.50)	10.00	30 (38)	25.50	988

Speed profiles on roundabouts

The speed profiles confirmed the experience in (12) for vehicles approaching the roundabouts, as it is shown in the following examples. Each speed profile that occurred for the vehicle entering the roundabout was related to the greater or lesser congestion level for conflicting and entry traffic.

In some cases, the test vehicle experienced entry and negotiation of the circulating area without stopping for then accelerating back to cruise speed as it is exiting (see Figure 3.10a), while in other situations the test vehicle experienced one stop at the entry line before finding a convenient headway, accelerated to travel the ring and to exit the roundabout (see Figure 3.10b). There were further cases of multiple stopping that the test vehicle also experienced depending

on the level of congestion of the entry approach (see Figure 3.10c), where the vehicle has waited for a useful gap for more time, thus entered the roundabout also facing low circulating traffic, or the vehicle spent the time in deceleration as it approached the roundabout, entered the circulating lanes at low speed and acceleration as it exited the roundabout. Concerning left turning movements, the test vehicle experienced entry and negotiation of the circulating area without stopping, and then accelerating back to cruise speed as it exited.D

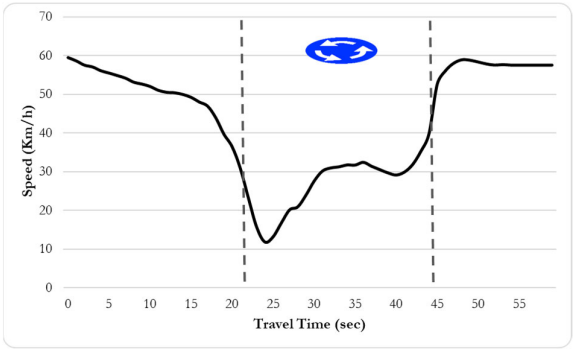

a)

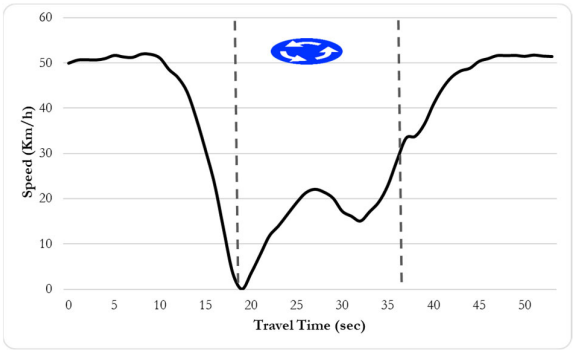

b)

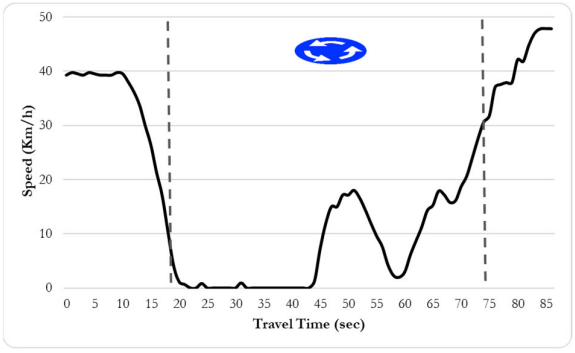

c)

Figure 3.10: Examples of speed profiles for through movements in roundabout 4 *(no stop, a)*, roundabout 2 *(one stop, b)* and roundabout 5 *(multiple stop, c)*

As previously introduced, all the surveyed trajectories were separated by driving direction considering both trough movements directions and the left turning manoeuvres. The experienced curvilinear paths by the test vehicle have proved to be similar and for this reason trajectory data were considered invariant for crossing manoeuvres. This hypothesis is supported by a two-tailed t-test which was performed on the observed distributions of speed and accelerations and decelerations in the AB and BA directions, as described in Table 3.5. Based on these results it can be stated that no significant difference exists between the two travelling directions through the roundabouts. In the following Figure 3.11 all instantaneous speed profiles are also shown for each roundabout of the study sample for the AB and BA through movements where a reference profile could be selected for the following analysis. The averaged speed profile of crossing movement for each direction and for each roundabout are presented (Fig.3.11). The construction of averaged speed values depends on the choice to standardize the registered runs according to an influence area of 500 meters; in this way it is possible to represent the collected profiles in several time series with comparable order of magnitude, and to calculate the average profile.

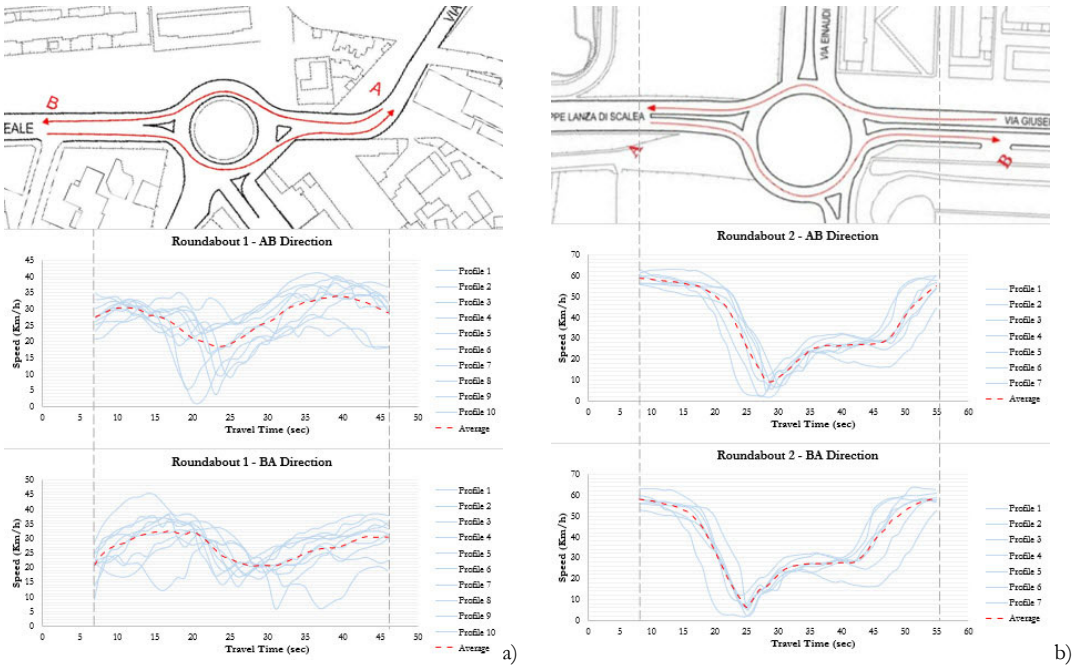

a) b)

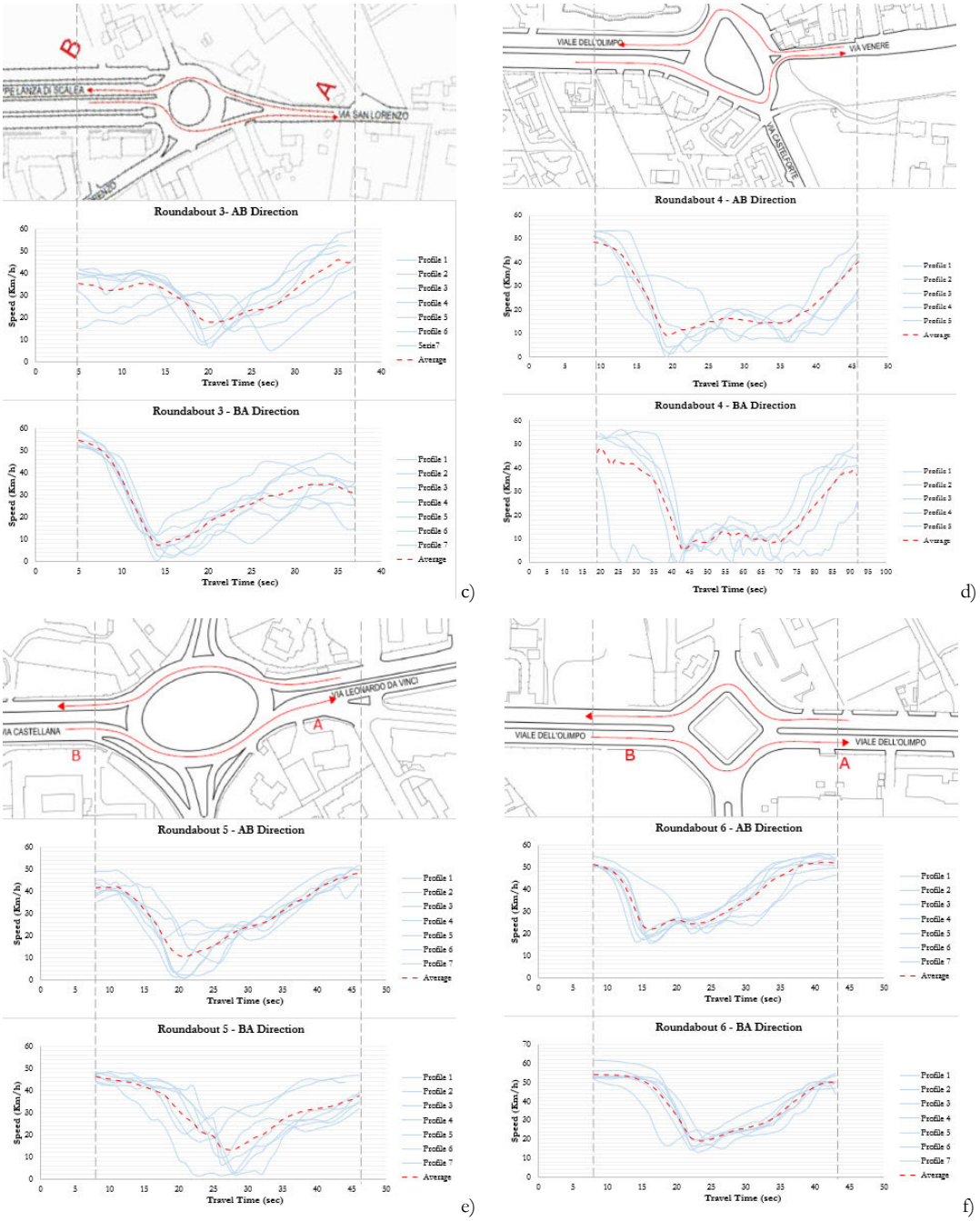

Figure 3.11: Recorded instantaneous speed profiles for AB and BA movements in each sampled roundabout

Table 3.5: Two-tailed t-test for distributions of observed kinematic parameters relating the AB and BA through movements

parameter	μ_{AB}[4] (s.e.)	μ_{BA}[3] (s.e.)	t-value[5]	t-critical value $t_{0.05,92}$	t-critical value $t_{0.01,92}$	p-value (α[6]=0.05)
Max. speed [m/s]	14.46 (0.38)	14.12 (0.36)	0.65	1.986	2.630	0.516
Max. acceleration [m/s²]	1.77 (0.07)	1.55 (0.07)	2.0	1.986	2.630	0.052
Max. deceleration [m/s²]	2.498 (0.108)	2.417 (0.11)	0.52	1.986	2.630	0.60
85th percentile acceleration [m/s²]	0.916 (0.030)	0.868 (0.025)	1.20	1.986	2.630	0.231
95th percentile acceleration [m/s²]	1.286 (0.039)	1.196 (0.042)	1.57	1.986	2.630	0.121
85th percentile deceleration [m/s²]	1.420 (0.081)	1.25 (0.059)	1.68	1.986	2.630	0.100
95th percentile deceleration [m/s²]	2.053 (0.089)	1.88 (0.085)	1.39	1.986	2.630	0.20

The VSP methodology for Estimating Emissions

As introduced in Chapter 1 the class of the instantaneous emission models relate the emission rates to second-by-second vehicle dynamic data. Concerning the simplified form of the VSP equation for a typical light passenger vehicle, it is based on the road grade, vehicle's speed, and acceleration (25):

$$VSP = v \cdot \left[1.1 \cdot a + 9.81 \cdot sin\left(arctan(grade)\right) + 0.132\right] + 0.000302 \cdot v^3 \quad (3.7)$$

with *VSP* in kW/ton, the instantaneous speed *v* in m/s, the acceleration (or deceleration) *a* in m/s². To estimate the pollutant emissions for the recorded speed profile *i*, Eq. 3.7 was used to calculate second-by-second emission rates for the vehicle test which experienced that speed profile *i*. In Table 3.6 one can see 14 modes of engine regime and emission factors by mode to estimate CO_2, CO, NO_x, and HC emissions by vehicle type (12).

[4] μ_{AB} and μ_{BA} represent the averaged values of the observations of each parameter in the two driving directions (AB and BA) for the sampled roundabouts.

[5] t-value is the result of the two tailed t-test done to compare the equality of the μ_{AB} and μ_{BA} of samples of two populations with equal sample size.

[6] α is the 5% significance level.

Table 3.6: Average values of CO_2, CO, NO_x, and HC emissions rates by VSP mode for LPDV

VSP range [Kw/ton]	VSP mode	Average modal emission rates [g/s]			
		CO_2	CO	NO_x,	HC
VSP < - 2	1	0.21	0.00003	0.0013	0.00014
- 2 ≤ VSP < 0	2	0.61	0.00007	0.0026	0.00011
0 ≤ VSP < 1	3	0.73	0.00014	0.0034	0.00011
1 ≤ VSP < 4	4	1.50	0.00025	0.0061	0.00017
4 ≤ VSP < 7	5	2.34	0.00029	0.0094	0.00020
7 ≤ VSP < 10	6	3.29	0.00069	0.0125	0.00023
10 ≤ VSP < 13	7	4.20	0.00058	0.0155	0.00024
13 ≤ VSP < 16	8	4.94	0.00064	0.0178	0.00023
16 ≤ VSP < 19	9	5.57	0.00061	0.0213	0.00024
19 ≤ VSP < 23	10	6.26	0.00101	0.0325	0.00028
23 ≤ VSP < 28	11	7.40	0.00115	0.0558	0.00037
28 ≤ VSP < 33	12	8.39	0.00096	0.0743	0.00042
33 ≤ VSP < 39	13	9.41	0.00077	0.1042	0.00040
VSP ≥ 39	14	10.48	0.00073	0.1459	0.00042

For the test vehicle operating during data collection, the emissions values of CO_2, CO, NO_x and HC pollutants were estimated from the distribution of time spent in each VSP mode obtained from the speed profiles (12):

$$E_{ij} = \sum_{k=1}^{N_k} F_{kj} \tag{3.8}$$

Where:

- E_{ij} = total emissions for source pollutant *j* and speed profile *i*, [g];
- k is the label for second of travel [s];
- F_{kj} is the emission factor for pollutant *j* in label for second of travel k [g/s];
- N_k is the number of seconds [s].

The influence area of 500 m was considered for each roundabout in order to have the same value of distance travelled from downstream to upstream and to ensure consistency among the runs through the examined roundabouts. It was defined as the sum of the deceleration distance of a vehicle travelling from the cruise speed as it approaches and the enters the roundabout, the acceleration distance as it exits the roundabout up to the section it reaches the cruise speed, and the travel distances during cruising before approaching and after exiting the roundabout. Taking into account that each roundabout selected is characterized by grades less than 2 percent this parameter was considered equal to zero in Eq. 3.7.

Results

Based on emission rates corresponding to each run and each through movement[7], the average CO_2, CO, NOx and HC emission rates were estimated for the sampled roundabouts (Figure 3.12). The total emissions for the different pollutants were estimated and compared; no critical issues were identified with respect to the EURO IV standards on pollutant emissions from vehicular sources. The results were also consistent with the expectation of lower CO and higher NOx emissions than gasoline vehicles; see in this regard (25). According with the EU's air quality directives, the CO_2 and NOx +HC emission targets for the test vehicle corresponds to 130 g/km and 0.30 g/km respectively; in some of the examined cases the CO_2 and NOx + HC emissions were found to be higher than expected. However, the differences in pollutant emissions concerning the roundabout sample here examined were due both to the different layouts and entry (or exit) dimensions, and to different amount of traffic volumes that were recorded in the field. In particular the previous factors caused different acceleration conditions that the test vehicle experienced during data collection.

Figure 3.13 to 3.18 show the speed profiles selected between the sampled roundabouts; a comparison in terms of relative frequencies of time spent in VSP mode and the spatial distribution of CO_2 pollutant emissions was carried out.

The speed profiles were chosen among all the recorded ones in the field to build the cumulative distributions of CO_2 from the second-by-second emission rates and the time spent in each VSP mode during the GPS runs. The relative increase in the percentage of CO_2 emissions (the steepness of the spatial distribution) with the distance travelled from the roundabout entry is greatest in short stop-and-go events and the acceleration phase. This aspect is particularly noticeable when one examines roundabout 4 (see Figure 3.16) having an atypical layout compared to roundabout 2 (see Figure 3.14) that is entirely consistent with the Italian standards on geometric design of road interchanges and intersections (25).

Repeated changes in the vehicle speeds in the ring provided greater CO_2 emission rates than at entries. Increases of the CO_2 emissions occurred when the test vehicle got in the ring with a minimum speed and started accelerating to reach its desired speed to exit (see Figure 3.15c and Figure 3.17c).

[7] In this study left turn movements collected during field observation were not considered for emission estimations.

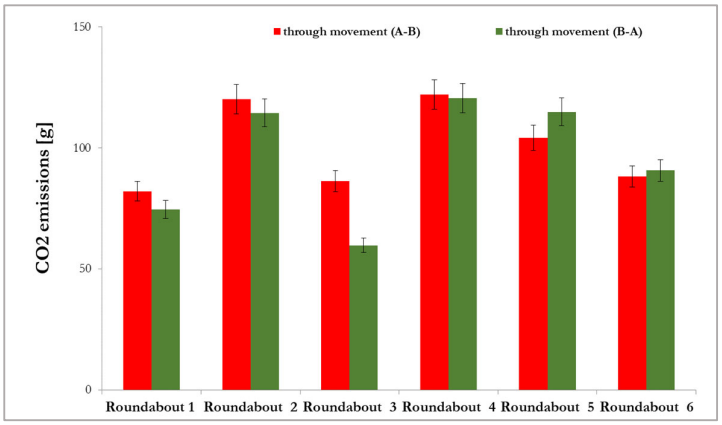

a)

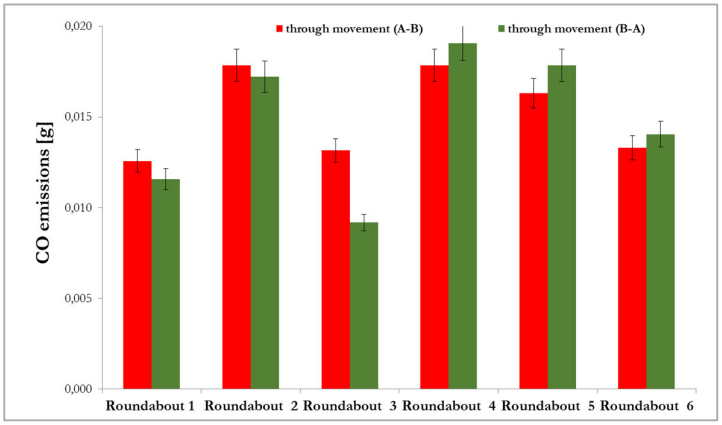

b)

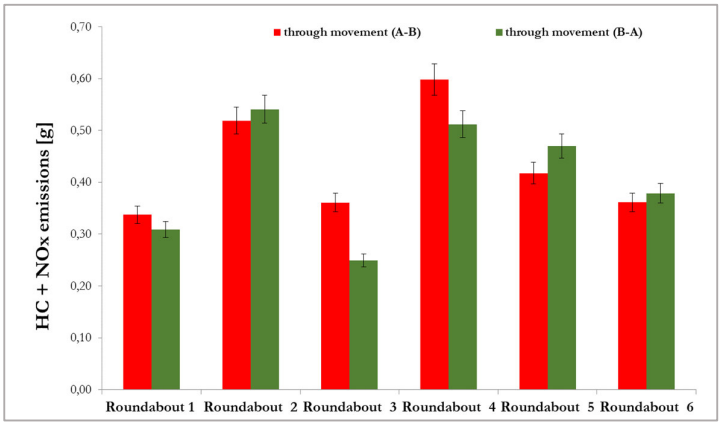

c)

Figure 3.12: CO_2, CO and HC+NOx total emission [g] in AB and BA movements through the surveyed roundabouts using the VSP methodology

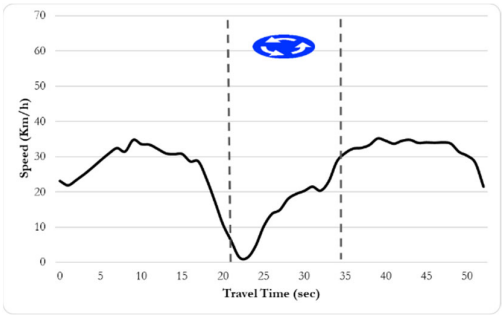

a)

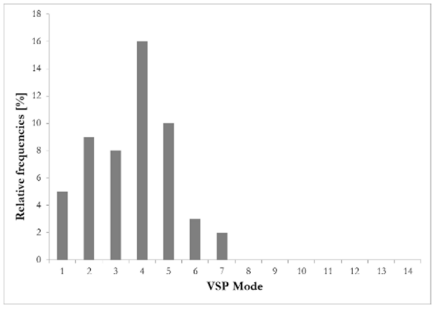

b)

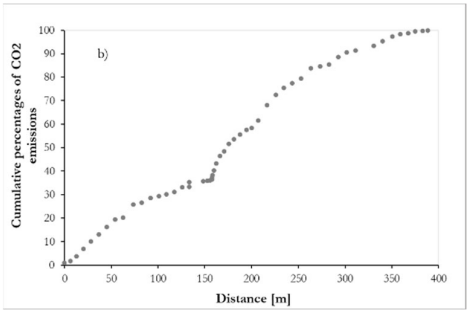

c)

Figure 3.13: Roundabout 1 AB movement; Speed profile 5 a), Time spent in VSP mode b); CO_2 spatial distribution c)

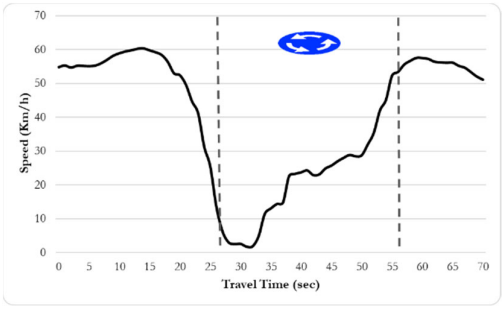

a)

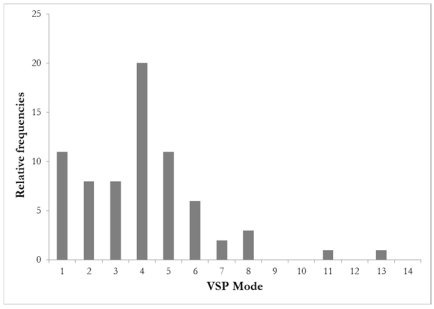

b)

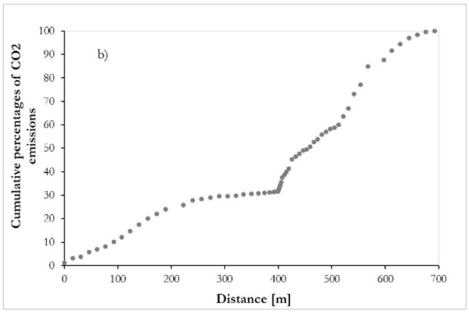

c)

Figure 3.14: Roundabout 2 BA movement; Speed profile 4 a), Time spent in VSP mode b); CO_2 spatial distribution c)

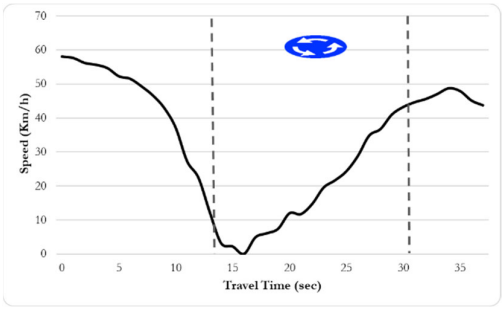

a)

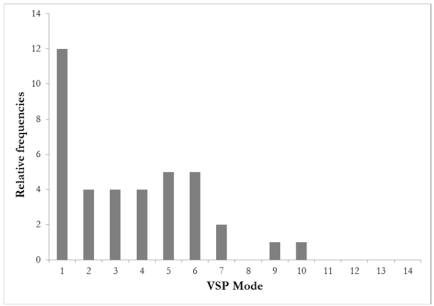

b)

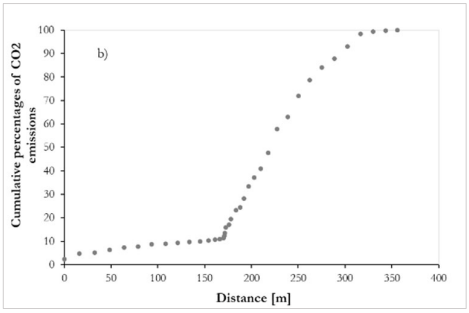

c)

Figure 3.15: Roundabout 3 BA movement; Speed profile 5 a), Time spent in VSP mode b); CO_2 spatial distribution c)

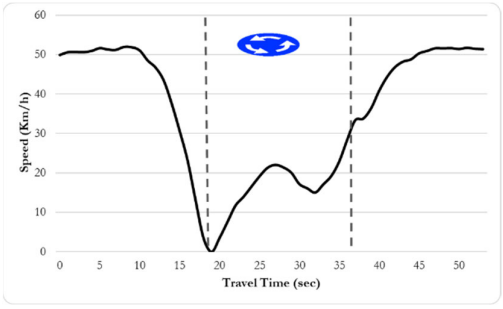

a)

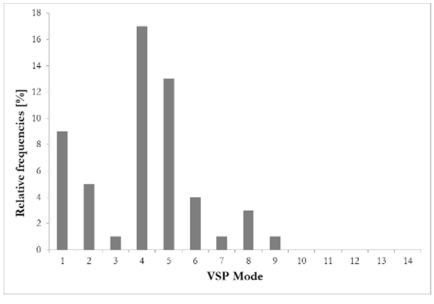

b)

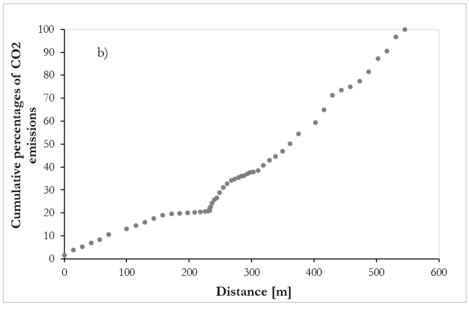

c)

Figure 3.16: Roundabout 4 AB movement; Speed profile 5 a), Time spent in VSP mode b); CO_2 spatial distribution c)

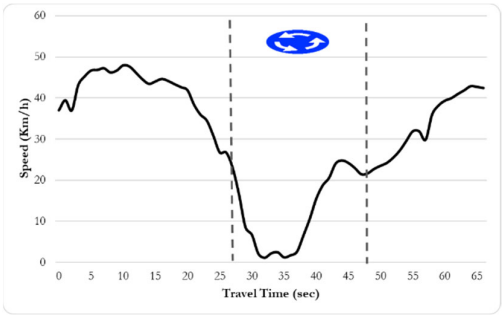

a)

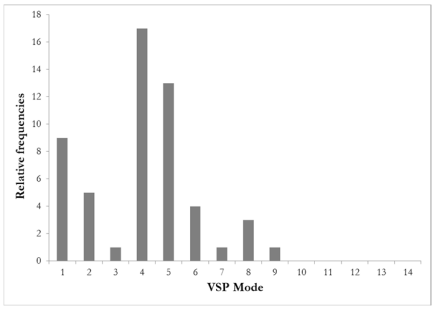

b)

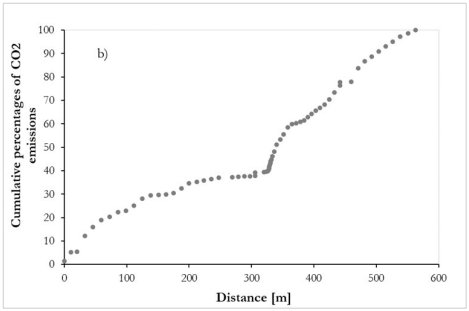

c)

Figure 3.17: Roundabout 5 AB movement; Speed profile 6 a), Time spent in VSP mode b); CO_2 spatial distribution c)

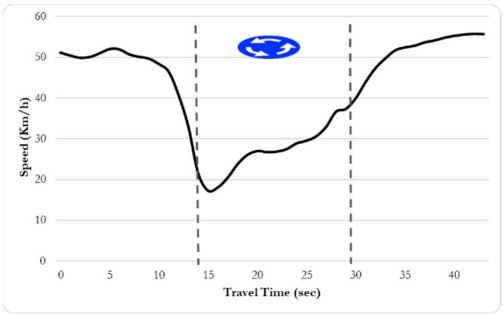

a)

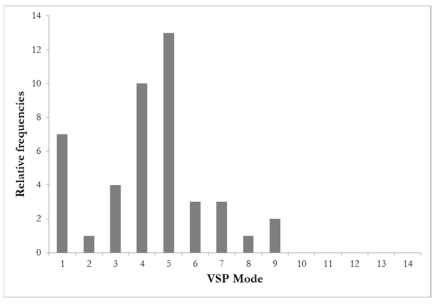

b)

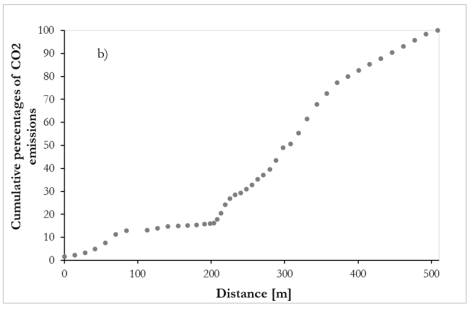

c)

Figure 3.18: Roundabout 6 AB movement; Speed profile 6 a), Time spent in VSP mode b); CO_2 spatial distribution c)

Focusing on roundabout 1 and roundabout 5, one can see that most of time is spent in the VSP modes 2 (deceleration), 3 (idle) and 4 (acceleration and cruising) (Figure 3.17b), while in Figure 17b the vehicle test keeps speeding up and the VSP modes higher than 4 are also experienced. This aspect is mainly due to the different sizes of the two roundabouts and to differences concerning the configuration of approaches; in roundabout 5, legs allow the vehicles to travel by means of fastest paths than those ones confluent to roundabout 1; see also Figure 3.6.

Few conflicting and entering traffic volumes produce very low probability for speed profiles with one or multiple stops in roundabout 6 (Figure 3.18a); during data collection the vehicle test experienced fast crossing maneuvers without stopping at the entry lane both for AB and for BA through movements. In Figure 3.18b this aspect is highlighted from lower frequency of time spent in VSP mode 3 (idle) than modes 4 and 5 (acceleration and cruising).

The percent of the time spent in VSP modes higher than 5 is low in most of cases, and it is noticeable only for layouts with two-lane approaches as well as bigger lane width.

According to (12) (26) acceleration events in the ring and exiting areas of a roundabout contributed to more than 25 percent of the emissions for a given speed profile.

Conclusions

The chapter describes the study conducted to assess pollutant emission estimation by means of an empirical approach using instantaneous speed data from a smartphone app and the vehicle-specific power (VSP) methodology. The main goal was to acquire vehicle dynamics data from roundabouts located in the road network of the City of Palermo, Italy, and to quantify emissions generated by an available light diesel vehicle used as the test vehicle.

Vehicle trajectory data were collected by using the app Speedometer GPS PRO for Android smartphone which recorded the second-by-second detailed GPS paths. The left turns and through movements were experienced entering each roundabout from the left lane (where a two-lane entry approaches were installed) for a total of 236 travel runs of through movements in both directions and left turn movements; over 15 h were gathered for the surveyed roundabouts. However, focus was made mainly on through movements in the analysis that will be done in the following activities (see next chapters).

With recorded field data from smartphone app, speed, and acceleration (and deceleration) were obtained directly giving the possibility to explore the driving performance at the roundabouts from an environmental point of view only. The results show the goodness about the

simultaneous use of smartphone app to collect data and the Vehicle-Specific Power methodology to estimate pollutant emissions at urban roundabouts. The approach is revealed friendly both in data collection and in the following data analysis.

References

1. F.A., Santagata. *AAVV Strade Pearson.* 2016.

2. Esposito T., Mauro R. *Fondamenti di Infrastrutture Viarie 1 - La geometria stradale.* s.l. : Hevelius Edizioni, 2001.

3. Tollazzi, T. *Alternative Types of Roundabouts and Informational Guide.* s.l. : Springer eds, 2015.

4. *Methodological Frontier in Operational Analysis for Roundabouts: A Review.* Giuffrè O, Granà A and Tumminello. s.l. : Front. Built Environ. 2:28, 2016.

5. Mauro, Raffaele. *Calculation of Roundabouts - Capacity, Waiting Phenomena and Reability.*

6. *Highway Capacity Manual, 6th Edn.* Washington, DC : Transportation Research Board, 2016.

7. *The Traffic Capacity of Roundabouts.* Kimber, R. M. Crowthorne, Berkshire : s.n., 1980, TRRL Laboratory, Vol. Report 942.

8. *Comparison between simulated and experimental crossing speed profiles on roundabout with different geometric features.* Vincenzo Gallellia, Rosolino Vaiana, Teresa Iuele. 111, 2014, Elsevier Ltd, Procedia - Social and Behavioral Sciences, p. 117-126.

9. Rodegerdts, L., & al. Roundabouts: An Informational Guide. (2nd ed.). *NCHRP Report 672, Transportation Research Board.* Washington, D.C. : s.n.

10. *Driver behavior characterization in roundabout crossings.* Ana Bastos Silva, Silvia Santos, Luìs Vasconcelos, Alvaro Seco, João Pedro Silva. Sevilla, Spain : Elsevier, 2014, Transportation Research Procedia 3, p. 80-89.

11. *The effects of route choice decisions on vehicle energy consumption and emissions.* Ahn, K., Rakha, H. 2008, Transportation Research Part D, Vol. 13(3), p. 151–167 .

12. P. Fernandes, S. R. Pereira, J. M. Bandeira, L. Vasconcelos, A. Bastos Silva & M. C. Coelho. Driving around turbo-roundabouts vs. conventional roundabouts: Are there advantages regarding pollutant emissions? *International Journal of Sustainable Transportation.* 2016, Vol. 10:9, p. 847-860.

13. *Effect of roundabout operations on pollutant emissions.* Margarida C. Coelho, Tiago L. Farias, Nagui M. Rouphail. Issue 5, 2006, Transportation Research Part D: Transport and Environment, Vol. Volume 11, p. 333-343.

14. *Emissions estimation at multilane roundabouts.* Salamati, K., Coelho, M., Fernandes, P., Rouphail, N., Frey, H., & Bandeira, J. 2389, 2013, Transportation Research Record: Journal of the Transportation Research Board, p. 12-21.

15. Jiménez-Palacios. Understanding and Quantifying Motor Vehicle Emissions with Vehicle Specific Power and TILDAS Remote Sensing. 1999.

16. *Travel behavior characterization using raw accelerometer data collected from smartphones.* Sheila Ferrera, Tomás Ruiza. 2014, Procedia - Social and Behavioral Sciences 160, p. 140-149.

17. *Treating uncertainty in the estimation of speed from smartphone traffic probes.* Giuseppe Guido, Vincenzo Gallelli, Frank Saccomanno, Alessandro Vitale, Daniele Rogano, Demetrio Festa. 47, 2014, Transportation Research Part C, p. 100-112.

18. *Determining transportation mode on mobile phones.* Reddy, S., Burke, J., Estrin, D., Hansen, M.H., & Srivastava, M.B. [a cura di] Proceedings of the 12th IEEE International Symposium on Wearable Computers Proceedings of ISWC '08. 2008. p. 25-28.

19. *Transportation mode identification and real-time co2 emission estimation using smartphones.* Manzoni, V., Maniloff, D., Kloeckl, K., & Ratti, C. Massachusetts Institute of Technology, Cambridge, Massachusetts, USA, Technical Report. : s.n., SENSEable City Lab.

20. *A strategy on how to utilize smartphones for automatically reconstructing trips in travel survey.* Nitsche, P., Widhalm, P., Breuss, S.,& Maurer P. 2012, Procedia - Social and Behavioral Sciences, Vol. 48, p. 1033-1046.

21. *UbiActive: A Smartphone-Based Tool for Trip Detection and Travel-Related Physical Activity Assessment.* Fan, Y., Chen, Q., Liao, C.-F., & Douma, F. Washington DC : s.n., 2013. Transportation Research Board 92st Annual Meeting.

22. *Evaluation of high sensitivity GPS receivers.* Zhang, J., Li, B., Dempster, A.G., Rizos, C. Taipei, Taiwan : s.n., 2010. Proceedings of 2010 International Symposium on GPS/GNSS.

23. *Acceleration-Deceleration Behaviour of Various Vehicle Types.* Bokare, P.S., Maurya, A.K. 25, 2017, Transportation Research Procedia, p. 4733–4749.

24. *Reconsideration of sample size require-ments for field traffic data collection with global positioning system devices.* . Li, S., Zhu, K., van Gelder, B., Nagle, J., Tuttle, C. 1804, 2002, Transportation Research Record, p. 17–22.

25. Margarida C. Coelho, H. Christopher Frey, Nagui M. Rouphail, Haibo Zhai, Luc Pelkmans,. Assessing methods for comparing emissions from gasoline and diesel light-duty vehicles based on microscale measurements. *Transportation Research Part D: Transport and Environment.* 2009, Vol. Volume 14, Issue 2, p. 91-99.

26. *An agent-based traffic regulation system for the roadside air quality control.* Abdelaziz el Fazziki, Djamal Benslimane, Abderrahmane Sadiq, Jamal Ouarzazi, Mohamed Sadgal. 2017, IEEE Access, Vol. 5.

27. Janson Olstam, J., Tapani, A. *Comparison of car-following models.* Linköping : VTI meddelande, 2004.

28. TTS - Trasport Simulation System. AIMSUN Version 8.3 User's Manual. 2020.

29. Gipps, P.G. A model for the structure of lane-changing decisions. *Transportation Research Part B: Methodological, Volume 20, Issue 5.* 1986, p. 403-414.

30. P.S. Bokare, A.K. Maurya. Acceleration-Deceleration Behaviour of Various Vehicle Types. *Transportation Research Procedia.* 2017, Vol. Volume 25, p. 4733-4749.

31. Orazio Giuffrè, Anna Granà, Maria Luisa Tumminello, Antonino Sferlazza. Estimation of Passenger Car Equivalents for single-lane roundabouts using a microsimulation-based procedure. *Expert Systems with Applications.* 2017, Vol. 79, p. 333-347.

32. Orazio Giuffrè, Anna Granà, Maria Luisa Tumminello, Antonino Sferlazza,. Capacity-based calculation of passenger car equivalents using traffic simulation at double-lane roundabouts. *Simulation Modelling Practice and Theory.* 2018, Vol. 81, p. 11-30.

33. J., Barcelò. *Fundamental od Traffic Simulation.* London : Springer, 2010.

34. *Assessing methods for comparing emissions from gasoline and diesel light-duty vehicles based on microscale measurements.* Margarida C. Coelho, H. Christopher Frey, Nagui M. Rouphail, Haibo Zhai, Luc Pelkmans,. 2009, Vol. Volume 14, Issue 2, p. 91-99.

35. *Method and case study for quantifying local emissions impacts of a 3 transportation improvement project involving road re-alignment and 4 conversion to a multi-lane roundabout.* Anya, A., Rouphail, N., Frey, H. C., & Liu, B. 2013. TRB 2013 Annual Meeting.

36. *Application of AIMSUN Microsimulation Model to Estimate Emissions on Signalized Arterial Corridors.* Anya, A. R., Rouphail, N. M., Frey, H. C., & Schroeder, B. 2428, 2014, Transportation Research Record, Vol. 1, p. 75-86.

37. *Speed and Acceleration Impact on Pollutant Emissions.* Andre, Michel & Pronello, C. s.l. : Speed and Acceleration Impact on Pollutant Emissions, 1996. 10.4271/961113.

38. *Regulated and unregulated diesel and cold start emissions at different temperature.* Weilenmann. M., Soltic. P., Saxer. C., Forss. A.M., Heeb. N. 39, 2005, Atmospheric Environment, p. 2433–2441.

Chapter 4

Estimating emissions on urban roundabouts in Palermo (Italy) using AIMSUN

Introduction

Microscopic simulation models can generate large amounts of vehicle activity that could be used to estimate emissions on road networks. For accurate estimation of the emissions from roundabouts, it is necessary to ensure that the simulated vehicle activity closely represents field observed vehicle activity. In this thesis an improvement in emissions estimations on urban roundabouts is proposed by calibrating the internal behavioral model parameters in the *AIMSUN Next* software from field observed vehicle data at second-by-second temporal resolution as shown in the previous chapter.

Simulated and observed vehicle activity data were characterized by Vehicle Specific Power (VSP), defined as the power per unit mass of vehicle. Emissions were estimated based on the VSP modal emission rates and the time spent by vehicles in each VSP mode. The emissions were compared for six roundabouts located in the urban area of Palermo City, Italy.

The calibration process here presented focused specifically on improving vehicle activity for better emissions estimates.

Application of microsimulation models: instantaneous simulated speed profiles

Background

AIMSUN Next (Advanced Interactive Microscopic Simulation for Urban and Non-Urban Networks) is the core simulation module developed by Transportation Systems Solution (TSS) in Barcelona, Spain. The 8.3 version of this software has been used to model the urban roundabouts identified as sample case study. The geometric characteristics of each roundabout have been considered; each intersection has been contextualized within the road network where it is operating considering traffic conditions and the surrounding built environment that were observed in field.

When using traffic microsimulation tools to simulate road networks model calibration should be considered in order to provide as realistic as possible output. It is well known that calibration

consists of the identification of model parameters having effects on the phenomenon under examination and the definition of the range of values for controllable parameters. The several studies as literature informs *(*e.g. FHWA[1] 2007*)*, recommend selecting few parameters for calibration and running the simulation repeatedly to narrow down to the best values for the set of selected parameters.

Vehicles in AIMSUN are generated at headway values sampled from a user-defined distribution. The default headway model is a negative exponential distribution (1). Each vehicle that can enter the network has a specific set of available vehicle attributes. It is possible to assign specific attributes to individual links or sections within the road network. Among these vehicle attributes one can remember length, width max. acceleration, normal deceleration, maximum deceleration, minimum distance between stopped vehicles, minimum headway and so on (1). The driver's behavior when vehicles enter the link section is constrained by local parameters as section speed limit, lane speed limit, visibility distance at junctions, reaction time variation and so on (1). Global parameters, in turn, are separately defined from vehicle or local parameters to control the behavior of vehicles everywhere in the road network such as the driver reaction time (1). At every simulation step, the position and speed of every vehicle are updated according to the internal behavioral models of AIMSUN; as introduced before, these models are characterized by multiple vehicle parameters and local and global parameters. New vehicles are generated in the system only after the statuses of vehicles already in the network are updated during each simulation step (1).

Several sub-models contribute to the behavioral core models in AIMSUN as follows (1):

- *Car-following model* – This algorithm serves to estimate a vehicle's speed at each time step based on the performance constraints of the vehicle and/or its driver and the behavior of the preceding vehicle.
- *Lane-changing model* – This algorithm models the decision process by which the necessity, desirability, and feasibility of a vehicle to change lanes are determined and the vehicle behavior is adjusted accordingly.
- *Gap accepting model for lane changing* – This model evaluates if a gap is acceptable for a lane change, based on cooperation of the upstream vehicles and calculated values for gap, speeds and the deceleration required to complete the maneuver.

[1] Report n. FHWA-HOP-07-079

- *Gap acceptance model for give-way behavior at stops* – The decision to allow a lower priority vehicle to cross a stop-controlled intersection is modeled by this algorithm, based on position and speeds of higher priority vehicle and level of risk of each driver.
- *Overtaking maneuver* – This algorithm models the decision to change to a faster lane based on the speed and position of the preceding vehicle or to a slower lane based on the driver characteristics.
- *On-ramp model* – This is an extension of the lane changing model with local parameters to distinguish ramps and the need for vehicles to merge into the main traffic stream on a freeway.
- *Off-ramp model* - Close to the on-ramp model, this algorithm is an application of the lane changing model to allow a vehicle exiting the freeway to diverge from the main traffic stream.
- *Look-ahead model* – This model is applied to avoid situations in which a vehicle is unable to complete a desired turning movement due to not reaching the correct lane in time and is lost from the network when the simulation is run with route-based demand.

However, they can concern every road unit that can be simulated in AIMSUN so that the role of model parameters of AIMSUN must be considered in relation to the study to be carried out at road network, corridor, or single road unit level. In AIMSUN, the position and speed of every vehicle in the network is updated after checking for lane-changing decisions and applying the car-following model and the gap acceptance model. The Gipps lane-changing process is used in conjunction with the Gipps car-following model which places limits on the driver's braking ability to maintain a safe distance with the preceding vehicle (2). The car following model can be relevant to investigate individual vehicle activity along urban roundabouts, considering that AIMSUN has the smallest number of modeling parameters when compared to popular micro-simulation tools such as VISSIM and PARAMICS (3).

The car following parameters have an impact in the second-by-second speed and position of each vehicle in the simulation and concerning the individual vehicle behavior considered at the micro-scale.

Network modelling

In this case study six roundabouts located in Palermo City, Italy, were selected and modeled in AIMSUN (Figure 4.1). As described in the previous chapter, the GPS trajectories were gathered

by using the Speedometer GPS PRO Android app in a light passenger diesel vehicle conforming to Euro IV Standard that was used as the available test vehicle. This test vehicle is also consistent with the specifications tested to derive emissions rates for the VSP modes (4). Second-by-second speeds were extracted from the GPS trajectories of the movements through the roundabouts traveled by the test vehicle which entered each roundabout from the left lane (7 to 10 runs per site in each driving direction for a total of 94 observations). Acceleration and deceleration values were then computed from speed data; see (5) for the method and expressions here used. The speed profiles with or without one complete stop were recognized, while those with multiple stopping on the entry approach were excluded due to their low relative occurrence (6). The observations were separated by driving direction where the respective trajectories occurred in the field based on the analogy observed for the curvilinear paths through the six roundabouts in AB and BA directions; see Fig. 4.1.

Figure 4.1: The pilot sample of roundabouts in Palermo modelled in AIMSUN

The network models of each roundabout were reproduced by using sections and nodes as AIMSUN provides. Sections were joined together to form the road segments between the nodes. AIMSUN allows to import Google Earth images (Year 2020) and Open Street Maps layouts to integrate the dimensions of the sections with the lengths and number of lanes as surveyed in the field (Figure 4.1). Sections were joined by nodes to allow the turning movements as performed in the field at each intersection. Google Earth's aerial views were also used to check that the sections had been connected properly and to check turning and through

movements. A speed limit of 50 km/h was assigned everywhere in the roundabout network models.

Another assumption concerned the influence area considered for each roundabout. It should be noted that this study concerned urban roundabouts located in different areas of the City; they are not belonging to corridors and can be considered to be operating as isolated intersections. Reference has been made to the speed-travel time profiles experienced by the test vehicle within the distance equal to the sum of the deceleration distance of a vehicle travelling from the cruise speed as it approaches and the enters the roundabout, and the acceleration distance as it exits the roundabout up to the section it reaches the cruise speed again. This distance was defined approximately with a length of three times the outer diameter of the roundabout each time considered. thus, it was possible to have speed profiles as coherent as possible among the roundabouts in order to extract the contribution of each roundabout to the emission phenomenon based on a congruent term of comparison. However, speed profiles were analyzed and the subsequent analysis preliminary to the emission estimation was also made with reference to a distance of about 500 m that included the time spent in the cruise mode.

O/D matrices and traffic characterization

Once the network model was built, centroids necessary for the insertion of a given matrix O/D were suitably entered. Different matrices were used, referring to light and heavy traffic, in order to build the traffic demand and to feed the network models (Figure 4.2).

The characterization of each individual category of vehicle was carried out in terms of size and class (car, heavy goods vehicles, public transport, etc.), and in terms of the kinematic and behavioral parameters that distinguish every category. It should be noted that a percentage of heavy vehicles under 10 % was surveyed in the field[2], while the O/D matrices considered for each roundabout of the sample were described and presented in the previous chapter.

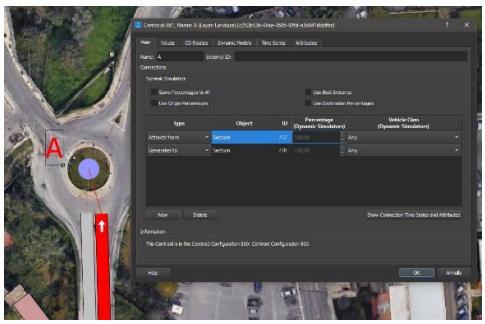

[2] Percentage of heavy vehicles under 10% was found in almost 85% of surveys, for all the directional movement

a)

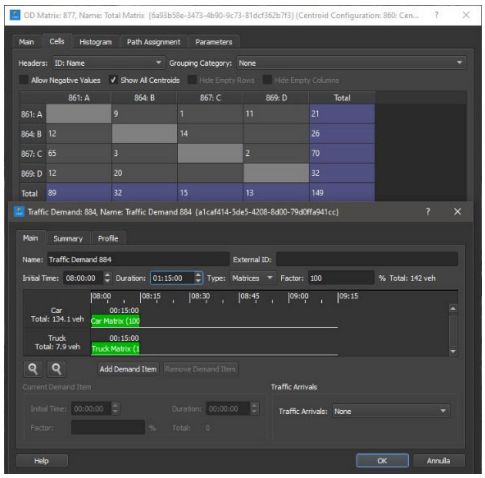

b)

Figure 4.2: Centroid definition *a)*, O/D Matrix and traffic demand settings *b)*

Dynamic design scenario

The next step was to create the design scenarios for which all simulations ran. Specifically, the collected traffic data of interest were selected among those implemented previously, and the statistics to be generated in output were specified.

In the specific case where the interest is directed to the instantaneous speed profiles it is necessary to set the saving of the trajectory data by specifying the class of vehicles and the O/D pairs for through movements.

Single scenarios were built considering the same morning peak-hour used as time slot for data collections. In particular each dynamic scenario was located into the 7:30-8:30 a.m. slot where 5400 seconds were considered as single replication, while 1800 seconds of warm-up time[3] were set. Once carried out the i-th replication in AIMSUN, imposing a resolution time scan per second, trajectory data useful for the construction of speed profiles are available in the database file[4] that can be found in the subfolder named "MIVEHDETAILEDTRAJECTORY" (Figure 4.3). The usable information is referred to the previously selected O/D pair and to the class of vehicles which have travelled it in the given time interval:

- *did*: replication or average identifier

[3] Simulation model runs usually start with zero vehicles on the network. If the simulation output is being compared to field measurements (as in calibration), then the artificial period where the simulation model starts out with zero vehicles (the warmup period) must be excluded from the reported statistics for system performance. AIMSUN Next do this automatically.

[4] The generated output file is a database with .sqlite extension.

- *oid*: vehicle ID
- *sectionId*: record sequence ID in vehicle trajectory
- *laneIndex*: vehicle section lane
- *xCoord*: vehicle x coordinate
- *yCoord*: vehicle y coordinate
- *timeSta*: simulation time (sec)
- *speed*: vehicle speed in km/h
- *travelledDistance*: vehicle distance travelled (km)
- *acceleration*: vehicle acceleration (m/sec^2)

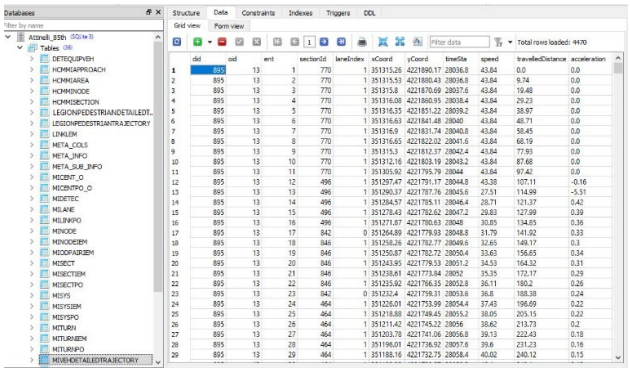

Figure 4.3: Database output file from AIMSUN

AIMSUN parameters calibration

The data collected by the light duty diesel vehicle test contained second-by-second speeds, accelerations, decelerations, and positions of the vehicle along the examined movements into the six roundabouts. The instantaneous speed profiles from the trajectories travelled across the study area were extracted as described in Chapter 3. Data from each trajectory were then investigated for parameter calibration in AIMSUN. Based on a preliminary sensitivity analysis, the following controllable parameters in AIMSUN have been chosen:

1. Maximum desired speed (MDS)
2. Maximum acceleration (MA)
3. Normal deceleration (ND)
4. Reaction time (RT)
5. Minimum headway – gap (MH)
6. Speed acceptance (SA)

The maximum desired speed refers to the maximum speed a vehicle can travel at any point along the network. The maximum acceleration is the maximum acceleration vehicles achieve on

the network under any circumstances. The normal deceleration is the maximum deceleration that a vehicle can achieve under normal circumstances (1). It is different from maximum deceleration, which occurs under special circumstances when severe braking is required. All three parameters follow a truncated normal distribution, defined using the mean, standard deviation, maximum and minimum values for a vehicle type (1), which in this research work is a LPDV.

As described in Chapter 3, the second-by-second speeds were extracted from the GPS trajectories experienced by the test vehicle in AB and BA directions; the values of accelerations and decelerations were then computed from speed data (5). The instantaneous speed profiles with or without one complete stop were recognized (6), while those with multiple stopping on the entry approach were excluded due to their low relative occurrence. The maximum, 95th and 85th percentile values of accelerations and decelerations and maximum value of speed were found from each trajectory collected for the AB and BA movements travelled across the six roundabouts, resulting in a total of 94 observations of each parameter and measurement value combination; see Figure 4.4 for the maximum acceleration and normal deceleration distributions. However, the maximum desired speed it was excluded from the calibration set, taking into account the urban speed limit that AIMSUN allows to establish. Thus, the urban speed limit of 50 km/h was set as the maximum speed at which each roundabout can be traveled under free flow conditions.

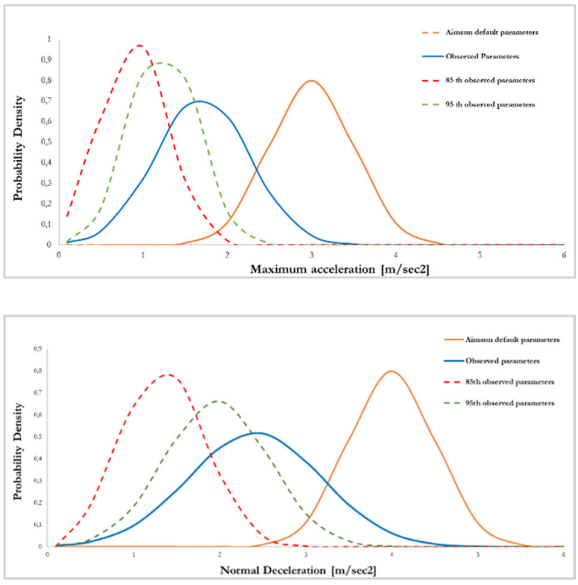

Figure 4.4*: Maximum acceleration (a) and Normal deceleration distribution (b)*

Concerning the two parameters of interest for calibration, the AIMSUN default values are higher than the 95th percentile or 85th percentile values. The lowest values are for the collected 85th percentile parameter distributions while in comparison, the 95th percentile values distribution appears shifted to the right and has smaller peak and larger variation. Both the peaks of the collected 95th and 85th percentile distributions occur far left of the AIMSUN default parameter distribution indicating that simulated vehicles use to experience high accelerations to high speeds and high decelerations when slowing down. The default parameters seem more acceptable to simulate driving behaviors on freeways rather than urban networks and more for intersections, even if it must be highlighted that in some cases (e.g. the case of the roundabout 1) the 95th and 85th percentile distributions of accelerations and decelerations are quite close to the default AIMSUN parameters distribution.

Based on previous results of AIMSUN calibration process for roundabouts in Palermo, Italy (7) (8), the set of the calibration parameters above was also combined with AIMSUN parameters having influence on gap-acceptance behavior. For single-lane entry approaches a value of the driver reaction time of 0.86 s instead of the default value of 0.80 s, the minimum gap of 1.58 s instead of the default value of 0.0 s and speed acceptance of 1.0 instead of 1.1 were considered (7). Then, for multi-lane entry approaches a value of the driver reaction time of 0.95 s instead of the default value of 0.80 s, the minimum gap of 1.33 s instead of the default value of 0.0 s and speed acceptance of 1.0 instead of 1.1 were used (8).

Instantaneous speed profiles in AIMSUN

Several simulation runs were carried out to build the simulated speed profiles and to compare them with the observed ones. In order to explain the proposed procedure, the comparison between the GPS trajectories collected in the field and the speed profiles returned by AIMSUN under default parameters is shown considering a single vehicle trajectory only among those observed in the field[5] regardless the driving direction (as described in the previous chapter). Note that the reference speed profile was selected based statistical indicators as GEH and RMSNE (9); in turn, the simulated speed profiles they were extracted for each driving direction where each simulated profile was averaged among 30 runs in AIMSUN. Figure 5 shows the comparison between the observed speed-time profiles and the simulated ones under default parameters in AIMSUN.

[5] This preliminary study considered the match between simulated profiles whose behavioural parameters considered are closely like those characterizing the recorded reference trajectory (one trajectory chosen for each roundabout analyzed).

The 95th and 85th percentile distributions of accelerations and decelerations were then considered for calibration purposes in order to investigate the better performance in estimating pollutant emissions from micro-simulated trajectory data returned from AIMSUN. In this regard, a sensitivity analysis was deepened concerning the 95th and 85th percentile distributions of maximum accelerations and normal decelerations (see Table 4.1). The behavioral parameters of AIMSUN such as the reaction time, the minimum headway and speed acceptance were then considered in combination with the kinematic parameter set.

Concerning the effects of the model calibration, Figure 6 shows as the speed profiles simulated under the 85th and 95th values of accelerations and decelerations extracted from all the on-field trajectory data regardless the driving direction are closer to the observed speed profiles (i.e. the observed speed profile each time selected as the reference profile for the roundabout under examination) than the speed profiles simulated under the default parameters of AIMSUN. The GEH index (9) resulted smaller than 5 in more than 95% of the cases when the speed series calibrated under the 85th and 95th values of accelerations and decelerations extracted from all the on-field trajectory data regardless the driving direction were compared with the corresponding empirical series. However, among these GEH values, the parameter set with the 95th distribution values of the relevant parameters gave the lowest value for each single GEH_i and the simulated profiles got close enough to the empirical ones.

Based on the investigated calibration, the instantaneous pollutant emissions were calculated as discussed below.

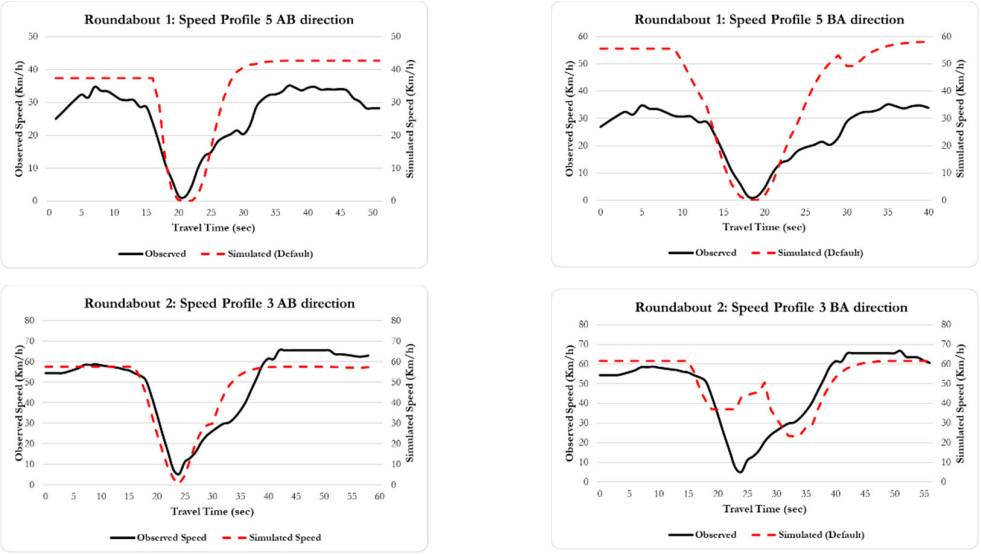

Figure 4.5*:* Observed speed-time profiles (reference) vs (default) simulated speed profiles for the roundabouts sample

Table 4.1: Summary of statistics for kinematic parameters from the examined roundabouts.

	Maximum Acceleration	85th Maximum Acceleration	95th Maximum Acceleration	Normal Deceleration	85th Normal Deceleration	95th Normal Deceleration
Average	1.66	0.89	1.24	2.46	1.34	1.96
Standard Deviation.	0.53	0.19	0.28	0.75	0.49	0.60
Max	3.55	1.36	1.86	5.34	2.67	4.24
Min	0.73	0.50	0.68	0.77	0.53	0.75

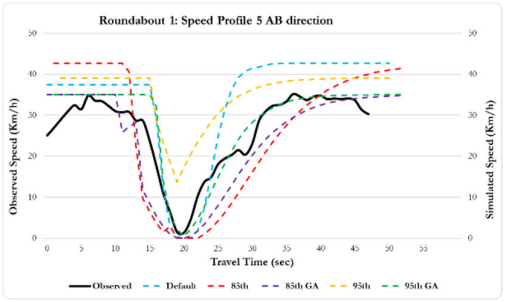
Roundabout 1: Speed Profile 5 AB direction
Observed Speed (Km/h)
Simulated Speed (Km/h)
Travel Time (sec)
Observed
Default
85th
85th GA
95th
95th GA

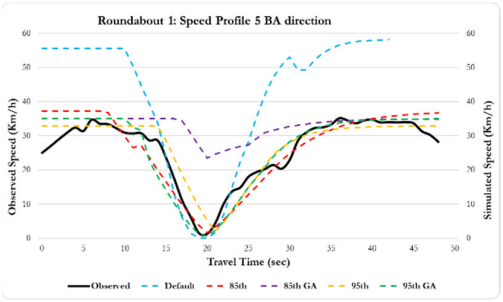
Roundabout 1: Speed Profile 5 BA direction
Observed Speed (Km/h)
Simulated Speed (Km/h)
Travel Time (sec)
Observed
Default
85th
85th GA
95th
95th GA

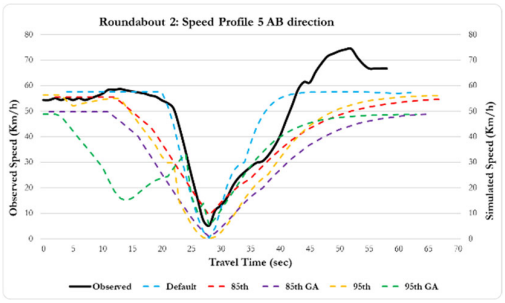
Roundabout 2: Speed Profile 5 AB direction
Observed Speed (Km/h)
Simulated Speed (Km/h)
Travel Time (sec)
Observed
Default
85th
85th GA
95th
95th GA

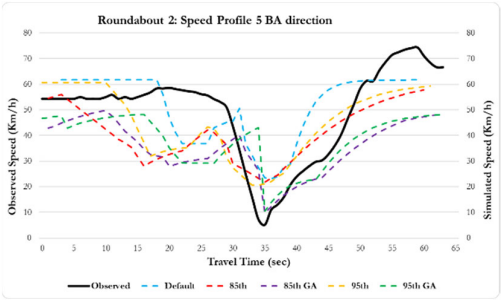
Roundabout 2: Speed Profile 5 BA direction
Observed Speed (Km/h)
Simulated Speed (Km/h)
Travel Time (sec)
Observed
Default
85th
85th GA
95th
95th GA

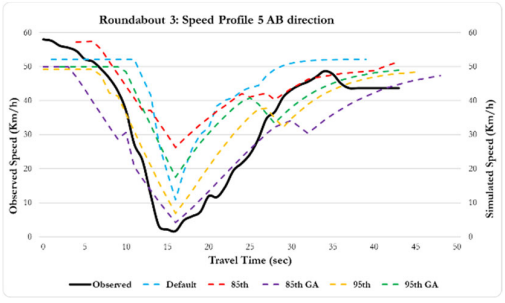
Roundabout 3: Speed Profile 5 AB direction
Observed Speed (Km/h)
Simulated Speed (Km/h)
Travel Time (sec)
Observed
Default
85th
85th GA
95th
95th GA

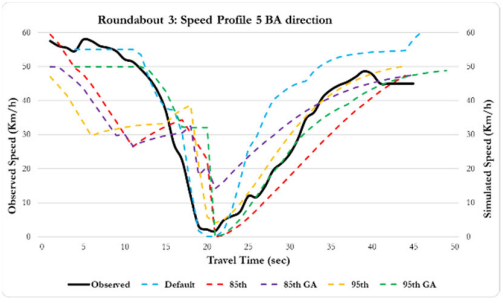
Roundabout 3: Speed Profile 5 BA direction
Observed Speed (Km/h)
Simulated Speed (Km/h)
Travel Time (sec)
Observed
Default
85th
85th GA
95th
95th GA

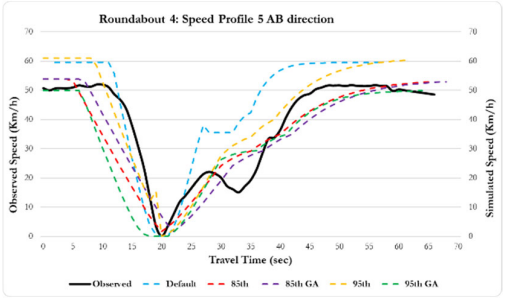
Roundabout 4: Speed Profile 5 AB direction
Observed Speed (Km/h)
Simulated Speed (Km/h)
Travel Time (sec)
Observed
Default
85th
85th GA
95th
95th GA

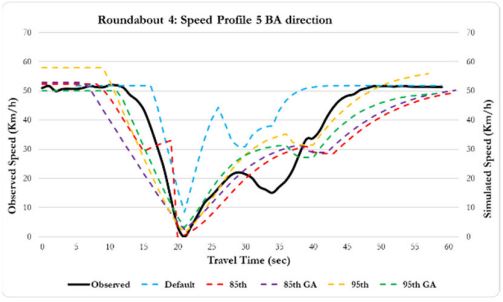
Roundabout 4: Speed Profile 5 BA direction
Observed Speed (Km/h)
Simulated Speed (Km/h)
Travel Time (sec)
Observed
Default
85th
85th GA
95th
95th GA

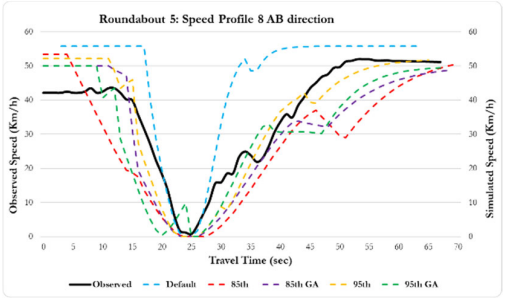
Roundabout 5: Speed Profile 8 AB direction
Observed Speed (Km/h)
Simulated Speed (Km/h)
Travel Time (sec)
Observed
Default
85th
85th GA
95th
95th GA

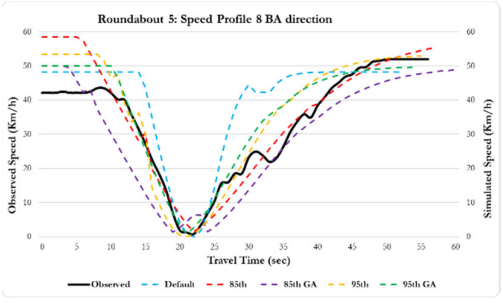
Roundabout 5: Speed Profile 8 BA direction
Observed Speed (Km/h)
Simulated Speed (Km/h)
Travel Time (sec)
Observed
Default
85th
85th GA
95th
95th GA

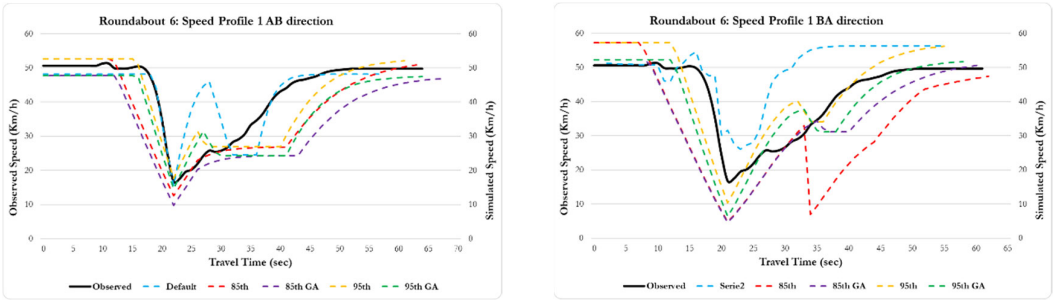

Figure 4.6: Comparison between observed speed profiles and simulated profiles under the 85th and 95th values of MA and ND. *Note that GA stands for simulation including the reaction time, speed acceptance and minimum headway parameters calibrated using Genetic Algorithm from literature GA (7) (8)*

Emission estimation from instantaneous speed profiles

As discussed in the previous chapter, the VSP expresses the instantaneous power generated by the engine to overcome the rolling resistance and aerodynamic drag, and to increase the kinetic and potential vehicle energy (10). The simplified form of the VSP equation for a typical light passenger vehicle is based on the road grade, vehicle's speed, and acceleration (4):

(4.1)

$$VSP = v \cdot \left[1.1 \cdot a + 9.81 \cdot sin\left(arctan(grade)\right) + 0.132\right] + 0.000302 \cdot v^3$$

where the *VSP* in kW/ton, the instantaneous speed *v* in m/s, the acceleration (or deceleration) *a* in m/s^2. There are 14 modes of engine regime and an emission factor by mode to estimate CO_2, CO, NO_x, and HC emissions by vehicle type (6) (11) (12).

The instantaneous VSP measurements from trajectory data showed in Figure 6 were detected at regular time points and the considered as time series to explain how close the observed and the simulated values were.

By way of example, the diagrams shown in Figures 4.7 to 4.9 describe the distribution of time spent in the VSP modes under parameters calibrated with the mean values of the 95th percentiles of the acceleration and deceleration; they matched the VSP distribution from empirical data more closely than the corresponding distributions under default parameters.

It should be noted that, with reference to the VSP bins showed in the Figures 4.7 to 4.9, bins 1-3 represent decelerations or idle events, bins 4-6 represent accelerations from low speeds, while bins 7-14 reflect acceleration events at high speeds (12). VSP bins 1-3 resulted slightly uniform between the observed, default simulated and calibrated values.

Under the default parameters, the simulated vehicle tended to spend most of the time in the mode 4, while the proportion of time tended to reduce from VSP mode 5 onward; in some cases, a proportion of time appears in VSP modes 11 to 12 that correspond to high acceleration events. Under the parameters calibrated with the mean values of 95th percentiles of acceleration and deceleration, the percentages of time spent were realistic from the VSP modes 1 to 2 (deceleration), mode 3 (idling) and 4 to 7 (acceleration and cruising). One can observe differences among the amount of the time spent in the VSP modes when the values based on the observed speed profiles and those simulated in AIMSUN are compared; this is especially true for the 4-6 VSP bins where the highest deviation between AIMSUN default parameters and the observed VSP mode is about 17%, however on average higher than events under calibration with the 95th values of the relevant parameters.

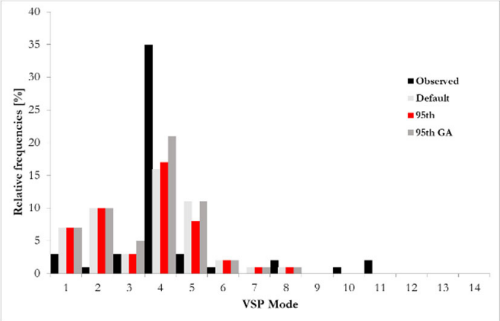

Roundabout 1: relative frequencies of time spent in VSP – AB direction

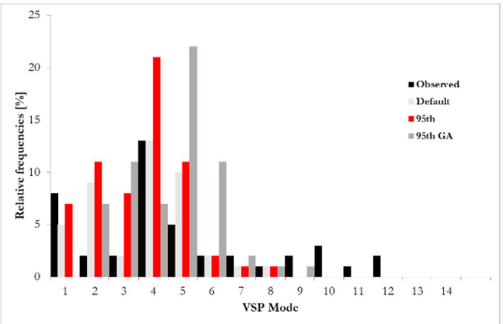

Roundabout 1: relative frequencies of time spent in VSP – BA direction

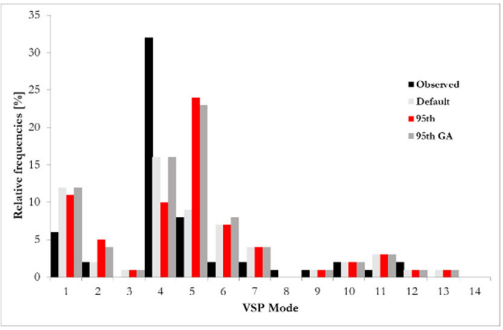

Roundabout 2: relative frequencies of time spent in VSP – AB direction

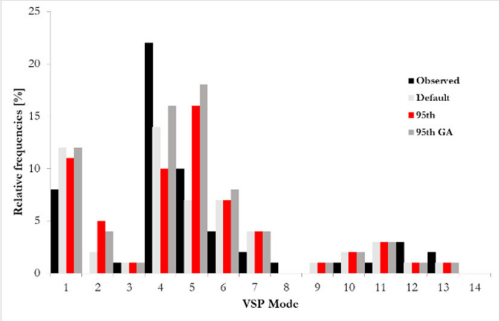

Roundabout 2: relative frequencies of time spent in VSP – BA direction

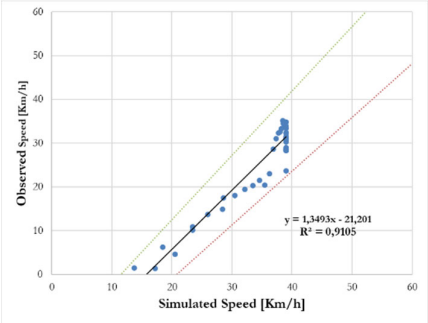

Roundabout 1: regression line of observed vs simulated speeds for AB direction (95th distribution parameters)

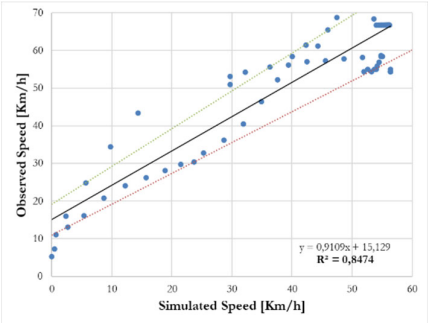

Roundabout 2: regression line of observed vs simulated speeds for AB direction (95th distribution parameters)

Figure 4.7: Relative frequencies of time spent in VSP modes; regression line of observed vs simulated speeds (Roundabouts 1 and 2)

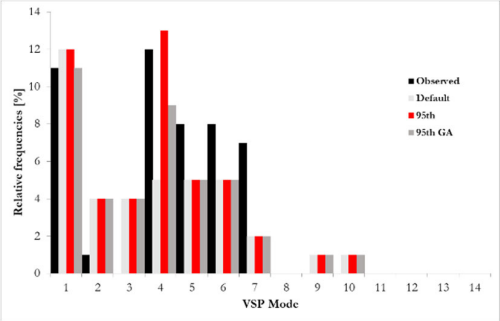

Roundabout 3: relative frequencies of time spent in VSP – AB direction

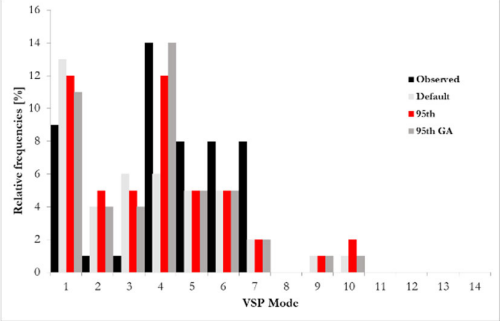

Roundabout 3: relative frequencies of time spent in VSP – BA direction

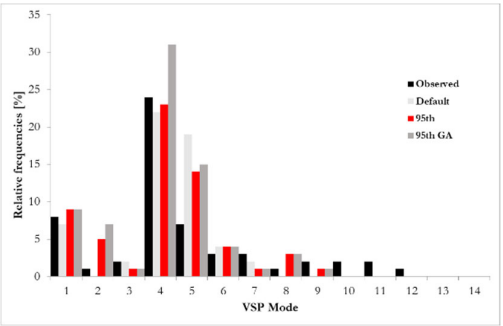

Roundabout 4: relative frequencies of time spent in VSP – AB direction

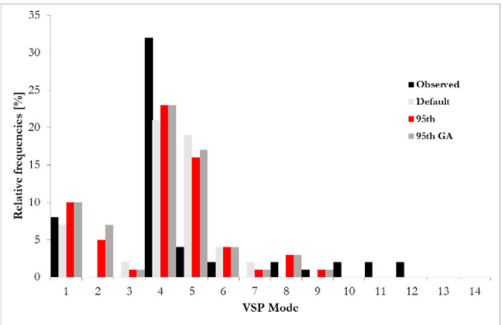

Roundabout 4: relative frequencies of time spent in VSP – BA direction

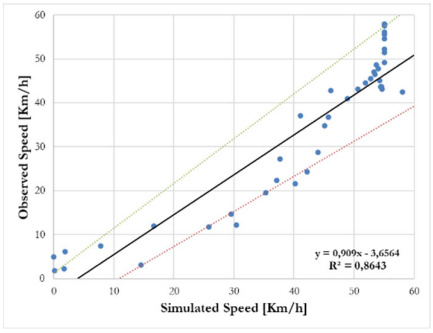

Roundabout 3: regression line of observed vs simulated speeds for BA direction (95th distribution parameters)

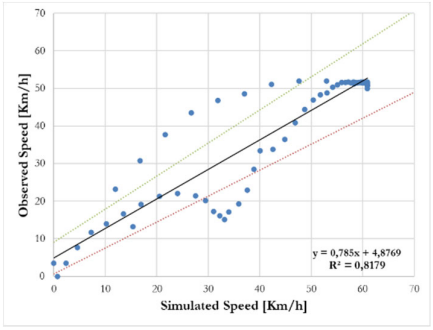

Roundabout 4: regression line of observed vs simulated speeds for AB direction (95th distribution parameters)

Figure 4.8: Relative frequencies of time spent in VSP modes; regression line of observed vs simulated speeds (Roundabouts 3 and 4)

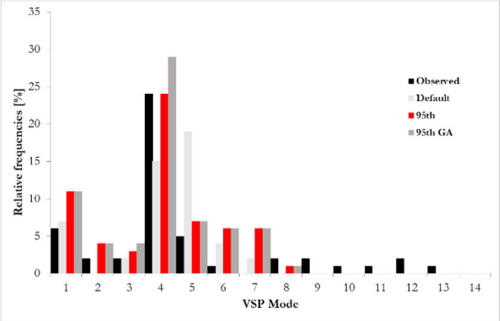

Roundabout 5: relative frequencies of time spent in VSP – AB direction

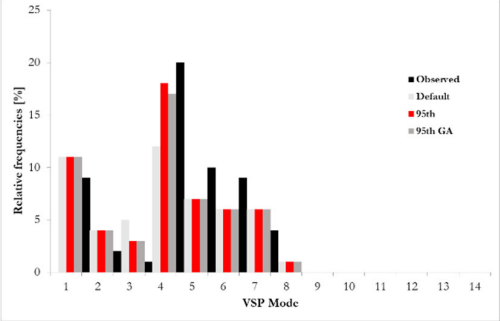

Roundabout 5: relative frequencies of time spent in VSP – BA direction

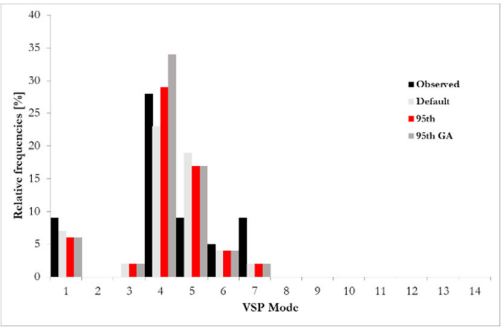

Roundabout 6: relative frequencies of time spent in VSP – AB direction

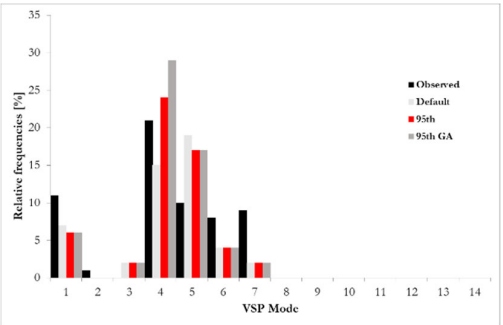

Roundabout 6: relative frequencies of time spent in VSP – BA direction

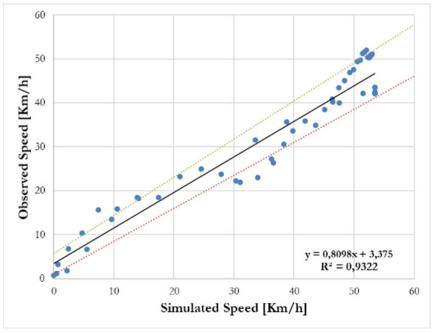

Roundabout 5: regression line of observed vs simulated speeds for BA direction (95th distribution parameters)

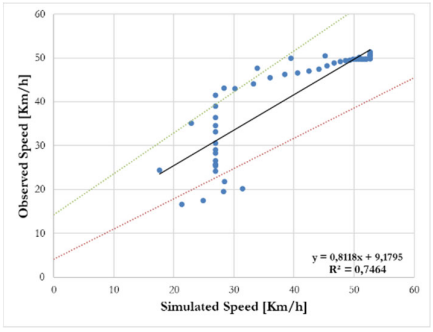

Roundabout 6: regression line of observed vs simulated speeds for AB direction (95th distribution parameters)

Figure 4.9: Relative frequencies of time spent in VSP modes; regression line of observed vs simulated speeds (Roundabouts 5 and 6)

It should be noted that the speed limit of 50 km/h constrained speed and as a consequence its (positive or negative) variation. This resulted more evident for simulation under the 85th percentile values of accelerations and decelerations than simulation with the 95th percentile values of the relevant parameters. In particular, the simulated vehicle activity under 85th percentile parameters extracted from vehicle activity data surveyed in the field did not closely represent empirical data; sampling data from this kind of distribution may get errors about the maximum accelerations or decelerations achievable in AIMSUN. For this reason, the corresponding the elative frequencies of time spent in VSP modes under calibration with the 85th percentile values of accelerations and decelerations have not been reported here.

It is also necessary to consider that the traffic demand observed during data collection for the all roundabout presented low traffic volume percentages, despite they were peak hours. This issue affected the peak values of acceleration and deceleration registered when AIMSUN ran, that were not so much close to observed peak values.

The same figures 4.7 to 4.9 show, be way of example, the regression lines made to compare the observed and simulated speeds under calibration with the mean values of the 95th percentiles of the relevant parameters. Note that the regression lines of observed versus simulated values of speeds as introduced above are reported with reference to one of the two driving directions that were investigated just for synthesis reasons. The results as shown by the plots confirmed the efficiency of simulation in AIMSUN; they were still the best results when simulation ran under AIMSUN behavioral parameters.

Based on the above, to better investigate the differences in vehicle activity, t-tests were performed on the binned VSP from simulation and field data: the null hypothesis (H_0) for the two-tailed t-test "there is no difference between the averages of the two distributions" was formulated. Then data were analyzed to determine the probability of an alternative hypothesis (H_1) which provides sufficient evidence to reject the null hypothesis.

In the specific case, null hypothesis stated that there is no difference between the averages of the samples of VSP distributions between the observed and simulated VSP modes for each roundabout and each movement (i.e. AB or BA movements). The following Tables 4.2 to 4.7 show the results of the t-test. The same tables show the KS test[6] results. It is well-known that the KS-test returns a D-statistic and a p-value corresponding to the D-statistic. The D-statistic is the absolute maximum distance (supremum) between the CDFs of the two samples. The

[6] See e.g. Kolmogorov–Smirnov test, Encyclopedia of Mathematics, EMS Press, 2001

closer this number is to 0, the more likely it is that the two samples were drawn from the same distribution.

Note that the p-value returned by the test has the same interpretation as other p-values. Reject the null hypothesis that the two samples were drawn from the same distribution if the p-value is less than the significance level (if alpha is 0.05 in the two-tailed test, then 0.025 should be considered as target value).

Table 4.2: Comparison between observed/simulated VSP modes for Roundabout 1 (AB and BA directions)

VSP mode (Roundabout 1) (Speed Profile 5 AB)		μ_1[7]	μ_2[4]	$t^8_{\alpha.n}$	t_{crit}	P-T Test (α[9] = 0.05)	D	P-KS Test
Obs. vs Default	380 m	2.871	1.695	0.946	1.990	0.347	0.392	0.001
	150 m	3.792	1.911	0.776	2.032	0.443	0.200	0.649
Obs. vs 85th	380 m	1.903	1.290	0.606	1.984	0.546	0.433	0.000
	150 m	1.440	1.544	-0.065	2.006	0.949	0.278	0.102
Obs. vs 85th +behavior	380 m	1.577	1.525	0.069	1.979	0.945	0.446	0.000
	150 m	1.429	1.464	-0.028	1.998	0.978	0.250	0.180
Obs. vs 95th	380 m	1.946	1.419	0.494	1.987	0.623	0.510	0.000
	150 m	1.900	2.056	-0.072	2.028	0.943	0.304	0.195
Obs. vs 95th +behavior	380 m	1.829	1.613	0.266	1.981	0.791	0.466	0.000
	150 m	1.967	1.790	0.117	2.007	0.907	0.207	0.514

VSP mode (Roundabout 1) (Speed Profile 5 AB)		μ_1	μ_2	$t_{\alpha.n}$	t_{crit}	P-T Test (α = 0.05)	D[4]	P-KS Test
Obs. vs Default	380 m	3.670	1.969	0.771	2.008	0.444	0.349	0.008
	150 m	2.436	1.343	0.283	2.052	0.780	0.333	0.109
Obs. vs 85th	380 m	1.754	1.342	0.585	1.980	0.560	0.436	0.000
	150 m	1.442	1.519	-0.065	1.998	0.949	0.182	0.601
Obs. vs 85th +behavior	380 m	1.597	1.585	0.017	1.986	0.986	0.472	0.000
	150 m	1.427	1.484	-0.039	2.017	0.969	0.348	0.096
Obs. v 95th	380 m	1.479	1.570	-0.130	1.980	0.897	0.468	0.000
	150 m	1.391	1.483	-0.070	2.002	0.944	0.267	0.200
Obs. v 95th +behavior	380 m	1.864	1.574	0.410	1.980	0.682	0.403	0.000
	150 m	1.986	1.492	0.391	2.000	0.697	0.156	0.795

Note that behavior means calibration including the contribution of AIMSUN behavioral parameters

[7] μ_{AB} and μ_{BA} stand for the mean values of the samples of the observations of each parameter in the two driving directions (AB and BA);

[8] t-value is the result of the two tailed t-test done to compare the equality of the μ_{AB} and μ_{BA} of samples of two populations with equal sample size;

[9] α is the significance level.

Table 4.3: Comparison between observed/simulated VSP modes for Roundabout 2 (AB and BA directions)

VSP mode (Roundabout 2) (Speed Profile 3 AB)		μ_1	μ_2	$t_{\alpha,n}$	t_{crit}	P-T Test (α = 0.05)	D	P-KS Test
Obs. vs Default	600 m	4.280	3.489	0.366	1.981	0.715	0.144	0.158
	240 m	3.525	5.303	-0.422	2.004	0.675	0.103	0.899
Obs. vs 85th	600 m	2.398	4.625	-1.476	1.983	0.143	0.119	0.277
	240 m	2.813	5.735	-1.071	2.008	0.289	0.171	0.232
Obs. vs 85th +behavior	600 m	2.254	4.529	-1.585	1.985	0.116	0.243	0.001
	240 m	0.754	3.345	-1.002	2.014	0.322	0.172	0.274
Obs. vs 95th	600 m	2.623	4.586	-1.275	1.979	0.205	0.063	0.938
	240 m	3.230	5.035	-0.677	2.000	0.501	0.112	0.706
Obs. vs 95th +behavior	600 m	2.338	4.460	-1.523	1.978	0.130	0.184	0.010
	240 m	2.118	5.659	-1.442	1.994	0.154	0.110	0.681
VSP mode (Roundabout 2) (Speed Profile 3 BA)		**μ_1**	**μ_2**	**$t_{\alpha,n}$**	**t_{crit}**	**P-T Test (α = 0.05)**	**D**	**P-KS Test**
Obs. vs Default	600 m	3.489	4.280	-0.366	1.981	0.715	0.254	0.036
	240 m	3.525	5.303	-0.422	2.004	0.675	0.168	0.927
Obs. vs 85th	600 m	2.286	4.643	-1.489	1.979	0.139	0.246	0.025
	240 m	1.313	6.156	-1.550	2.002	0.127	0.333	0.039
Obs. vs 85th +behavior	600 m	2.369	4.567	-1.371	1.979	0.173	0.304	0.002
	240 m	1.295	5.591	-1.377	1.998	0.173	0.294	0.085
Obs. vs 95th	600 m	2.895	4.469	-0.921	1.977	0.359	0.143	0.443
	240 m	2.011	4.396	-0.795	1.993	0.429	0.162	0.676
Obs. vs 95th +behavior	600 m	3.756	4.543	-0.448	1.980	0.655	0.172	0.274
	240 m	3.518	3.394	0.040	1.998	0.968	0.212	0.403

Note that behavior means calibration including the contribution of AIMSUN behavioral parameters

Table 4.4: Comparison between observed/simulated VSP modes for Roundabout 3 (AB and BA directions)

VSP mode (Roundabout 3) (Speed Profile 5 AB)		μ_1	μ_2	$t_{\alpha,n}$	t_{crit}	P-T Test (α = 0.05)	D	P-KS Test
Obs. vs Default	380 m	3.232	0.774	1.051	1.995	0.297	0.487	0.000
	150 m	3.008	0.739	0.500	2.048	0.621	0.368	0.116
Obs. vs 85th	380 m	1.675	1.260	0.211	1.991	0.834	0.300	0.043
	150 m	5.090	1.691	1.276	2.037	0.211	0.500	0.014
Obs. vs 85th +behavior	380 m	1.709	1.245	0.325	1.983	0.746	0.346	0.003
	150 m	1.263	1.525	-0.119	2.003	0.906	0.200	0.537
Obs. vs 95th	380 m	2.165	1.109	0.644	1.986	0.521	0.362	0.003
	150 m	1.621	0.916	0.253	2.011	0.801	0.240	0.414
Obs. vs 95th +behavior	380 m	2.288	1.014	0.682	1.990	0.497	0.405	0.001
	150 m	1.808	1.963	-0.048	2.021	0.962	0.381	0.071
VSP mode (Roundabout 3) (Speed Profile 5 BA)		**μ_1**	**μ_2**	**$t_{\alpha,n}$**	**t_{crit}**	**P-T Test (α = 0.05)**	**D**	**P-KS Test**
Obs. vs Default	380 m	4.139	0.682	1.543	1.993	0.127	0.395	0.002
	150 m	4.897	2.392	0.715	2.023	0.479	0.261	0.360
Obs. vs 85th	380 m	0.663	1.236	-0.319	1.988	0.750	0.200	0.295
	150 m	2.910	1.300	0.772	2.008	0.444	0.140	0.576
Obs. vs 85th +behavior	380 m	1.953	1.160	0.512	1.986	0.610	0.375	0.002
	150 m	2.761	0.916	0.719	2.013	0.476	0.400	0.026
Obs. vs 95th	380 m	2.313	1.396	0.519	1.986	0.605	0.306	0.016
	150 m	3.254	-0.133	1.290	2.008	0.203	0.519	0.001
Obs. vs 95th +behavior	380 m	4.030	2.773	0.544	2.012	0.589	0.426	0.000
	150 m	4.030	2.773	0.544	2.012	0.589	0.192	0.674

Note that behavior means calibration including the contribution of AIMSUN behavioral parameters

Table 4.5: Comparison between observedvssimulated VSP modes for Roundabout 4 (AB and BA directions)

VSP mode (Roundabout 4) (Speed Profile 5 AB)		μ_1	μ_2	$t_{\alpha,n}$	t_{crit}	P-T Test (α = 0.05)	D	P-KS Test
Obs. vs Default	540 m	3.364	2.362	0.520	1.990	0.605	0.268	0.029
	240 m	6.559	1.801	1.853	2.005	0.069	0.344	0.034
Obs. vs 85th	540 m	2.009	2.324	-0.294	1.978	0.769	0.261	0.015
	240 m	4.003	2.595	0.996	2.002	0.323	0.250	0.139
Obs. vs 85th +behavior	540 m	2.017	2.212	-0.177	1.978	0.860	0.319	0.001
	240 m	4.481	2.907	1.133	2.005	0.262	0.282	0.070
Obs. vs 95th	540 m	2.799	2.473	0.222	1.982	0.825	0.344	0.001
	240 m	8.168	5.777	1.992	2.015	0.053	0.429	0.008
Obs. vs 95th +behavior	540 m	2.018	2.474	-0.438	1.977	0.662	0.222	0.048
	240 m	3.634	2.633	0.734	1.995	0.466	0.140	0.765

VSP mode (Roundabout 4) (Speed Profile 5 BA)		μ_1	μ_2	$t_{\alpha,n}$	t_{crit}	P-T Test (α = 0.05)	D	P-KS Test
Obs. vs Default	540 m	3.202	2.355	0.446	1.990	0.657	0.236	0.078
	240 m	6.008	1.478	1.415	2.015	0.164	0.321	0.088
Obs. vs 85th	540 m	2.591	2.278	0.310	1.978	0.757	0.377	0.000
	240 m	0.823	1.757	-0.555	1.993	0.581	0.154	0.708
Obs. vs 85th +behavior	540 m	1.836	2.480	-0.623	1.977	0.534	0.282	0.005
	240 m	0.418	1.939	-1.456	1.990	0.149	0.167	0.564
Obs. vs 95th	540 m	2.327	2.484	-0.114	1.980	0.909	0.313	0.003
	240 m	3.156	1.886	0.615	2.010	0.541	0.250	0.300
Obs. vs 95th +behavior	540 m	2.120	2.453	-0.291	1.978	0.772	0.209	0.093
	240 m	0.131	1.612	-0.784	1.993	0.436	0.132	0.874

Note that behavior means calibration including the contribution of AIMSUN behavioral parameters

Table 4.6: Comparison between observedvssimulated VSP modes for Roundabout 5 (AB and BA directions)

VSP mode (Roundabout 5) (Speed Profile 8 AB)		μ_1	μ_2	$t_{\alpha,n}$	t_{crit}	P-T Test (α = 0.05)	D	P-KS Test
Obs. vs Default	550 m	3.553	2.642	0.392	1.998	0.697	0.286	0.029
	240 m	3.681	2.109	0.430	2.024	0.670	0.258	0.216
Obs. vs 85th	550 m	1.480	2.709	-1.271	1.978	0.206	0.208	0.076
	240 m	2.232	2.674	-0.397	1.984	0.692	0.196	0.251
Obs. vs 85th +behavior	550 m	1.930	2.794	-0.725	1.981	0.470	0.179	0.210
	240 m	1.376	2.686	-0.782	1.991	0.437	0.255	0.078
Obs. vs 95th	550 m	2.306	2.707	-0.287	1.985	0.775	0.194	0.174
	240 m	2.747	2.593	0.080	1.995	0.937	0.238	0.159
Obs. vs 95th +behavior	550 m	2.104	2.620	-0.415	1.982	0.679	0.162	0.309
	240 m	1.437	2.690	-0.699	1.993	0.487	0.106	0.941

VSP mode (Roundabout 5) (Speed Profile 8 BA)		μ_1	μ_2	$t_{\alpha,n}$	t_{crit}	P-T Test (α = 0.05)	D	P-KS Test
Obs. vs Default	550 m	2.753	2.605	0.091	1.989	0.928	0.289	0.021
	240 m	2.847	1.235	0.570	2.021	0.572	0.241	0.321
Obs. vs 85th	550 m	1.896	2.667	-0.584	1.984	0.561	0.281	0.018
	240 m	2.451	2.554	-0.063	1.991	0.950	0.195	0.377
Obs. vs 85th +behavior	550 m	1.746	2.747	-0.985	1.979	0.326	0.185	0.195
	240 m	1.499	2.683	-0.868	1.987	0.388	0.261	0.072
Obs. vs 95th	550 m	2.515	2.597	-0.056	1.986	0.955	0.286	0.016
	240 m	1.976	2.337	-0.170	2.000	0.866	0.263	0.120
Obs. vs 95th +behavior	550 m	2.193	2.660	-0.372	1.983	0.711	0.236	0.078
	240 m	1.758	2.297	-0.291	1.996	0.772	0.189	0.479

Note that behavior means calibration including the contribution of AIMSUN behavioral parameters

Table 4.7: Comparison between observed vs simulated VSP modes for Roundabout 6 (AB and BA directions)

VSP mode (Roundabout 6) (Speed Profile 5 AB)		μ_1	μ_2	$t_{\alpha,n}$	t_{crit}	P-T Test (α = 0.05)	D	P-KS Test
Obs. vs Default	540 m	3.364	2.362	0.520	1.990	0.605	0.268	0.029
	240 m	6.559	1.801	1.853	2.005	0.069	0.344	0.034
Obs. vs 85th	540 m	2.009	2.324	-0.294	1.978	0.769	0.261	0.015
	240 m	4.003	2.595	0.996	2.002	0.323	0.250	0.139
Obs. vs 85th +behavior	540 m	2.017	2.212	-0.177	1.978	0.860	0.319	0.001
	240 m	4.481	2.907	1.133	2.005	0.262	0.282	0.070
Obs. vs 95th	540 m	2.799	2.473	0.222	1.982	0.825	0.344	0.001
	240 m	8.168	5.777	1.992	2.015	0.053	0.429	0.008
Obs. vs 95th +behavior	540 m	2.018	2.474	-0.438	1.977	0.662	0.222	0.048
	240 m	3.634	2.633	0.734	1.995	0.466	0.140	0.765
VSP mode (Roundabout 6) (Speed Profile 5 BA)		μ_1	μ_2	$t_{\alpha,n}$	t_{crit}	P-T Test (α = 0.05)	D	P-KS Test
Obs. vs Default	540 m	3.202	2.355	0.446	1.990	0.657	0.236	0.078
	240 m	6.008	1.478	1.415	2.015	0.164	0.321	0.088
Obs. vs 85th	540 m	2.591	2.278	0.310	1.978	0.757	0.377	0.000
	240 m	0.823	1.757	-0.555	1.993	0.581	0.154	0.708
Obs. vs 85th +behavior	540 m	1.836	2.480	-0.623	1.977	0.534	0.282	0.005
	240 m	0.418	1.939	-1.456	1.990	0.149	0.167	0.564
Obs. vs 95th	540 m	2.327	2.484	-0.114	1.980	0.909	0.313	0.003
	240 m	3.156	1.886	0.615	2.010	0.541	0.250	0.300
Obs. vs 95th +behavior	540 m	2.120	2.453	-0.291	1.978	0.772	0.209	0.093
	240 m	0.131	1.612	-0.784	1.993	0.436	0.132	0.874

Note that behavior means calibration including the contribution of AIMSUN behavioral parameters

The following Tables 4.8 to 4.13 show the results of the tests that were performed to explore any discrepancy between the VSP modal distributions simulated both AB and BA directions for each speed profile and each roundabout of the sample.

Table 4.8: Comparison between simulated VSP modes (AB and BA directions) for roundabout 1

VSP mode (Roundabout 1) (Speed Profile 5)		μ_1	μ_2	$t_{\alpha,n}$	t_{crit}	P-T Test (α = 0.05)	D	P-KS Test
Default (AB) vs Default (BA)	380 m	2.871	3.670	-0.340	1.998	0.735	0.505	0.000
	150 m	4.006	3.446	0.149	2.007	0.882	0.159	0.866
85th AB vs 85th BA	380 m	1.903	1.754	0.152	1.986	0.879	0.315	0.004
	150 m	0.608	1.372	-0.842	2.048	0.407	0.230	0.442
85th +behavior (AB) vs 85th +behavior (BA)	380 m	1.577	1.597	-0.029	1.982	0.977	0.178	0.287
	150 m	0.177	1.553	-0.993	2.048	0.329	0.435	0.010
95th (AB) vs 95th (BA)	380 m	1.946	1.479	0.477	1.992	0.635	0.660	0.000
	150 m	1.899	1.411	0.228	2.042	0.821	0.412	0.016
95th +behavior (AB) vs 95th +behavior (BA)	380 m	1.829	1.864	-0.045	1.982	0.964	0.092	0.951
	150 m	1.736	1.986	-0.134	2.030	0.894	0.156	0.880

Note that behavior means calibration including the contribution of AIMSUN behavioral parameters

Table 4.9: Comparison between simulated VSP modes (AB and BA directions) for roundabout 2

VSP mode (Roundabout 2) (Speed Profile 3)		μ_1	μ_2	$t_{\alpha.n}$	t_{crit}	P-T Test (α = 0.05)	D	P-KS Test
Default (AB) vs Default (BA)	600 m	3.489	2.768	0.310	1.982	0.757	0.346	0.002
	240 m	3.529	2.152	0.416	1.993	0.679	0.447	0.001
85th AB vs 85th BA	600 m	2.398	2.286	0.093	1.979	0.926	0.254	0.020
	240 m	0.930	1.769	-0.416	1.994	0.679	0.263	0.120
85th +behavior (AB) vs 85th +behavior (BA)	600 m	2.254	2.369	-0.100	1.981	0.920	0.213	0.077
	240 m	0.834	1.761	-0.454	2.000	0.651	0.316	0.035
95th (AB) vs 95th (BA)	600 m	2.623	2.895	-0.186	1.979	0.853	0.171	0.232
	240 m	2.742	2.120	0.248	1.997	0.805	0.184	0.497
95th +behavior (AB) vs 95th +behavior (BA)	600 m	2.338	3.756	-1.056	1.981	0.293	0.336	0.001
	240 m	2.682	4.032	-0.578	1.995	0.565	0.316	0.040

Note that behavior means calibration including the contribution of AIMSUN behavioral parameters

Table 4.10: Comparison between simulated VSP modes (AB and BA directions) for roundabout 3

VSP mode (Roundabout 3) (Speed Profile 5)		μ_1[1]	μ_2[1]	$t_{\alpha.n}$[2]	t_{crit}	P-T Test (α = 0.05)	D[4]	P-KS Test
Default (AB) vs Default (BA)	380 m	3.232	4.139	-0.339	1.990	0.735	0.257	0.113
	150 m	3.274	5.837	-0.719	2.009	0.476	0.111	0.994
85th AB vs 85th BA	380 m	1.675	0.663	0.537	1.989	0.593	0.175	0.495
	150 m	2.232	2.856	-0.311	2.012	0.757	0.156	0.496
85th +behavior (AB) vs 85th +behavior (BA)	380 m	1.709	1.953	-0.165	1.985	0.870	0.109	0.913
	150 m	1.258	3.103	-0.880	2.007	0.383	0.296	0.153
95th (AB) vs 95th (BA)	380 m	2.165	2.313	-0.082	1.986	0.935	0.102	0.954
	150 m	1.064	3.562	-0.911	2.007	0.367	0.333	0.078
95th +behavior (AB) vs 95th +behavior (BA)	380 m	2.288	1.396	0.496	1.989	0.621	0.374	0.002
	150 m	1.505	-0.133	0.586	2.009	0.561	0.407	0.016

Note that behavior means calibration including the contribution of AIMSUN behavioral parameters

Table 4.11: Comparison between simulated VSP modes (AB and BA directions) for roundabout 4

VSP mode (Roundabout 4) (Speed Profile 5)		μ_1	μ_2	$t_{\alpha.n}$	t_{crit}	P-T Test (α = 0.05)	D	P-KS Test
Default (AB) vs Default (BA)	540 m	3.364	3.202	0.067	1.982	0.947	0.423	0.000
	240 m	4.927	3.267	0.593	1.989	0.554	0.318	0.018
85th AB vs 85th BA	540 m	2.009	2.591	-0.584	1.978	0.560	0.203	0.102
	240 m	4.097	1.769	2.005	1.995	0.049	0.227	0.179
85th +behavior (AB) vs 85th +behavior (BA)	540 m	2.017	1.836	0.169	1.978	0.866	0.231	0.041
	240 m	4.358	0.346	3.243	1.997	0.002	0.296	0.034
95th (AB) vs 95th (BA)	540 m	2.799	2.327	0.292	1.980	0.771	0.301	0.005
	240 m	6.005	1.550	2.535	1.999	0.014	0.250	0.108
95th +behavior (AB) vs 95th +behavior (BA)	540 m	2.018	2.120	-0.092	1.978	0.927	0.123	0.644
	240 m	3.639	1.502	1.504	1.996	0.137	0.182	0.423

Note that behavior means calibration including the contribution of AIMSUN behavioral parameters

Table 4.12: Comparison between simulated VSP modes (AB and BA directions) for roundabout 5

VSP mode (Roundabout 5) (Speed Profile 8)		μ_1	μ_2	$t_{\alpha,n}$	t_{crit}	P-T Test (α = 0.05)	D	P-KS Test
Default (AB) vs Default (BA)	550 m	3.553	2.753	0.310	1.989	0.757	0.526	0.000
	240 m	3.645	2.814	0.225	2.000	0.823	0.314	0.050
85th AB vs 85th BA	550 m	1.480	1.896	-0.311	1.983	0.756	0.187	0.193
	240 m	1.741	4.332	-1.998	2.000	0.050	0.343	0.024
85th +behavior (AB) vs 85th +behavior (BA)	550 m	1.930	1.746	0.147	1.979	0.884	0.109	0.805
	240 m	3.543	3.254	0.308	1.997	0.759	0.171	0.640
95th (AB) vs 95th (BA)	550 m	2.306	2.515	-0.121	1.981	0.904	0.168	0.349
	240 m	5.144	2.775	1.185	2.011	0.242	0.143	0.839
95th +behavior (AB) vs 95th +behavior (BA)	550 m	2.104	2.193	-0.061	1.980	0.951	0.146	0.503
	240 m	3.424	2.211	0.723	2.007	0.473	0.286	0.094

Note that behavior means calibration including the contribution of AIMSUN behavioral parameters

Table 4.13: Comparison between simulated VSP modes (AB and BA directions) for roundabout 6

VSP mode (Roundabout 6) (Speed Profile 5)		μ_1	μ_2	$t_{\alpha,n}$	t_{crit}	P-T Test (α = 0.05)	D	P-KS Test
Default (AB) vs Default (BA)	540 m	3.364	3.202	0.067	1.982	0.947	0.423	0.000
	240 m	4.927	3.267	0.593	1.989	0.554	0.318	0.018
85th AB vs 85th BA	540 m	2.009	2.591	-0.584	1.978	0.560	0.203	0.102
	240 m	4.097	1.769	2.005	1.995	0.049	0.227	0.179
85th +behavior (AB) vs 85th +behavior (BA)	540 m	2.017	1.836	0.169	1.978	0.866	0.231	0.041
	240 m	4.358	0.346	3.243	1.997	0.002	0.296	0.034
95th (AB) vs 95th (BA)	540 m	2.799	2.327	0.292	1.980	0.771	0.301	0.005
	240 m	6.005	1.550	2.535	1.999	0.014	0.250	0.108
95th +behavior (AB) vs 95th +behavior (BA)	540 m	2.018	2.120	-0.092	1.978	0.927	0.123	0.644
	240 m	3.639	1.502	1.504	1.996	0.137	0.182	0.423

Note that behavior means calibration including the contribution of AIMSUN behavioral parameters

Note that the results in Table 4.2 to 4.13 include both the cases with cruising and those ones without cruising just for completeness of information. Overall, the results highlighted the role of calibration except for roundabout 2 and roundabout 5 where the need for calibration resulted less marked; these roundabouts are large circular schemes of recent construction and, among the other things, they are usually travelled at enough high speeds. However, Tables 4.8 to 4.13 confirmed that it cannot conclude that a significant difference exist between the two driving directions. Calibrating the parameters with 95th percentile values resulted in most of the cases here examined to be effective in producing a VSP distribution more consistent with the VSP distribution from field-collected vehicle activity and in reducing the errors in emissions estimates as one can see from Figure 4.10 to 4.15, where emissions of CO_2, CO, and HC + NO_X in grams are given.

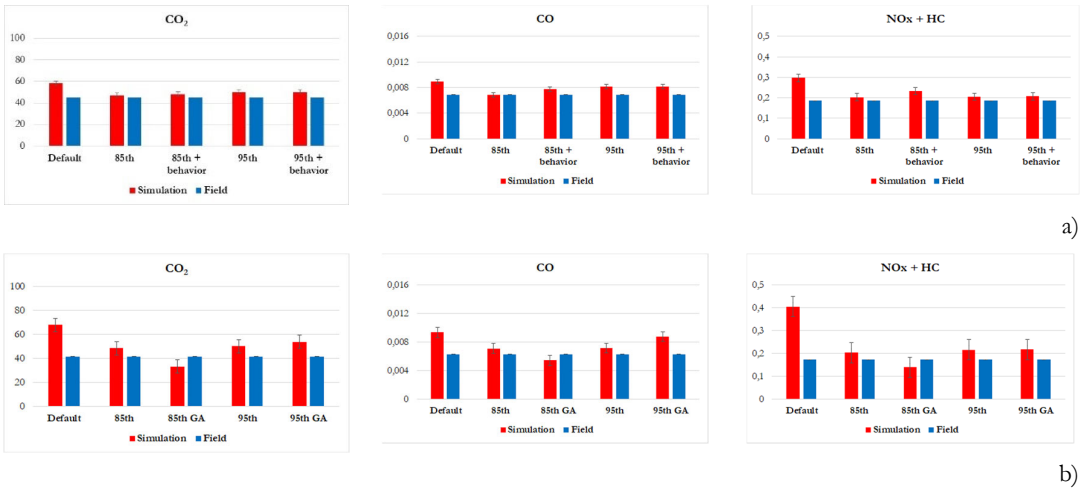

Figure 4.10: CO_2, CO, NO_x, + HC emissions in Roundabout 1: *a)* AB direction *b)* BA direction

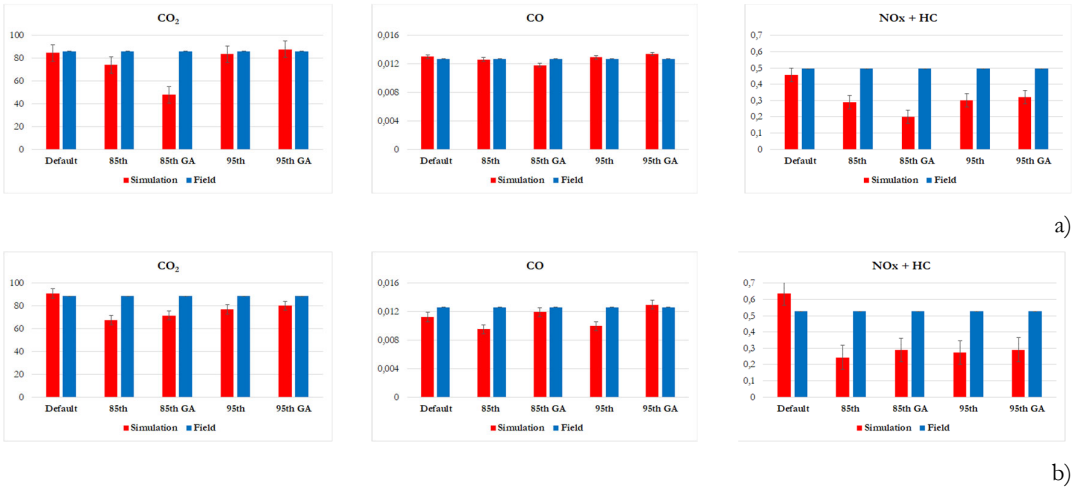

Figure 4.11: CO_2, CO, NO_x, + HC emissions in Roundabout 2: *a)* AB direction *b)* BA direction

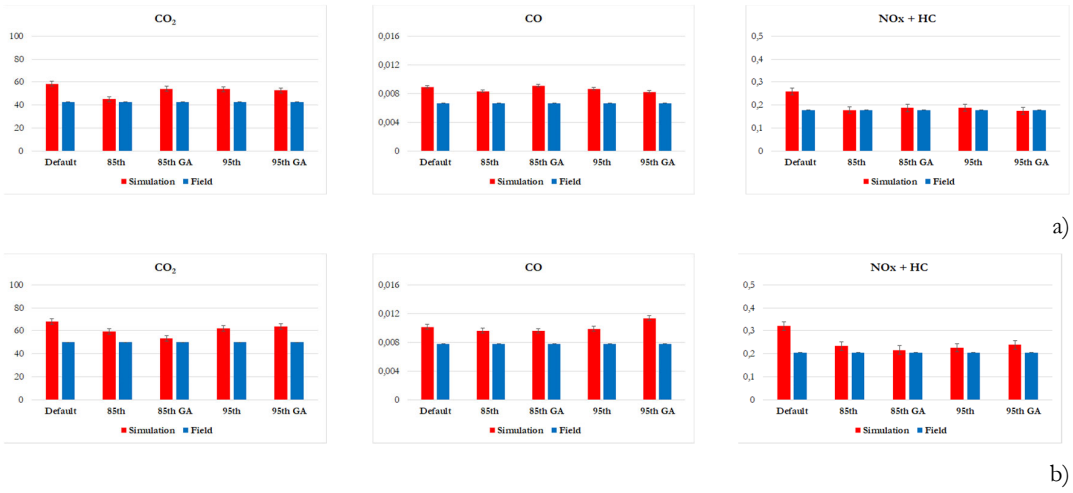

Figure 4.12: CO_2, CO, NO_x, + HC emissions in Roundabout 3: *a)* AB direction *b)* BA direction

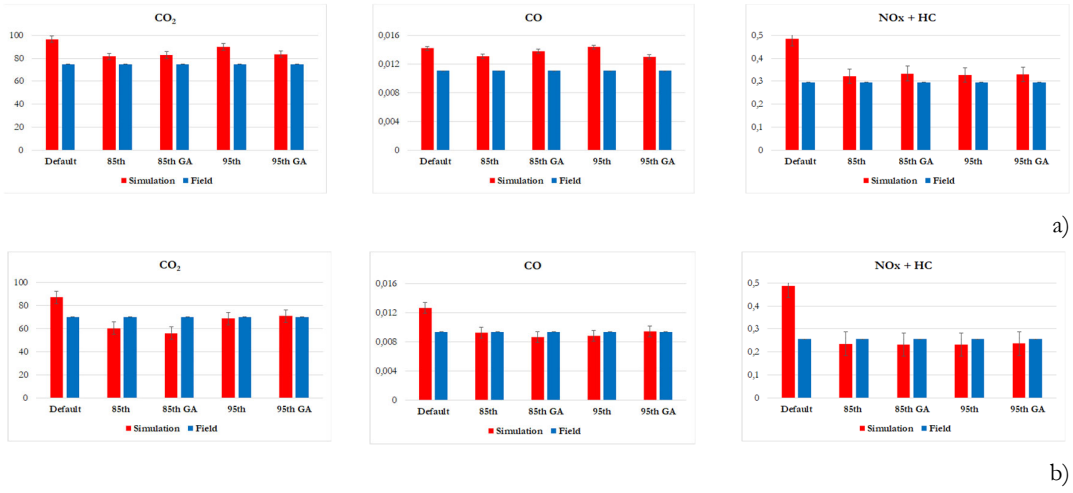

Figure 4.13: CO_2, CO, NO_x, + HC emissions in Roundabout 4: *a)* AB direction *b)* BA direction

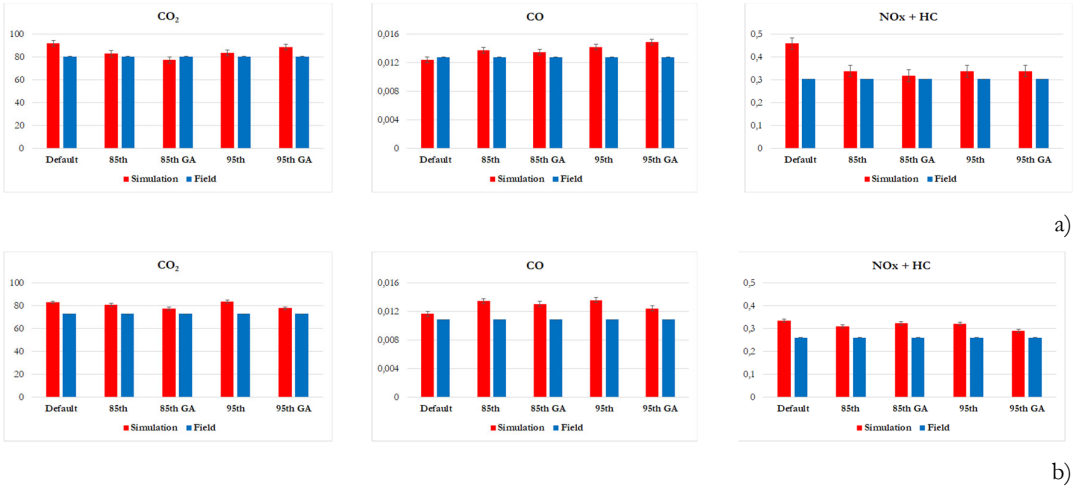

Figure 4.14: CO_2, CO, NO_x, + HC emissions in Roundabout 5: *a)* AB direction *b)* BA direction

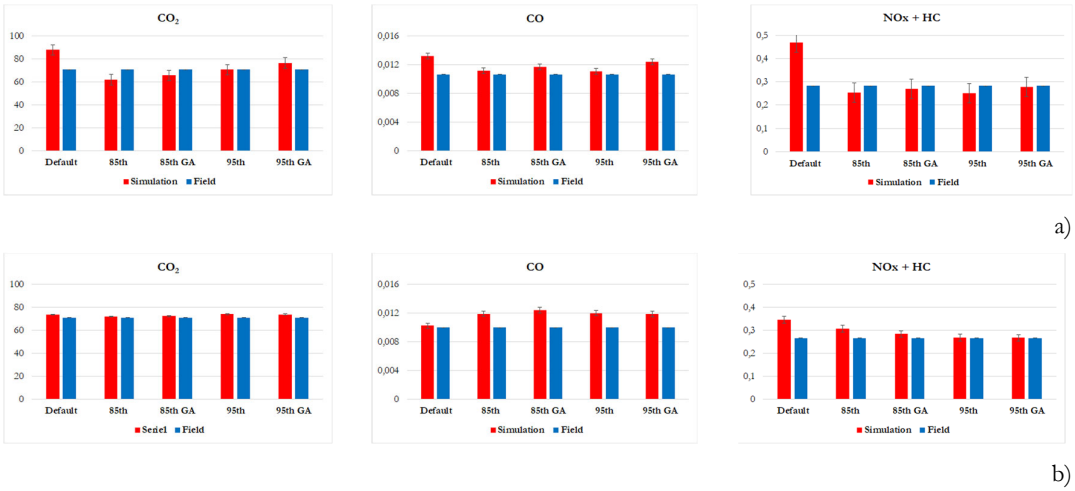

Figure 4.15: CO_2, CO, NO_x, + HC emissions in Roundabout 6: *a)* AB direction *b)* BA direction

The results show that the vehicle activity data under default simulation cause in most of cases a slight overestimation of the emissions across all pollutants. One can observe that the accuracy tends to be improved under calibration with the 95th percentiles of the relevant parameters only. The emissions estimate from the simulation model under calibration with the 95^{th} percentile parameters are closer to the CO_2 and CO emissions based on data surveyed in the fields; underestimation occurred only for HC + NO_X emissions at roundabout 2. The contribution of AIMSUN behavioral parameters (7) (8) leans towards improved results only for

roundabouts with atypical design due to the constraints of the surrounding built environment; see Fig. 4.1. Under 95th calibrated parameters, vehicle activity on roundabout is more realistic because the accelerations and speeds are closer to the range of values observed during data collection.

It should be also noted the role of the kinematic parameters as accelerations and decelerations that affected emissions generated from vehicle activity. In particular, except the very low speeds (0 to 4 km/h) and accelerations (0 to 0.14 m/sec^2), higher average speed and consequently the high average acceleration have influence on pollutant emissions (13).

In order to highlight this aspect, the graphs in Fig 4.16 compare the second-by-second acceleration (or deceleration) activity simulated under calibration with the 95th percentile parameters; by way of example, reference is made to NO_X for each roundabout and both driving directions.

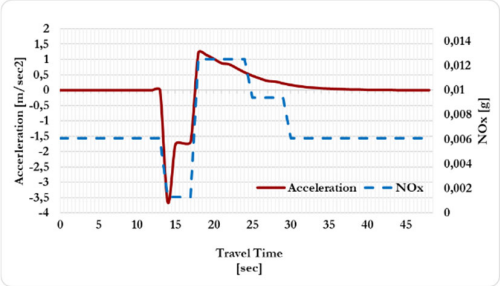

Roundabout 1, AB direction

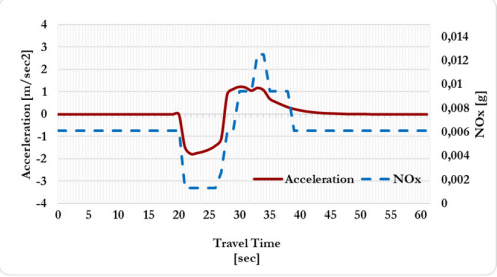

Roundabout 1, BA direction

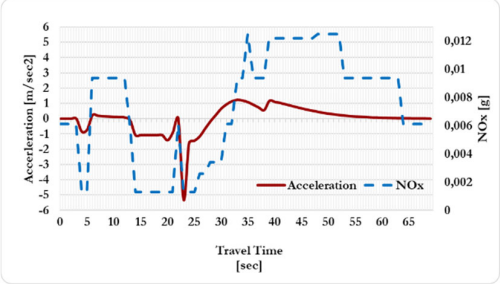

Roundabout 2, AB direction

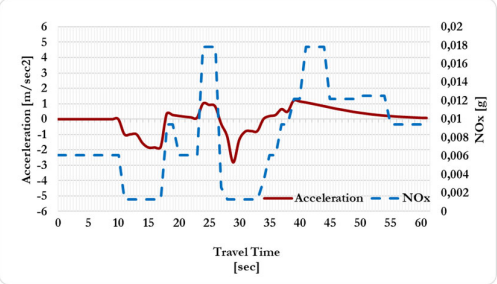

Roundabout 2, BA direction

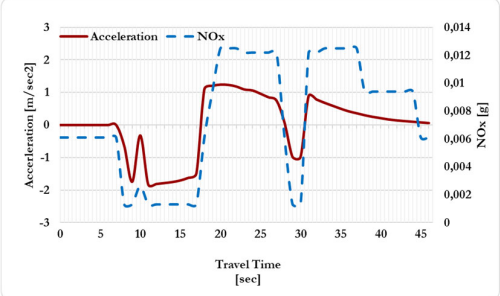

Roundabout 3, AB direction

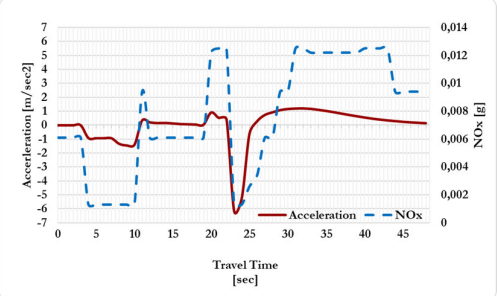

Roundabout 3, BA direction

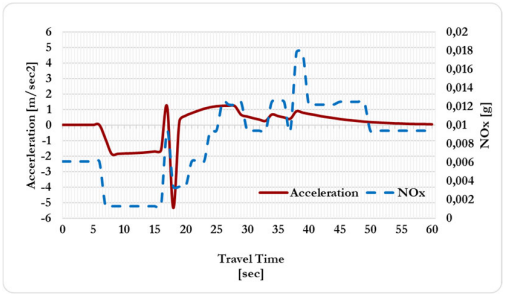

Roundabout 4, AB direction

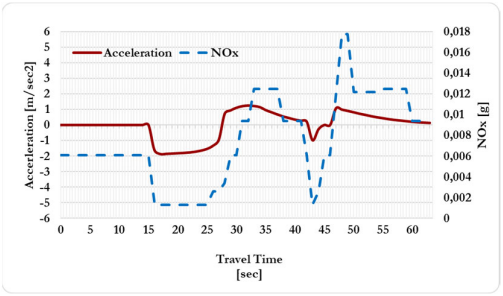

Roundabout 4, BA direction

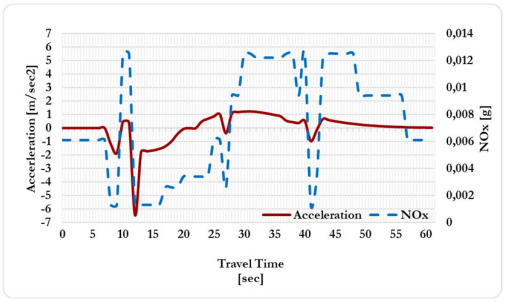

Roundabout 5, AB direction

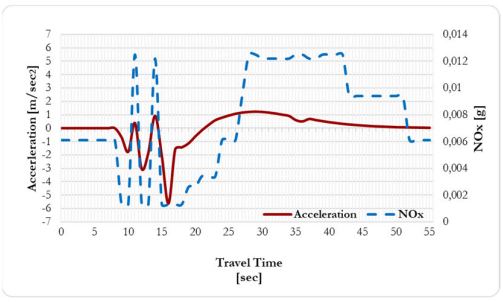

Roundabout 5, BA direction

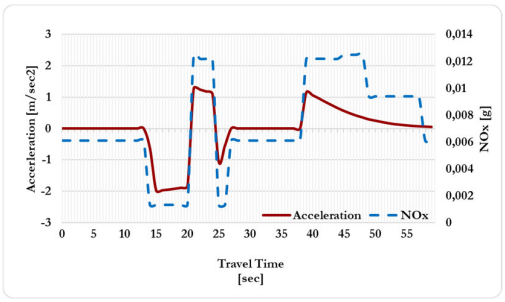

Roundabout 6, AB direction

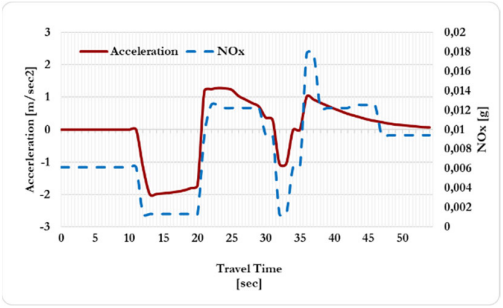

Roundabout 6, BA direction

Figure 4.16: *Second-by-second acceleration and NO_X emission from calibration*

One can observe the significant differences in the instantaneous (simulated) emissions among the roundabouts, mainly caused by the discrepancy between field-based and simulated vehicle activity. Under simulation runs, in fact, the vehicles often achieved higher speeds and accelerations than in the field, spending significant proportions of time in the higher VSP modes associated with higher emission rates. Acceleration events are more frequent in the case of the simulated profiles because of very low conflicting traffic volumes that AIMSUN returned at roundabouts under examination (14). NO_X emissions calculated using the VSP methodology were, however, enough realistic, and consistent with the estimates based on vehicle activity data collected in the field.

Conclusions

This work explored the integration of the VSP methodology and a micro-simulation model to estimate the emissions at urban roundabouts. Measurements of kinematic parameters from vehicle trajectory data collected in the field using a smartphone app were employed to calibrate the model parameters in AIMSUN. Individual vehicle trajectories from AIMSUN under defaults parameters were extracted and compared with the instantaneous speed profiles detected in the field. Calibration was made to provide second-by-second (simulated) speed profiles as close as possible to the observed ones and to improve the emissions estimations. The use of the VSP methodology as available in literature and used in practice allowed to make the comparisons among the emissions estimates from field-observed speed profiles and those ones simulated in AIMSUN.

Despite the efforts of the calibration process, the novel aspect of the study was the smart collection of vehicle activity data across existing roundabouts that made easy the comparison with simulation outputs. Another issue is associated with the use of kinematic parameters extracted from the corresponding distributions surveyed in the field,

The results show that the vehicle activity data simulated under default parameters can overestimate the emission values across all pollutants here examined. The emissions estimated from the simulation model under calibration with the 95^{th} percentile parameters are closer to the field-based estimates for CO_2 and CO; in some cases, loss of efficiency in estimates was obtained (e.g. roundabouts 2 and 4 for HC + NO_X) due to the dispersion observed in the distribution of the time spent in each VSP mode among the roundabouts and their typical operations where curvilinear trajectories have significant effects on speeds. The urban speed limit further constrained vehicle activity both in the field and in AIMSUN.

Another important issue is about the acceleration variations, which are more pronounced in the case of simulated profiles, denoting higher differences in NO_X and HC emissions than the field-based ones.

The results demonstrate the versatility of microsimulation models to investigate about environmental performances of urban hotspots such as roundabouts. An extensive application of the procedure here presented on a wider sample of road units may support the generalization of the results. Future applications of the AIMSUN model once it is properly calibrated for emissions estimation on urban arterials, may include the assessment of the emissions impacts from different traffic management strategies.

References

1. TTS - Trasport Simulation System. AIMSUN Version 8.3 User's Manual. 2020.

2. Gipps, P.G. A model for the structure of lane-changing decisions. *Transportation Research Part B: Methodological, Volume 20, Issue 5*. 1986, pp. 403-414.

3. Janson Olstam, J., Tapani, A. *Comparison of car-following models*. Linköping : VTI meddelande, 2004.

4. Margarida C. Coelho, H. Christopher Frey, Nagui M. Rouphail, Haibo Zhai, Luc Pelkmans,. Assessing methods for comparing emissions from gasoline and diesel light-duty vehicles based on microscale measurements. *Transportation Research Part D: Transport and Environment*. 2009, Vol. Volume 14, Issue 2, pp. 91-99.

5. P.S. Bokare, A.K. Maurya. Acceleration-Deceleration Behaviour of Various Vehicle Types. *Transportation Research Procedia*. 2017, Vol. Volume 25, pp. 4733-4749.

6. P. Fernandes, S. R. Pereira, J. M. Bandeira, L. Vasconcelos, A. Bastos Silva & M. C. Coelho. Driving around turbo-roundabouts vs. conventional roundabouts: Are there advantages regarding pollutant emissions? *International Journal of Sustainable Transportation*. 2016, Vol. 10:9, pp. 847-860.

7. Orazio Giuffrè, Anna Granà, Maria Luisa Tumminello, Antonino Sferlazza. Estimation of Passenger Car Equivalents for single-lane roundabouts using a microsimulation-based procedure. *Expert Systems with Applications*. 2017, Vol. 79, pp. 333-347.

8. Orazio Giuffrè, Anna Granà, Maria Luisa Tumminello, Antonino Sferlazza,. Capacity-based calculation of passenger car equivalents using traffic simulation at double-lane roundabouts. *Simulation Modelling Practice and Theory*. 2018, Vol. 81, pp. 11-30.

9. J., Barcelò. *Fundamental od Traffic Simulation*. London : Springer, 2010.

10. Jiménez-Palacios. Understanding and Quantifying Motor Vehicle Emissions with Vehicle Specific Power and TILDAS Remote Sensing. 1999.

11. *Method and case study for quantifying local emissions impacts of a 3 transportation improvement project involving road re-alignment and 4 conversion to a multi-lane roundabout*. Anya, A., Rouphail, N., Frey, H. C., & Liu, B. 2013. TRB 2013 Annual Meeting.

12. *Application of AIMSUN Microsimulation Model to Estimate Emissions on Signalized Arterial Corridors*. Anya, A. R., Rouphail, N. M., Frey, H. C., & Schroeder, B. 2428, 2014, Transportation Research Record, Vol. 1, pp. 75-86.

13. *Speed and Acceleration Impact on Pollutant Emissions.* Andre, Michel & Pronello, C. s.l.: Speed and Acceleration Impact on Pollutant Emissions, 1996. 10.4271/961113.

14. *Effect of roundabout operations on pollutant emissions.* Margarida C. Coelho, Tiago L. Farias, Nagui M. Rouphail. Issue 5, 2006, Transportation Research Part D: Transport and Environment, Vol. Volume 11, pp. 333-343.

15. *An agent-based traffic regulation system for the roadside air quality control.* Abdelaziz el Fazziki, Djamal Benslimane, Abderrahmane Sadiq, Jamal Ouarzazi, Mohamed Sadgal. 2017, IEEE Access, Vol. 5.

16. *Assessing methods for comparing emissions from gasoline and diesel light-duty vehicles based on microscale measurements.* Margarida C. Coelho, H. Christopher Frey, Nagui M. Rouphail, Haibo Zhai, Luc Pelkmans,. 2009, Vols. Volume 14, Issue 2, pp. 91-99.

Chapter 5

Environmental assessment of converting a multi-lane roundabout into a turbo-roundabout. An exploratory study.

Introduction

Currently roundabout configurations are widespread both in urban and rural road networks but greatly vary for size and shape. Roundabout designs can be traced back to:

- single lane schemes having a single lane on the entry (and exit) approaches and the ring roadway.
- "multi-lane" counterparts having a different number of lanes on one or more approaches and the ring roadways enough wide to accommodate more than one vehicle that travel side-by-side.

If it is true that based on traffic demand more entry capacity occurs on multi-lane roundabouts than single-lane roundabouts, it is also true that the transition from a single-lane ring road to a two- or multi-lane ring roadway has introduced several safety issues: the increase in the number of potential conflict points, the increase in travel speeds, the possibility of lane changes within the ring. Taking into account the absence of curbs on the roundabout driveway ring and approaches, it is also possible to interfere between the trajectories of vehicles circulating along the multiple-lane ring carousel with consequent conflict points attributable to the interweaving of vehicle trajectories. In order to integrate the benefits of single-lane and multi-lane roundabouts and to improve their performance, the turbo concept was introduced in the Netherlands in the late 90s; see in this regard (1)(2).

The turbo-roundabouts are characterized by the physical separation of the lanes on the ring, the entry and exit approaches with broken curbs only where vehicles must perform their maneuvers, and by a different mode of use of the maneuvering areas compared to the traditional layout. Several advantages have been established compared to traditional schemes of roundabout from the point of view of traffic safety and performance efficiency, also in terms of the environmental load due to road traffic (3)(4)(5). Several investigations are underway to understand the operational benefits of one or the other scheme in relation to operational aspects and issues of

insertion into the road network, and the natural or constructed context with which the roundabouts interfere (6).

Characteristics of turbo-roundabouts

The main differences between a turbo-roundabouts and the other roundabouts are found in the geometry of the central island and the physical separation of the lanes on the ring lanes and the approaches. The separation of traffic streams produces a characteristic way of using maneuvering areas on turbo-roundabouts: unlike traditional roundabouts, in turbo roundabouts, depending on their destination, users are bound to pre-select the lane required before entering the ring and subsequently with the help of road signs and curbs make a precise trajectory, without being able to modify it as a result of a possible error. It is therefore also necessary to install suitable vertical signs at a certain distance before entering the ring, in order to suggest to the user, the choice of the appropriate lane with sufficient notice. The characteristics of turbo-roundabouts are determined by their particular planimetric configuration:

- the elimination of the lane change maneuver inside the ring and the consequent reduction of the number conflict points
- the inhibition of the possibility of traveling the ring road according to median trajectories, which produce the partial occupancy of both concentric lanes
- the decrease in the operating speeds of users both along the entries and inside the roundabout.

Turbo-roundabouts may have different configurations, varying the number of lanes on both inbound and outbound arms, the number of ring lanes, and the geometry of the central island, e.g. see Figure 5.1. The layouts proposed by (1) (see also Fig. 5.1):

- case of three or four arms flowing at the intersection
  - *basic turbo-roundabout*
  - *egg turbo-roundabout*
  - *spiral turbo-roundabout*
  - *knee turbo-roundabout*
  - *rotor turbo-roundabout*
- case of three arms only:
  - *star turbo-roundabout*
  - *stretched knee turbo-roundabout*

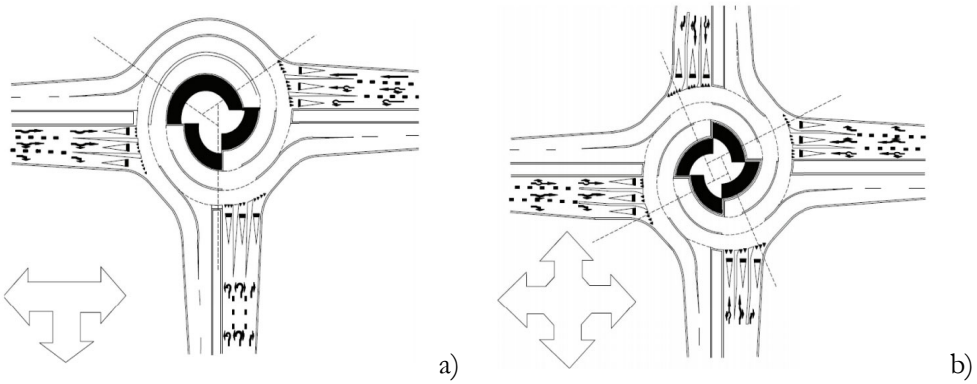

Figure 5.1: Examples of turbo layouts: a) Star turbo-roundabout; b) Rotor turbo-roundabout

The main goal regarding a turbo-roundabout, compared to a traditional roundabout, lies in the reduction of potential conflict points whose number, as is well known, can affect the safety of the intersection. Andrighettoni and Mauro (8) pointed out that a basic turbo-roundabout compared to a double-lane roundabout allows to achieve a reduction of the potential collision points by 55% to 37.5% depending on whether all the points of conflict, equal to twenty-two, or only the most frequent ones, total of sixteen, are considered in the comparison. The following Figure 5.2 compares the conflict points between the two intersection patterns.

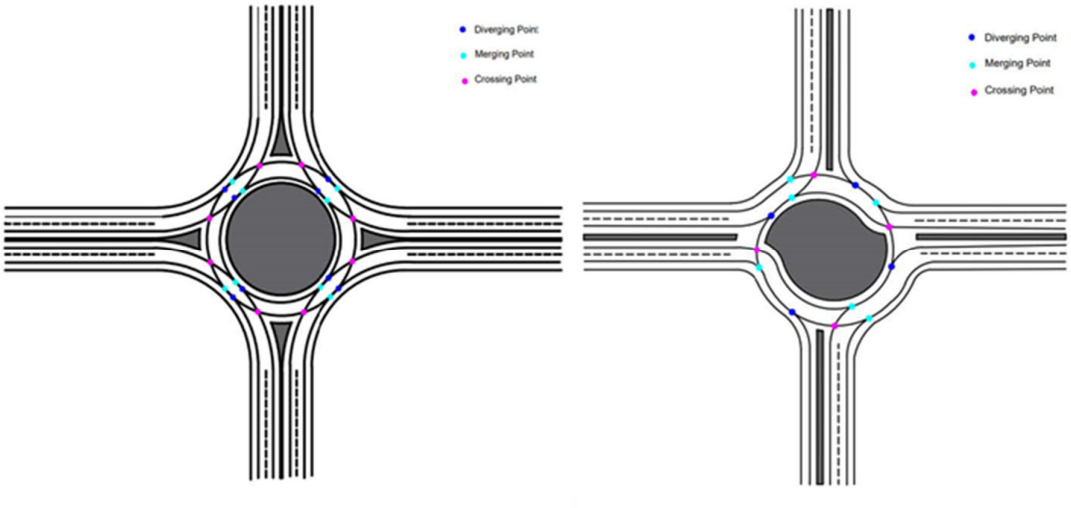

Fig. 5.2 Turbo-roundabout vs double-lane roundabout potential collision points

According to the indications found in the Roundabout - Application and design manual[1]:

- the capacity of the intersection is increased, however depending on traffic demand

[1] See https://core.ac.uk/download/pdf/30821772.pdf (last accessed April 23, 2021)

- the capacity of the turbo-roundabout is higher than a "single lane" roundabout (1 1/2 to 2 1/2 higher) and the "double lane" roundabout (1 to 1 1/2 higher)
- the capacity of the turbo-roundabout is equal to or higher than the traffic light intersection
- waiting times are shorter than at the traffic light intersection
- road safety has increased
- turbo-roundabout has greater safety of the non-traffic lighted and traffic light intersection, although it is less safe than the "single-lane" roundabout
- the overall surface of the turbo-roundabout is approximately equal to the traffic light intersection, assuming that the traffic light intersection involves the passage of two heavy vehicles at the same time in all directions where possible for both schemes
- the construction costs of turbo-roundabouts are generally high but life cycle costs are lower than those of traffic light intersections.

Design aspects

Turbo-roundabouts derive from a particular planimetric conformation that recalls the shape of a turbine (see e.g. Figure 5.3). Compared to the traditional roundabouts in which all vehicles move side by side, each in their own lane, the vehicles reach the entrance of the ring roadway and then set the trajectory and complete their maneuvers towards the desired exit, in a turbo-roundabout, instead, the vehicles select the correct lane already starting from the entry arm according to the exit to be reached.
The main advantages of turbo-roundabouts can be traced back to:

- fewest potential conflict points between vehicle trajectories
- lower speed along the ring road
- reducing the risk of collision between side-by-side vehicles
- improvement of the overall capacity of the intersection due to continuity between the entry lanes and the corresponding ones on the ring roadway.

However, in case of incorrect lane preselection some turbo-roundabouts do not allow U-turn.
Before illustrating the different phases of a turbo-roundabout design, a brief description of the essential elements should be given:

1. the single-lane entry arms may give priority to traffic circulating on one or two lanes of the driveway ring
2. at least two arms of two-lane entrance give priority to traffic circulating on two lanes (but not more than two) of the driveway ring
3. the spiral layout guides traffic from the entrance to the desired destination, avoiding the conflict points in crossing
4. the dividing curbs allow the preselection of the lane on the entry arms and the journey of the correct lane along the ring, thus accentuating the curvature of trajectories
5. at least two exit arms are two-lanes
6. once the driver entered from the outer entry lane, he or she can still decide whether to turn right at the adjacent exit approach or make the crossing movement but cannot perform the left turns (the driver in this case should have preselected the inner lane at entries).

Fig. 5.3: Turbo-roundabout in Reeuwijk, Netherlands (Source: Google)

The turbo-roundabout consists of a sequence of spirals. These spirals are composed of string segments, often semicircles, that follow one another; each arc has a greater radius than the previous one.

The construction of a basic turbo-roundabout is based on spiral lines that determine the limits of the lanes. Each spiral consists of three semicircle whose radius increases progressively. The semicircle is interrupted at the translation axis (see Figure 5.4). The arcs to the right of the translation axis have C_{right} as their center, the arcs to the left of the translation axis have C_{left} as their center. Figure 5.4 summarizes details about the turbo block such as reported by the guidelines of several countries where turbo-roundabouts have been built for some time (9).

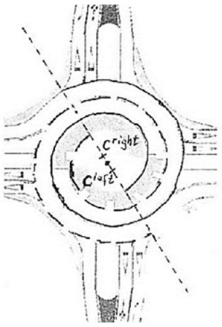

Element	Turbo roundabout template							
	Mini		Regular		Medium		Large	
	Dutch Slovenian Serbian	Croatian	Dutch Slovenian Serbian	Croatian	Dutch Slovenian Serbian	Croatian	Dutch Slovenian Serbian	Croatian
R_1 / m	10,50	10,45	12,00		15,00	14,95	20,00	19,95
R_2 / m	15,85		17,15		20,00		24,90	
R_3 / m	16,15		17,45		20,30		25,20	
R_4 / m	21,15	21,20	22,45		25,20	25,25	29,90	29,95
L_1 / m	5,35	5,40	5,15		5,00	5,05	4,90	4,95
L_2 / m	5,00	5,05	5,00		4,90	4,95	4,70	4,75
Δv / m	5,75		5,35	5,30	5,15		5,15	
Δu / m	5,05		5,05	5,00	4,95		4,75	

Fig. 5.4: Geometric characteristics of turbo roundabouts from European countries

Figure 5.5 shows the shift between the centers along the translation axis and the bias, i.e., the distance between the C_{right} center (or C_{left}) and the absolute center of the turbo-roundabout which is equal to half the shift. The shift corresponds to the minimum width value of a lane.

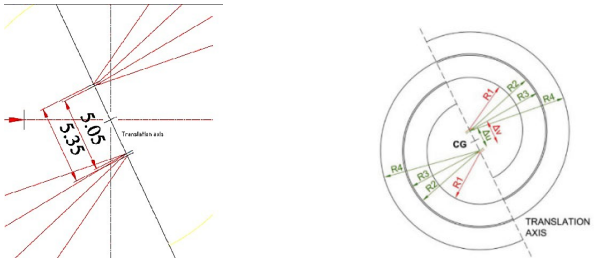

Fig. 5.5: Details about the turbo block

Geometric elements and their role in construction of the layout are summarized in Table 5.1. More precisely, this table refers to the case where the smallest radius is 12 m.

The most important geometric parameters that affect the performance of the turbo-roundabout are the radii of the different circular arcs and the ring lanes widths: different R_1 values that correspond to the most common cases of turbo-roundabouts in the technical practice are available in literature manuals[2].

[2] See again https://core.ac.uk/download/pdf/30821772.pdf (last accessed April 23, 2021)

Table 5.1: Geometric design parameters

Cross section elements	width				
inner radius	12.00				
inner edge line offset	0.45				
inside lane	4.65				
divider inner line offset	0.20				
divider (divider)	0.30				
divider outer line offset	0.20				
outside lane	4.35				
outer edge line offset	0.45				
Roadway widths, shifts, and biases					
inside roadway width		5.30			
outsider roadway width		5.00			
shift1 (inside to middle)			5.35		
shift2 (middle to outside)				5.05	
bias1 = shift1 / 2 (applies to R1 and R1')			2.675		
bias2 = shift2 / 2 (applies to all other radii)				2.525	
bias difference				0.15	
Radii for lane lines	arc centre bias	radius	start position	end position	'position' is relative to overall centre. start position = radius - bias; end position = radius + bias
R1' = inside lane, inner line	2.675	12.45	9.775	15.125	R1' = inner radius + inner edge line offset
R3' = outside lane, inner line	2.525	17.65	15.125	20.175	R3' = R1' + shift1 - bias difference
difference			*5.350*	*5.050*	*differences match shift1 and shift2; also, end position of R1' matches start position of R3'.*
R2' = inside lane, outer line	2.525	16.95			R2' = R3' - width of divider and divider offsets
R4' = outside lane, outer line	2.525	22.00			R4' = R2' + shift2 = R3' + outside lane width
Radii for roadway edges	arc centre bias	radius	start position	end position	start position = radius - bias; end position = radius + bias
R1 = inside roadway, inner edge	2.675	12.00	9.325	14.675	R1 = inner radius
R2 = inside roadway, outer edge	2.525	17.15	14.625	19.675	R2 = R1 + inside roadway width - bias difference
difference			*5.300*	*5.000*	*differences match roadway widths*
R3 = outside roadway, inner edge	2.525	17.45			R3 = R2 + divider width
R4 = outside roadway, outer edge	2.525	22.45			R4 = R3 + outside roadway width

The same table thus identifies different dimensions of the radii (R_1 to R_4) that can be used for designing the turbo block. According to experience in the Netherlands (1), turbo-roundabouts are characterized by greater safety when the internal radius (R_1) is equal to 12 m (2); this radius, indeed, affects the speed along the turbo-roundabout (the lower the radius, the lower the speed along the turbo-roundabout).

Environmental issues

Over the past decade, research has established several benefits in terms of capacity and safety for users for both modern roundabouts and turbo-roundabouts and traditional schemes (10) (11). The environmental aspect, and in particular the impact on pollutant emissions from traffic, is still of great interest in the scientific world.

Some researchers (12) based their investigations on the hypothesis that vehicles that are forced to follow the specific trajectories imposed by the turbo-roundabout will have a significant impact on emissions. Specifically, using the VSP methodology and microsimulation techniques it has been shown that a turbo layout compared to a single-lane roundabout produces a reduction in emissions, but higher CO_2 and NO_X emissions at turbo-roundabouts than two-lane roundabouts were provided for low levels of pollution (about 3 to 6%).

Fernandes et al. (13) used the empirical VSP methodology to compare the emissions produced by vehicles that travel existing turbo-roundabouts and two-lane roundabouts. The results showed that emissions from turbo-roundabout vehicles are 15-22% higher than those derived from traditional schemes. Another interesting approach was to study the environmental performance of a corridor with turbo roundabouts compared to a similar corridor with two-lane roundabouts. In this case, the authors have also found a small increase of polluting emissions regarding the configuration of the corridor with turbo-roundabouts.

Case study

This study was carried out to assess the feasibility of converting an existing two-lane roundabout into a turbo-roundabout and their impacts from an environmental perspective. Specifically, the hypothesis of converting the intersection between Giuseppe Lanza Di Scalea str, Besta str and L Einaudi str (neighborhood street) into turbo-roundabout has been assessed in order to looking for its environmental performance; for further information see (14).

The roundabout was built as part of the redevelopment of Giuseppe Lanza Di Scalea str (Northbound – Southbound) since 2014, in order to improve vehicular circulation in this area of Palermo. The road plan is placed into the Z.E.N. district to allow direct connection with the Luigi Einaudi str (Westbound) and Fabio Besta str (Eastbound).

The roundabout is newly built as previously mentioned, and it is characterized by a radius of 40 m (including the ring road); it occupies a total area of 5900 square meters. Lanza di Scalea str and Einaudi str, both having two entry and exit lanes, are connected to three of the 4 sides of

the roundabout. The fourth leg, Besta str is a two-lane road, one in each direction. Public transport runs on all roads approaching the intersection (see Fig. 5.6).

Fig. 5.6: Via Besta roundabout (Source: Google Heart)

The following project hypotheses have considered the space requirements of heavy vehicles. For a correct analysis of the constraints present in the area of the existing roundabout was also taken into account the town development plan of Palermo City since 2004.

Fig. 5.7: PRG of Palermo

By means of the PRG the node location has been identified and the historical green areas and urbanized areas have been identified as constraints, which inevitably condition the planimetric configuration. The overall center of the roundabout has been identified, as shown in Figure 5.8. Since the position of the roundabout center does not lie on the major road axis but it was shifted to the left, the shift to the position centered on the axis of the major roads have been thought before conceptualizing and planning the turbo roundabout with comparable size; see Figure 5.9 where the central island and the ring road were also plotted.

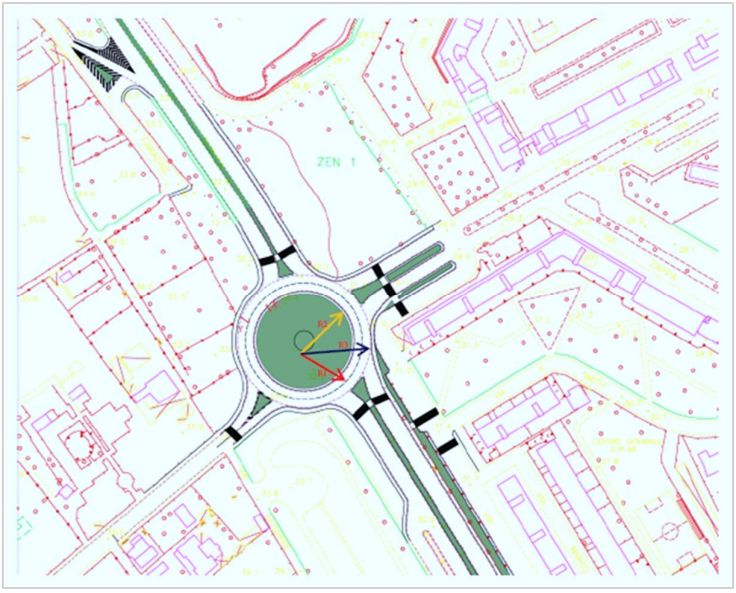

Fig. 5.8: Geometric design of the two-lane roundabout (14)

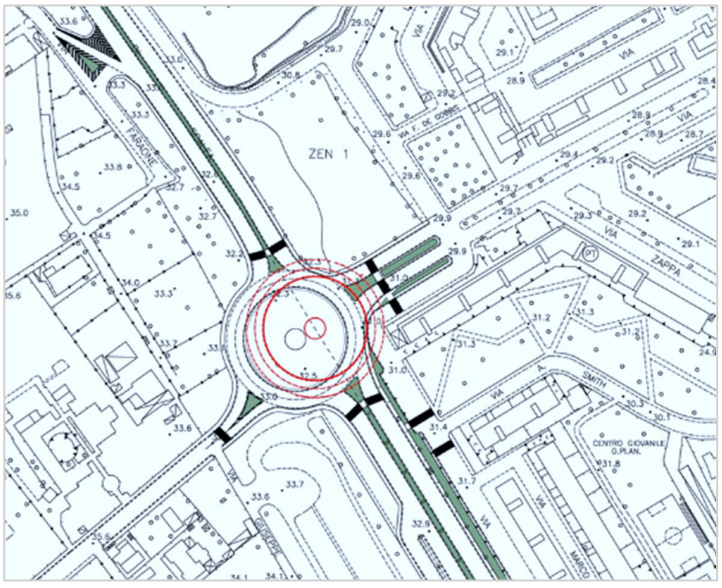

Fig. 5.9: Roundabout positioning (14)

Several design hypotheses have been examined for the turbo roundabout starting from the choice of the inner radius of the central island R_1, considering values of 20 m and 15 m and experimenting with an eccentric layout for the latter value.

To compare the environmental performance with the traditional roundabout layout in terms of pollutant emissions, the configuration adopted was that with a radius of the central island equal to 15 m (as in the following Table 5.2).

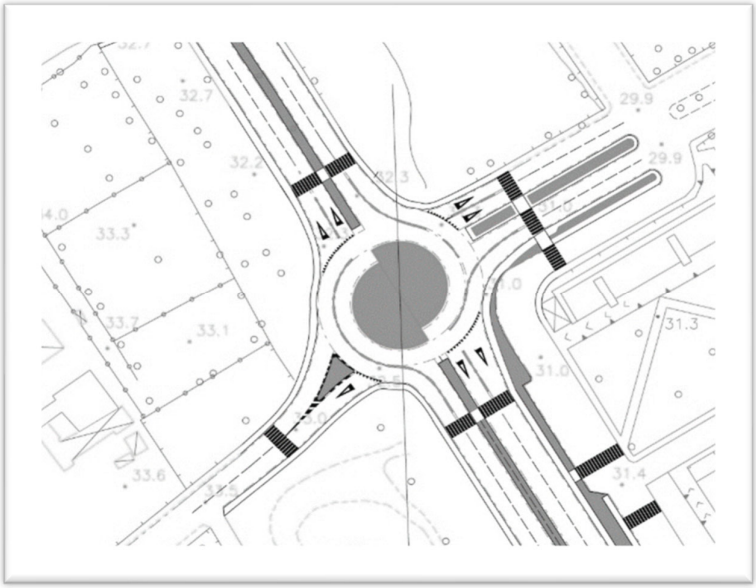

Fig. 5.10: Design configuration with a 15 m of central island radius

Table 5.2: Turbo roundabout geometry

Cross section elements and roadway edges [m]					
Inner radius[a]	15	Outside roadway width	5.25	$R_4=R_3$+ outside roadway width	25.925
Inner edge line offset	0.45	$Shift_1$ (inside to the middle)	5.55	Arc centre bias (R_1)	2.775
Divider inner line offset	0.20	$Shift_2$ middle to the outside	5.30	Start position	12.225
Divider width	0.30	$Bias_1$ ($Shift_1$ /2)	2.775	End position	17.775
Divider outer line offset	0.20	$Bias_2$ ($Shift_2$ /2)	2.65	Arc centre bias (R_2)	2.65
Outer edge line offset	0.45	$R_2=R_1$+ inside roadway width-bias difference	20.375	Start position	17.725
Inside roadway width	5.50	$R_3=R_2$+divider width	20.675	End position	23.025

[a] inside circulatory roadway (inner edge).

Data collection

At the roundabout site hourly patterns of traffic flows showed two distinguishable peaks in the morning and the late afternoon, and no significant peak at noon or in the late evening; the morning peak was usually followed by a lean flow until another peak in the late afternoon. Thus, manual traffic-counting was done during the morning (7:00 - 8:00 a.m.) and afternoon (6:00 - 8:00 p.m.) peak hours on weekdays (Thursday to Friday) in July 2020 after the spring lockdown due to the COVID-19 emergency; traffic on each approach was recorded separately by travel direction and then classified for each maneuver.

It was noted that the morning peak was often enough sharp with the peak reached over a short time period that suddenly dropped to its lowest point; the afternoon peak was characterized by a wider peak that was reached and dispersed over a longer time period than the morning peak. Based on what observed, it was decided to exclude morning data in favor of those recorded during peak afternoon hours. Traffic data recording was carried out simultaneously from fixed positions at each entry (exit) to detect through movements in both directions. Entering, circulating, and exiting traffic flow data were both manually counted by two operators and videotaped in specific positions in each roundabout approach within the system's viewable area so that they can be then identified in the network model of the roundabouts built in AIMSUN (15). The traffic data allowed to obtain the O/D matrix in Table 5.3, which constituted the necessary input for the following microsimulation runs in AIMSUN. A total entry flow of 3324 vehicles per hour was registered where about 10 percent made by heavy vehicles.

Table 5.3: O/D Matrix of traffic volumes at the two-lane roundabout

O/D Matrix	A	B	C	D
A	-	51	28	9
B	101	-	27	2
C	37	8	-	0
D	3	9	1	-

This section is also about the data collection that was done to understand user behavior through the roundabout under examination via the recording and analysis of data on vehicle dynamics. Thanks to the ongoing digital transition and a great availability of smart tools to detect GPS trajectories on road segments and intersection, the idea of detecting data on location, travel time, distance, grade, second-by-second speed, and acceleration by learning them from vehicle

trajectory data, was implemented using the app Speedometer GPS PRO for Android smartphone installed in a Euro IV light passenger diesel vehicle used as the test vehicle[3].

Four GPS runs for each manoeuvre were experienced by the test vehicle (through movements AB-BA in both directions entering the roundabout from the left lane) for a total of 10 Km (see Figure 5.11).

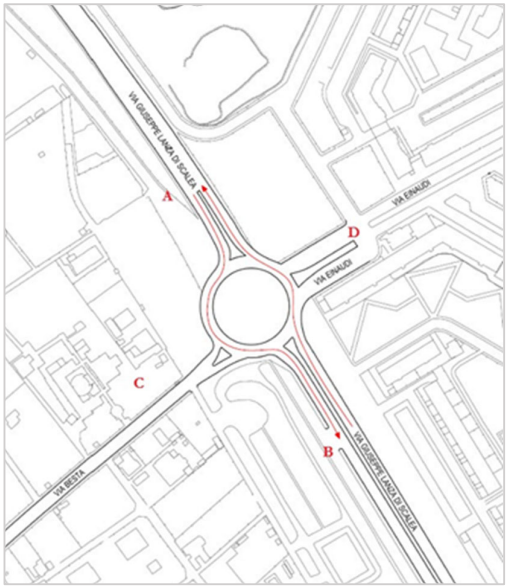

Fig. 5.11: Roundabout nodes configuration

Speed Profiles by using smartphone

Starting from the recorded trajectory data, speed profiles were built for the through movements in both directions of Lanza di Scalea str, and for the left turn to Besta str.

Based on (10) and (11), vehicles entering a roundabout may experience three types of speed profiles: non-stop (type I), one stop (type II), multiple stops (type III). However, the probability of experiencing one of these types is closely related to the level of intersection congestion. In the present case, given the low traffic volumes that were observe, the test vehicle experienced speed profiles that did not stop completely just before reaching the entry line to give priority to the circulating vehicles. For the purposes of the study, three speed-travel time profiles per driving direction were considered as representative profiles of the maneuvers being examined in an area of about 500 m. Among the assumptions introduced in the previous chapter, in order to have a common base of comparison among the roundabouts in view of estimating the

[3] [3] The LPDV test vehicle used for data collection is a Toyota Urban Cruiser equipped with a 1.4 lt engine (95hp).

contribution of each roundabout to the emission phenomenon, the effective influence area excluded cruising and was considered equal to about three times the outer diameter for each roundabout. Table 5.4 shows detailed information on the vehicle activity data detected in the field for each of the runs experienced by the test vehicle through the roundabout, while table 5.5 shows a summary of the mean values of the maximum speed, maximum acceleration and maximum deceleration, the 85th and 95th percentile values of accelerations and decelerations calculated from the corresponding values extracted from the vehicular trajectories (3 runs per by driving direction) experienced in the field. The assumption of using the 85th and 95th percentile values of accelerations and decelerations was suggested by (16) where the vehicle attribute parameters of AIMSUN were then supplied with the values of the 95th (or 85th) percentiles of the accelerations and decelerations extracted from the distributions measured in the field on urban arterial corridors that also included roundabouts. This choice may seem limiting to driving behavior at first, but it was founded on the driving behavior actually observed in urban roundabouts where the speed limit of 50 km / h is in force.

Note that the left turn-related data (i.e. BC direction in Table 5.5) were also recorded but only through movements were considered in the following analysis.

Table 5.4: Summary of vehicle activity parameters by movement

AB driving direction										
	Acceleration [m/s²]			**Deceleration [m/s²]**			**Speed [km/h]**			
Profile	**85th**	**95th**	**Max**	**85th**	**95th**	**Max**	**Average**	**Median**	**Min**	**Max**
1	0.82	1.167	1.45	1.27	1.57	2.95	41.28	47.17	13.08	53.05
2	0.93	1.278	1.67	1.38	2.15	3.0	41.97	49.18	9.29	54.62
3	0.74	0.8618	1.25	0.75	1.03	1.41	40.45	45.60	17.07	54.39
BA driving direction										
	Acceleration [m/s²]			**Deceleration [m/s²]**			**Speed [km/h]**			
Profile	**85th**	**95th**	**Max**	**85th**	**95th**	**Max**	**Average**	**Median**	**Min**	**Max**
1	0.66	0.79	1.56	0.96	1.69	2.08	36.12	44.10	8.35	52.30
2	0.78	1.10	1.24	0.84	1.97	3.33	38.66	45.60	10.02	53.17
3	0.85	1.39	1.97	1.01	1.71	1.81	39.21	48.00	5.05	56.37

Table 5.5: Summary of the mean values of the vehicle activity parameters by movement

Trajectory	**Max speed [km/h]**	**Max. acceleration [m/s²]**	**Max. deceleration [m/s²]**	**85th percentile acceleration [m/s²]**	**95th percentile acceleration [m/s²]**	**85th percentile deceleration [m/s²]**	**95th percentile deceleration [m/s²]**
AB direction	15.0	1.46	2.48	0.830816	1.10	1.13	1.58
BA direction	14.98	1.78	3.13	0.79408	1.17	0.96	1.74
BC direction	13.0	2.29	3.24	0.795194	1.14	1.27	2.10

The observations were then separated by driving direction where the respective trajectories occurred in the field. Given the analogy among the curvilinear paths experienced by the test vehicle in the two driving directions, a two-tailed t-test was performed on the distributions of the observations of each relevant parameter in AB and BA directions (see Table 5.6). Based on the p-values in the Table 5.6, it cannot conclude that a significant difference exists between the two driving directions. Similar considerations can be made with reference to the results of the KS-test.

Table 5.6: Two-tailed t-test and KS-test for the parameter's distributions detected in the field

Speed [m/sec]	Distance[1] [m]	μ_1[2]	μ_2[2]	$t_{\alpha=0.05}$[3]	n[4]	t_{crit}	p-t test (α = 0.05)	D[5]	p-KS Test
Profiles 1	500	11.31	10.03	1.78	54	1.980	0.077	0.185	0.234
(AB - BA)	250	9.18	7.21	2.00	52	2.007	0.051	0.414	0.009
Profiles 2	500	11.66	10.74	1.27	105	1.982	0.207	0.185	0.234
(AB - BA)	250	8.61	9.02	-0.36	44	2.015	0.7170	0.414	0.009
Profiles 3	500	11.23	10.89	0.51	110	1.982	0.613	0.167	0.380
(AB - BA)	250	8.28	8.49	-0.20	35	2.030	0.839	0.333	0.109

[1] these values are differentiated both for the distance including cruising and the distance without cruising; [2] μ_{AB} and μ_{BA} stand for the mean values of the samples of the observations of each parameter in the two driving directions (i.e. AB and BA); [3] t-value is the result of the two tailed t-test which was done to compare the equality of the means μ_{AB} and μ_{BA} of samples of two populations with equal sample size; [4] n stands for degree-of-freedom; [5] D is the max difference between the cumulated distributions of the samples as given by the KS-test.

Figure 5.12 shows an example of speed profile among those recorded during data collection. Note that the total emission associated with each of the speed profiles detected in the field also included the emissions corresponding to the time spent in the cruise mode. This time has been needed to cover the difference between the whole influence area of the roundabout (about 500 m) and the distance (approximately 250 meters including a length of three times the outer diameter) defined as the sum of the deceleration distance of a vehicle travelling from the cruise speed as it approaches and the enters the roundabout, and the acceleration distance as it exits the roundabout up to the section it reaches the cruise speed (see the continuous line in Figure 5.12); based on the observed cruise and circulating speeds, the last was identified to extract the specific contribution of the total traffic volume entering the roundabout on the emission phenomenon. Note that this case study of roundabout is characterized by grades less than 2 percent so that this parameter was neglected.

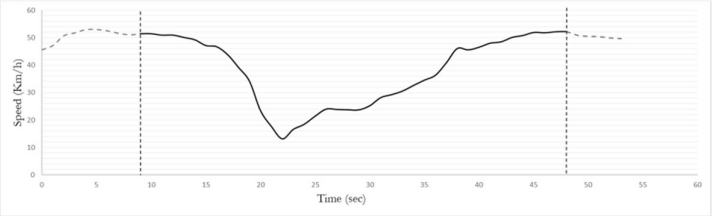

Fig. 5.12: An example of speed profile for though movement (A-B direction)

According to (*12*)(*13*)(*17*), CO_2, CO, NO_X and HC emissions from instantaneous speed profiles were calculated using the VSP methodology based on the speed profiles both detected in the field and simulated in AIMSUN for the existing two-lane roundabout. As introduced for the pilot sample (see the previous chapters), the versatility of the micro-simulation model for a calibration aimed at improving the accuracy of emissions estimates was tested in order to ensure that second-by-second trajectories experienced in the field properly reflected the speed-time profiles simulated in AIMSUN.

In order to quantify the emission impacts and compare the emissions from vehicles moving through the two-lane roundabout and the turbo-roundabout, the pollutant emissions were estimated from the VSP modal emission rates, and the distribution of time spent in each VSP mode from the speed profiles that were simulated in AIMSUN. In this regard see next section.

Emission estimation

The VSP empirical methodology for calculating emissions is based on the instantaneous power generated by the engine to overcome aerodynamic and rolling resistance and increasing the kinetic and potential energy of the vehicle (*17*). The choice of this approach is strongly influenced by the type of data available: the trajectory data with sampling per second in terms of speed, acceleration, deceleration, and slope allow to estimate the instantaneous emissions, with sampling per second too. The expression for the calculation of VSP and CO_2, CO, NOx, HC emission rates for each VSP mode have been already introduced in the previous chapters and for this reason it will not show here. Table 5.7, in turn, shows the results of two-tailed t-test for the VSP distributions detected in the field in AB and BA directions through the existing two-lane roundabout. Similar considerations can be made with reference to the results of the KS-test.

Table 5.7: T-Test and KS Test results for VSP modes in both directions though the existing roundabout

VSP [Kw/ton]	distance [1] [m]	μ_1[2]	μ_2[2]	t-value [3] (α = 0.05)	n[4]	t_{crit}	p-t test	D[5]	p-KS test
Profiles 1	500	2.78	1.95	0.68	101	1.98	0.50	0.172	0.315
(AB - BA)	250	1.72	-1.07	1.48	49	2.01	0.15	0.400	0.011
Profiles 2	500	2.52	2.15	0.26	95	1.98	0.79	0.167	0.356
(AB - BA)	250	0.83	-1.88	1.05	38	2.02	0.30	0.375	0.051
Profiles 3	500	2.55	2.06	0.38	111	1.98	0.70	0.156	0.464
(AB - BA)	250	0.15	-0.73	0.44	44	2.01	0.66	0.292	0.216

[1] these values are differentiated both for the distance including cruising and the distance without cruising; [2] μ_{AB} and μ_{BA} stand for the mean values of the samples of the observations of each parameter in the two driving directions (i.e. AB and BA); [3] t-value is the result of the two tailed t-test which was done to compare the equality of the means μ_{AB} and μ_{BA} of samples of two populations with equal sample size; [4] n stands for degree-of-freedom; [5] D is the max difference between the cumulated distributions of the samples as given by the KS-test.

Based on the p-values of the t-test in the Table 5.7, it cannot conclude that a significant difference exists between the two driving directions. Note that the results were shown both for the total distance travelled by the test vehicle and for the distance without cruising in order to maintain consistency among the runs and calculate the pollutant emissions for each speed profile through the examined roundabout.

The instantaneous emission rates were calculated based on speed profiles experienced by the tested vehicle and estimated from the distribution of time spent in each VSP mode obtained from the speed profiles. Based on VSP computations and the assignment of VSP modes as shown in the previous chapters for light passenger diesel vehicles, emissions by pollutant source and each profile were summed considering the emission factor (g/s) assigned to the i^{th} second of the speed profile corresponding to the instantaneous VSP mode.

The total emission of each pollutant was obtained as the average of the emissions per pollutant source and speed profile. The graphs in Figure 5.13 show the VSP mode relative frequencies in percent, tested for the speed profiles collected in the A-B and B-A directions; one can see that the time percentages were on the whole consistent with each other by driving direction especially in the VSP modes 1 to 2 (deceleration) and 4 to 5 (acceleration).

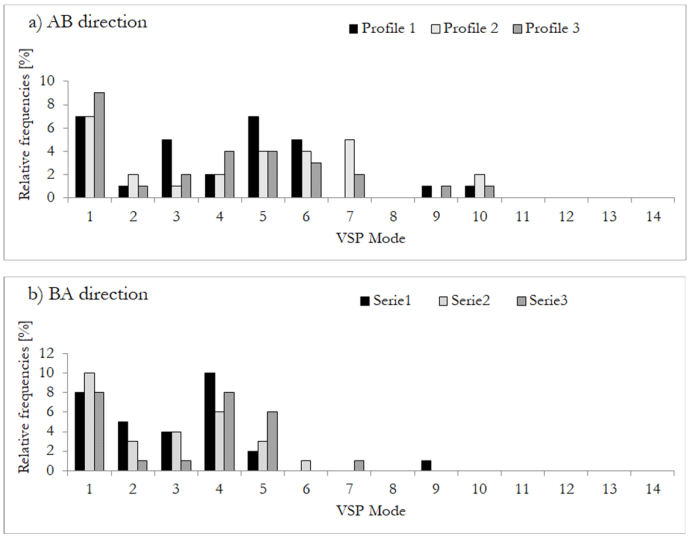

Fig. 5.13: Distribution of time spent by VSP mode by driving direction

Speed profiles from microsimulation

The *AIMSUN* software was used to simulate the traffic conditions as consistent as possible with data collection. All simulations have been developed in the same time period as surveyed in the field (6:00 to 8:00 p.m.), considering a preventive warm-up time to equalize adequately traffic flows deployed through O/D matrix.

Geometry modelling within the software editor considered the circulation rules provided for roundabouts, carefully implementing entry widths and ring size. The edited distances were inserted in line with the distances collected by the test vehicle, taking into account mainly the extent of the total influence area here considered. In particular, a georeferenced excerpt imported from the open-source database *OpenStreetMaps* was used as the starting geometry see Figure 5.14).

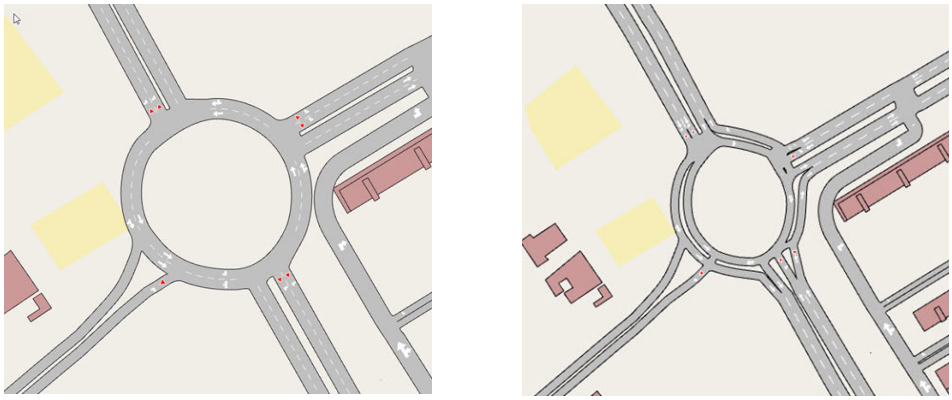

a) *b)*

Fig. 5.14: a) Standard multi-lane roundabout network model; b) Turbo-roundabout network model

Once the geometry has been completed, the centroids to insert the input traffic from O/D matrix have been defined. O/D matrices were differentiated in order to consider both light and heavy traffic as detected in field. Vehicle categories were also defined in terms of size and class (passenger cars, trucks) and kinematic and behavioral parameters.

Detectors needed to support generation of the second-by-second speed profiles were identified and localized along the possible vehicle paths through both roundabouts. Once the microsimulation ran by using the time scan per second, the trajectory data were extracted and processed using access database worksheets so that the simulated profiles could be generated both for the existing roundabout and the turbo roundabout.

The speed profiles were then used for estimating the instantaneous emissions by means of the VSP methodology. Aggregated emission data provided by the software have not been considered since they were not consistent with the purposes of the study. The Geoffrey E. Havers' statistic GEH as referred by (18) was used as joint measure to provide an overall view of the goodness of fit of the simulated traffic data to those observed in the field. This index calculates for each counting station:

(5.1)

$$GEH = \sqrt{\frac{2(y_{i,sim} - y_{i,obs})^2}{y_{i,sim} + y_{i,obs}}}$$

where $x_{i,obs}$ and $y_{i,sim}$ are the simulated and the observed values. It estimates an aggregated index by means of the following algorithm:

For i = m (number of counting stations)

If GEHi ≤ 5, then set GEHi = 1

Otherwise set GEHi = 0

Endif;

End for;

Let $GEH = \frac{1}{m}\sum_{i=1}^{m} GEH_i$

If GEH ≥ 85% then accept the model

Otherwise reject the model

Endif.

Thus, for each pair of simulated and observed values each GEH_i was verified. Based on current interpretation, since the deviation of the simulated values with respect to the measurement resulted smaller than 5% in at least 85% of the cases, then the model was accepted.

Calibration

Software calibration was carried out to obtain speed profiles consistent with those collected in the field in order to improve the accuracy of the emission estimates. A sensitivity analysis has been performed to identify the set of parameters more appropriate to improve the match between the observed and simulated speed - time profiles.

According to (16), the parameters considered were:

- *the maximum acceleration MA (m/s^2)*: vehicle attribute parameter which represents the highest acceleration that a vehicle can achieve under any driving circumstances in the network
- *the normal deceleration ND (m/s^2)*: vehicle attribute parameter which represents the maximum deceleration that a vehicle operates under normal conditions

Note that the two vehicle attributes of AIMSUN, namely the Maximum Acceleration and Normal Deceleration, have a default value of 3 m/s^2 a default value of 4 m/s^2, respectively. According to Anya et al (16) where AIMSUN was calibrated using analogous field-data to estimate emissions for urban arterials, the values of the 95^{th} (or 85^{th}) percentiles of the accelerations and deceleration distributions measured within the distance travelled by the test vehicle through the roundabout were used for calibration purposes. Thus, the following combinations have been examined:

- 95^{th} (or 85^{th}) percentile values of accelerations and decelerations extracted from each field-observed trajectory
- 95^{th} (or 85^{th}) percentile values of accelerations and decelerations extracted from all the field-observed trajectories experienced per driving direction
- 95^{th} (or 85^{th}) percentile values of accelerations and decelerations extracted from all the field-observed trajectories experienced by the test vehicle regardless of the driving direction

Before proceeding with the calculation of pollutant emissions using the VSP methodology, the observed and simulated speeds were compared.

The combinations of AIMSUN parameters as above introduced were considered for AB and BA driving directions (see Figure 5.15). The kinematic and behavioral parameters were extracted from each instantaneous speed profile detected in the field at the roundabout in Fig. 5.15a, so as to compare the results of microsimulation with the observed ones for each profile.

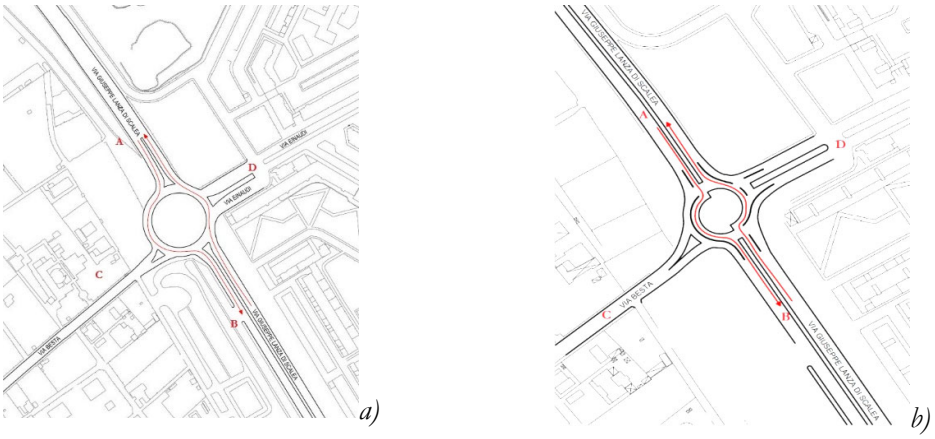

Fig. 5.15: Existing and turbo layouts considered for analysis

The simulated speed profiles for through movements in both directions under the default parameters and those calibrated with the 85th and 95th percentile values of the relevant parameters extracted from all the field-observed trajectories travelled by the test vehicle regardless of the driving direction were shown in the following figures (see Figures 5.16 to 5.18); the speed profiles observed in the field at the existing roundabout were reported in all the graphs for comparison purposes.

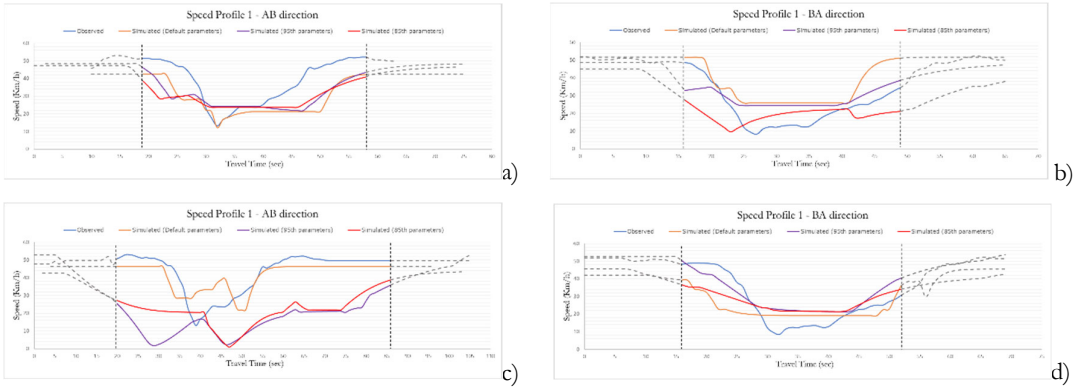

Fig. 5.16: Observed and simulated speed profiles under calibration with default, 85th and 95th percentile values of the relevant parameters): a) b) Speed Profile 1 for the standard roundabout; c) d) Speed Profile 1 for the turbo-roundabout.

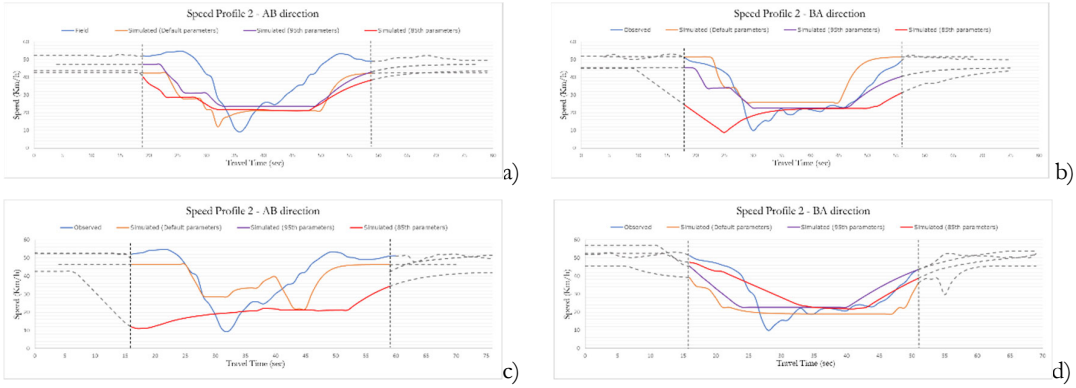

Fig. 5.17: Observed and simulated speed profiles under calibration with default, 85th and 95th percentile values of the relevant parameters: a) b) Speed Profile 2 for standard roundabout; c) d) Speed Profile 2 for the turbo-roundabout.

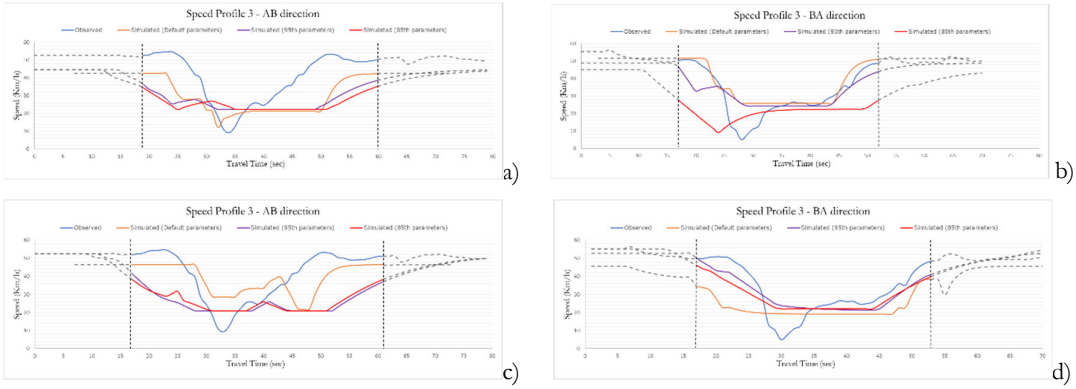

Fig. 5.18: Observed and simulated speed profiles under calibration with default, 85th and 95th percentile values of the relevant parameters: a) b) Speed Profile 3 for standard roundabout; c) d) Speed Profile 3 for the turbo-roundabout.

The GEH statistic as referred by (*18*) was used as joint measure to provide an overall view of the calibration, namely the goodness of fit of the simulated data to those observed in the field; see equation 1. Based on the analyzed speed profiles, each GEHi was verified for each pair of simulated and observed speed values.

Based on current interpretation since the deviation of the simulated values with respect to the measurement was smaller than 5% in at least 85% of the cases, then the model was accepted. Another goodness-of-fit measurement was employed to quantify the amount of error between two data sets, i.e. the Root Mean Squared Normalized Error (RMSNE) that measured the percentage deviation of the simulation output from the observed data (*18*). This statistic measures the percentage of the typical relative error, and it can be used to determine the width of the confidence intervals for the predictions.

The values of RMSNE resulted less than 15 percent, so it considered as acceptable for the purposes of this analysis. In particular highest RMSNE values were recorded for speed profiles

simulated starting from the default AIMSUN parameters (3.00 m/sec^2 for the maximum acceleration and 4 m/sec^2 for the normal deceleration), compared to results from speed profiles simulated using the 95th or 85th values of acceleration and deceleration extracted from the empirical distributions.

By way of example, Fig. 5.19 shows two scattergram plots used to compare the observed versus the simulated speeds both for standard layout that turbo-roundabout. Reference is done to calibration under the 95th values of the relevant parameters; similar results were obtained also for the other profiles so as to confirm the acceptability of the model calibration.

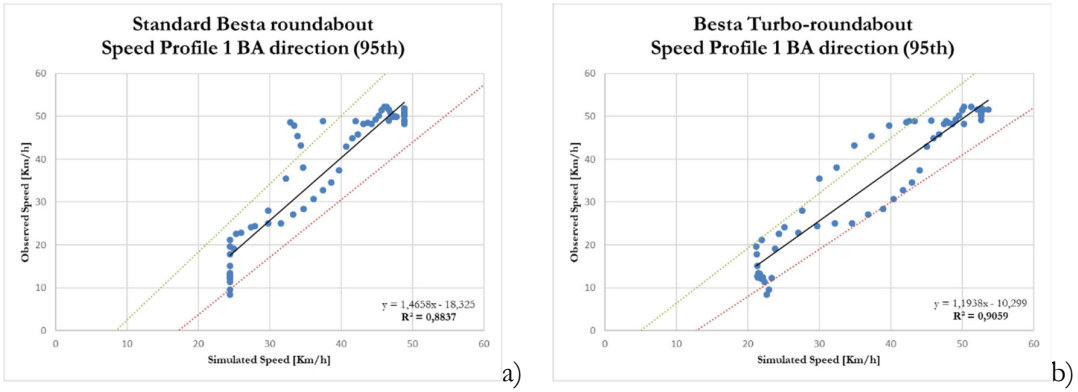

Fig. 5.19: Scattegram plot to compare simulated and observed speeds into a 95% confidence interval. a) standard roundabout b) turbo layout

The next step was to calculate VSP modes starting from simulated speed profiles for each direction and each layout.

Once the VSP modes were estimated, in hypothesis testing, the first step was to formulate the null hypothesis (H_0) for the two-tailed t-test as "there is no difference between the averages of the two distributions". Then data were analyzed to determine the probability associated with an alternative hypothesis (H_1) which will provide sufficient evidence to reject the null hypothesis. For this study, the null hypothesis stated that there is no difference between the averages of the samples of the VSP distributions between the observed and simulated VSP modes for the standard roundabout in each driving directions (AB or BA).

Tables 5.8 and 5.9 show the results of the t-test concerning profile 1 just a reference profile; the results of the KS test are also showed. In turn, Tables 5.10 and 5.11 show the result of the same test performed for the turbo-roundabout; however, the observed VSP modes concern the roundabout.

Table 5.8: Observed vs simulated VSP modes for roundabout (Speed Profile 1 AB direction)

VSP [Kw/ton]	distance [1]	μ_1[2]	μ_2[2]	t-value [3] (α = 0.05)	t_{crit}	p-t test	D[4]	p-KS test
Obs. vs Default	500 m	2.778	1.939	0.721	1.985	0.473	0.381	0.000
	250 m	2.280	1.694	0.331	1.991	0.742	0.325	0.022
Obs. vs 85th	500 m	2.778	1.862	0.841	1.991	0.403	0.500	0.000
	250 m	2.280	1.152	0.776	1.997	0.440	0.275	0.080
Obs. vs 95th	500 m	2.778	2.025	0.661	1.987	0.510	0.215	0.097
	250 m	2.280	0.959	0.816	1.992	0.417	0.225	0.231

[1] these values are differentiated both for the distance including cruising and the distance without cruising; [2] μ_{AB} and μ_{BA} stand for the mean values of the samples of the observations of each parameter in the two driving directions (i.e. AB and BA); [3] t-value is the result of the two tailed t-test which was done to compare the equality of the means μ_{AB} and μ_{BA} of samples of two populations with equal sample size; [4] D is the max difference between the cumulated distributions of the samples as given by the KS-test.

Table 5.9: Observed vs simulated VSP modes for roundabout (Speed Profile 1 BA direction)

VSP mode	distance [1]	μ_1[1]	μ_2[1]	$t_{\alpha=0.05}$ [2]	t_{crit}	P-T Test (α = 0.05)	D[3]	P-KS Test
Obs. vs Default	500 m	1.954	2.546	-0.457	1.981	0.648	0.288	0.006
	250 m	1.583	2.414	-0.482	1.990	0.631	0.286	0.029
Obs. vs 85th	500 m	1.954	1.328	0.775	1.983	0.440	0.196	0.095
	250 m	1.583	0.890	0.640	1.990	0.524	0.184	0.346
Obs. vs 95th	500 m	1.954	1.944	0.011	1.979	0.991	0.255	0.017
	250 m	1.583	2.161	-0.494	1.986	0.622	0.265	0.052

[1] these values are differentiated both for the distance including cruising and the distance without cruising; [2] μ_{AB} and μ_{BA} stand for the mean values of the samples of the observations of each parameter in the two driving directions (i.e. AB and BA); [3] t-value is the result of the two tailed t-test which was done to compare the equality of the means μ_{AB} and μ_{BA} of samples of two populations with equal sample size; [4] D is the max difference between the cumulated distributions of the samples as given by the KS-test.

Table 5.10: Observed vs simulated VSP modes for turbo-roundabout (Speed Profile 1 AB direction)

VSP mode	distance [1]	μ_1[1]	μ_2[1]	$t_{\alpha,n}$ [2]	t_{crit}	P-T Test (α = 0.05)	D[4]	P-KS Test
Obs. vs Default	500 m	2.778	2.404	0.266	1.980	0.790	0.306	0.006
	250 m	2.726	2.392	0.222	1.983	0.825	0.263	0.031
Obs. vs 85th	500 m	2.778	1.413	1.336	1.998	0.186	0.268	0.010
	250 m	2.726	1.126	1.604	1.993	0.113	0.316	0.005
Obs. vs 95th	500 m	2.778	1.390	1.302	1.993	0.197	0.258	0.014
	250 m	2.726	0.452	2.328	1.995	0.023	0.421	0.000

[1] these values are differentiated both for the distance including cruising and the distance without cruising; [2] μ_{AB} and μ_{BA} stand for the mean values of the samples of the observations of each parameter in the two driving directions (i.e. AB and BA); [3] t-value is the result of the two tailed t-test which was done to compare the equality of the means μ_{AB} and μ_{BA} of samples of two populations with equal sample size; [4] D is the max difference between the cumulated distributions of the samples as given by the KS-test.

Table 5.11: Observed vs simulated VSP modes for turbo-roundabout (Speed Profile 1 BA direction)

VSP mode	distance [1]	μ_1[1]	μ_2[1]	$t_{\alpha,n}$ [2]	t_{crit}	P-T Test (α = 0.05)	D[4]	P-KS Test
Obs. vs Default	500 m	1.954	1.899	0.052	1.976	0.958	0.327	0.001
	250 m	1.553	0.161	0.959	1.993	0.341	0.539	0.000
Obs. vs 85th	500 m	1.954	1.814	0.183	1.988	0.855	0.182	0.161
	250 m	1.553	0.156	1.144	2.010	0.258	0.385	0.004
Obs. vs 95th	500 m	1.954	2.248	-0.309	1.978	0.758	0.177	0.217
	250 m	1.553	0.795	0.501	1.992	0.618	0.500	0.000

[1] these values are differentiated both for the distance including cruising and the distance without cruising; [2] μ_{AB} and μ_{BA} stand for the mean values of the samples of the observations of each parameter in the two driving directions (i.e. AB and BA); [3] t-value is the result of the two tailed t-test which was done to compare the equality of the means μ_{AB} and μ_{BA} of samples of two populations with equal sample size; [4] D is the max difference between the cumulated distributions of the samples as given by the KS-test.

Table 5.12: Comparison between simulated VSP modes (AB and BA directions) for turbo-roundabout

VSP mode (Speed Profile 1)	distance [1]	μ_1[1]	μ_2[1]	$t_{\alpha,n}$ [2]	t_{crit}	P-T Test (α = 0.05)	D[4]	P-KS Test
Default (AB) vs Default (BA)	500 m	2.404	1.899	0.396	1.978	0.693	0.618	0.000
	250 m	2.392	1.553	0.509	1.986	0.612	0.765	0.000
85th AB vs 85th BA	500 m	1.413	1.814	-0.971	1.973	0.333	0.165	0.155
	250 m	1.126	0.156	1.700	1.989	0.093	0.348	0.005
95th (AB) vs 95th (BA)	500 m	1.390	2.248	-1.122	1.979	0.264	0.237	0.015
	250 m	0.452	0.795	-0.330	2.014	0.743	0.306	0.020
VSP mode (Speed Profile 2)	**distance [1]**	**μ_1[1]**	**μ_2[1]**	**$t_{\alpha,n}$ [2]**	**t_{crit}**	**P-T Test (α = 0.05)**	**D[4]**	**P-KS Test**
Default (AB) vs Default (BA)	500 m	2.404	1.899	0.396	1.978	0.693	0.618	0.000
	250 m	2.373	0.161	1.282	1.993	0.204	0.727	0.000
85th AB vs 85th BA	500 m	1.499	2.114	-0.930	1.979	0.354	0.351	0.000
	250 m	2.436	1.223	1.339	2.008	0.187	0.507	0.000
95th (AB) vs 95th (BA)	500 m	2.002	2.019	-0.017	1.977	0.987	0.249	0.019
	250 m	1.187	1.198	-0.007	1.989	0.994	0.265	0.085
VSP mode (Speed Profile 3)	**distance [1]**	**μ_1[1]**	**μ_2[1]**	**$t_{\alpha,n}$ [2]**	**t_{crit}**	**P-T Test (α = 0.05)**	**D[4]**	**P-KS Test**
Default (AB) vs Default (BA)	500 m	2.404	1.899	0.396	1.978	0.693	0.618	0.000
	250 m	2.364	1.055	0.671	1.993	0.504	0.664	0.000
85th (AB) vs 85th (BA)	500 m	1.712	1.996	-0.351	1.977	0.726	0.215	0.054
	250 m	0.984	1.179	-0.174	1.991	0.862	0.349	0.009
95th (AB) vs 95th (BA)	500 m	1.707	2.343	-0.760	1.977	0.449	0.211	0.062
	250 m	0.483	1.193	-0.592	1.994	0.556	0.301	0.036

[1] these values are differentiated both for the distance including cruising and the distance without cruising; [2] μ_{AB} and μ_{BA} stand for the mean values of the samples of the observations of each parameter in the two driving directions (i.e. AB and BA); [3] t-value is the result of the two tailed t-test which was done to compare the equality of the means μ_{AB} and μ_{BA} of samples of two populations with equal sample size; [4] D is the max difference between the cumulated distributions of the samples as given by the KS-test. Note that AB and BA are directions in Fig. 17.

The same tests were used to study any discrepancy between the simulated VSP distributions in AB and BA directions for speed profile and each roundabout; in this regard see tables 5.12 and 5.13.

Table 5.13: Comparison between simulated VSP modes (AB and BA directions) for standard roundabout

VSP mode (Speed Profile 1)	distance [1]	μ_1[1]	μ_2[1]	$t_{\alpha,n}$ [2]	t_{crit}	P-T Test (α = 0.05)	D[4]	P-KS Test
Default (AB) vs Default (BA)	500 m	1.939	2.546	-0.484	1.982	0.629	0.514	0.000
	250 m	1.694	2.414	-0.371	1.988	0.711	0.328	0.013
85th (AB) vs 85th (BA)	500 m	1.862	1.328	0.864	1.976	0.389	0.304	0.001
	250 m	1.152	0.890	0.273	1.992	0.786	0.335	0.001
95th (AB) vs 95th (BA)	500 m	2.025	1.944	0.098	1.976	0.922	0.266	0.009
	250 m	0.959	2.161	-0.942	1.993	0.350	0.482	0.000
VSP mode (Speed Profile 2)	**distance** [1]	μ_1[1]	μ_2[1]	$t_{\alpha,n}$ [2]	t_{crit}	**P-T Test (α = 0.05)**	**D**[4]	**P-KS Test**
Default (AB) vs Default (BA)	500 m	1.939	2.546	-0.484	1.982	0.629	0.514	0.000
	250 m	1.706	2.283	-0.260	1.996	0.796	0.285	0.063
85th (AB) vs 85th (BA)	500 m	1.748	1.591	0.275	1.975	0.783	0.222	0.028
	250 m	0.776	1.627	-0.930	1.998	0.356	0.406	0.002
95th (AB) vs 95th (BA)	500 m	2.017	1.926	0.116	1.976	0.908	0.293	0.002
	250 m	1.400	0.953	0.309	1.991	0.758	0.395	0.003
VSP mode (Speed Profile 3)	**distance** [1]	μ_1[1]	μ_2[1]	$t_{\alpha,n}$ [2]	t_{crit}	**P-T Test (α = 0.05)**	**D**[4]	**P-KS Test**
Default (AB) vs Default (BA)	500 m	1.939	2.546	-0.484	1.982	0.629	0.514	0.000
	250 m	1.739	2.356	-0.306	1.991	0.760	0.282	0.050
85th (AB) vs 85th (BA)	500 m	1.640	1.647	-0.014	1.975	0.989	0.245	0.010
	250 m	1.451	0.077	1.540	1.990	0.128	0.309	0.024
95th (AB) vs 95th (BA)	500 m	1.718	2.133	-0.538	1.981	0.592	0.289	0.003
	250 m	1.646	1.718	-0.059	1.996	0.953	0.400	0.001

[1] these values are differentiated both for the distance including cruising and the distance without cruising; [2] μ_{AB} and μ_{BA} stand for the mean values of the samples of the observations of each parameter in the two driving directions (i.e. AB and BA); [3] t-value is the result of the two tailed t-test which was done to compare the equality of the means μ_{AB} and μ_{BA} of samples of two populations with equal sample size; [4] D is the max difference between the cumulated distributions of the samples as given by the KS-test. Note that AB and BA are directions in Fig. 17.

Based on the results of the t-test above it cannot conclude that a significant difference exists between the two driving directions especially with reference to the 95th percentile values of accelerations and decelerations extracted from each field-observed trajectory experienced per driving direction at each roundabout. Note that the KS test did not return the same analytical outcome.

The simulated VSP modes closer to what was detected in the field can be seen in Figure 5.20 where, by way of example, simulation ran using the 95th percentile values of accelerations and decelerations extracted from each field-observed trajectory experienced at each roundabout. Calibrating the parameters with 95th percentile values tended to be more realistic in producing a VSP distribution more consistent with the VSP distribution from field-collected vehicle activity and in reducing the errors in emissions estimates.

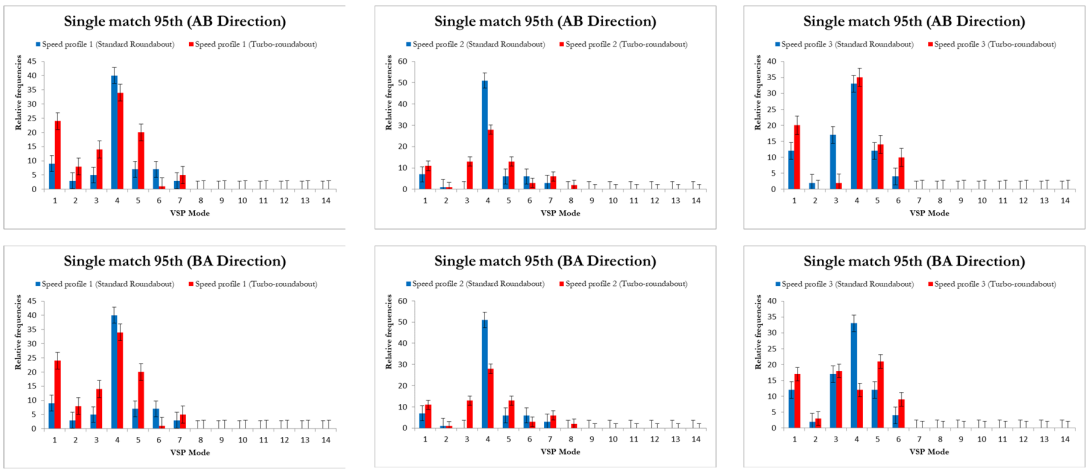

Fig. 5.20: VSP mode distributions for standard and turbo roundabout

Pollutant emissions from VSP modes with scanning per second were calculated based on emission rates by VSP mode for the light passenger vehicles diesel (see in this regard the previous chapter 3). Grams per second of CO_2, CO, (NO_x+ HC) have been calculated for each speed profile here examined.

It should be noted that calibration under the 85th and 95th values of acceleration and deceleration was also combined to the AIMSUN behavioral parameters (e.g. reaction time and minimum gap) having influence on gap-acceptance behavior in roundabouts as done in the previous chapter 4 based on (19). However, it did not significantly improve the accuracy of the vehicle activity simulated under the default parameters provided by AIMSUN software and then the accuracy of the emission estimates; for this reason, it was neglected in this explorative study. This aspect was not surprising as the existing roundabout presents a standard configuration in terms of geometry and alignments of the entry approaches.

At last, Fig 5.21 to 5.23 shows the mean emissions values of CO_2, CO, (NO_x+ HC) in grams for each roundabout calculated to describe the overall environmental performance of each roundabout.

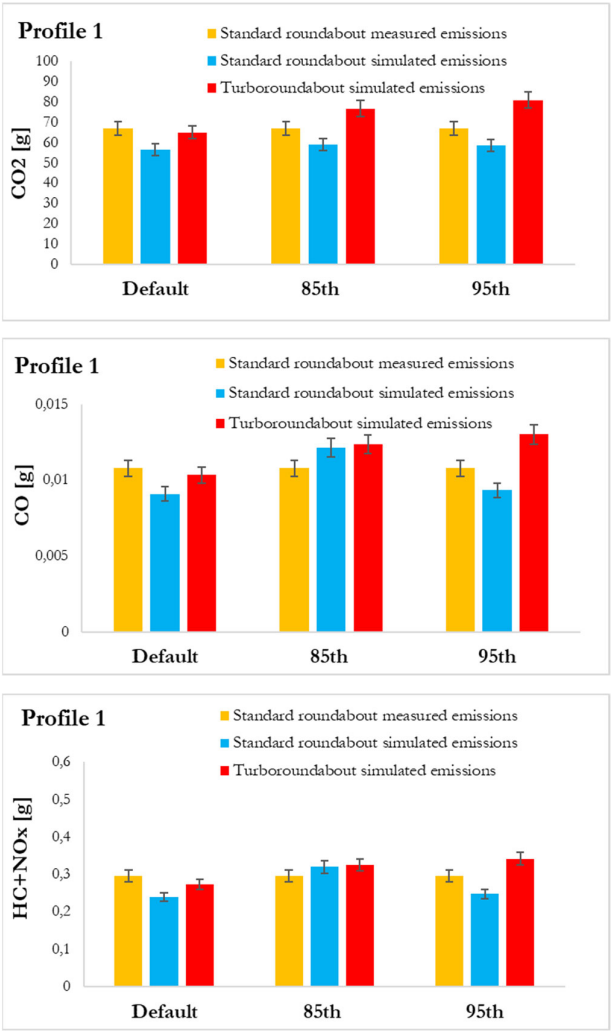

Fig. 5.21: Roundabout vs turbo roundabout emissions (profile 1)

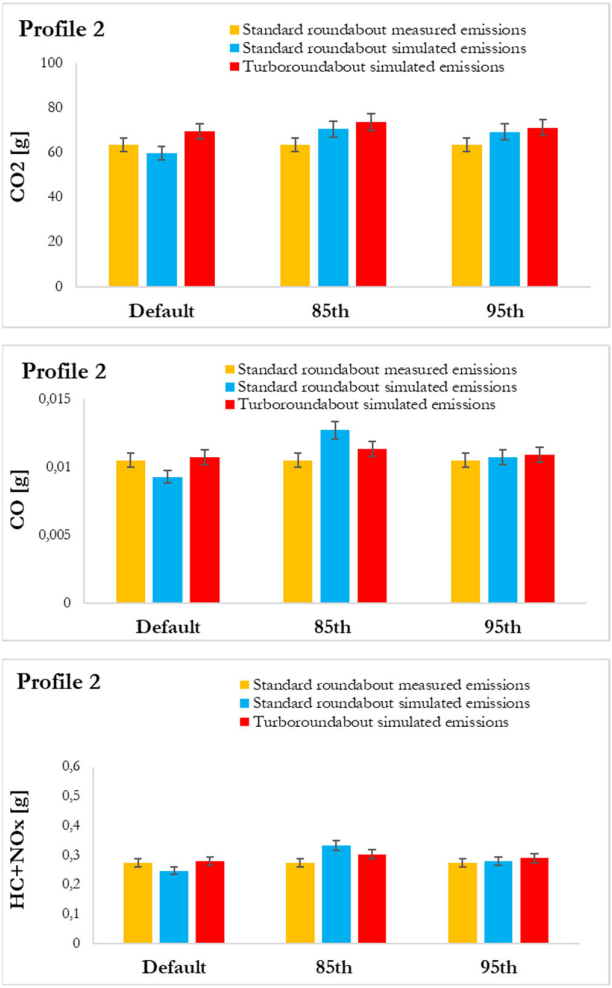

Fig. 5.22 Roundabout vs turbo roundabout emissions (profile 2)

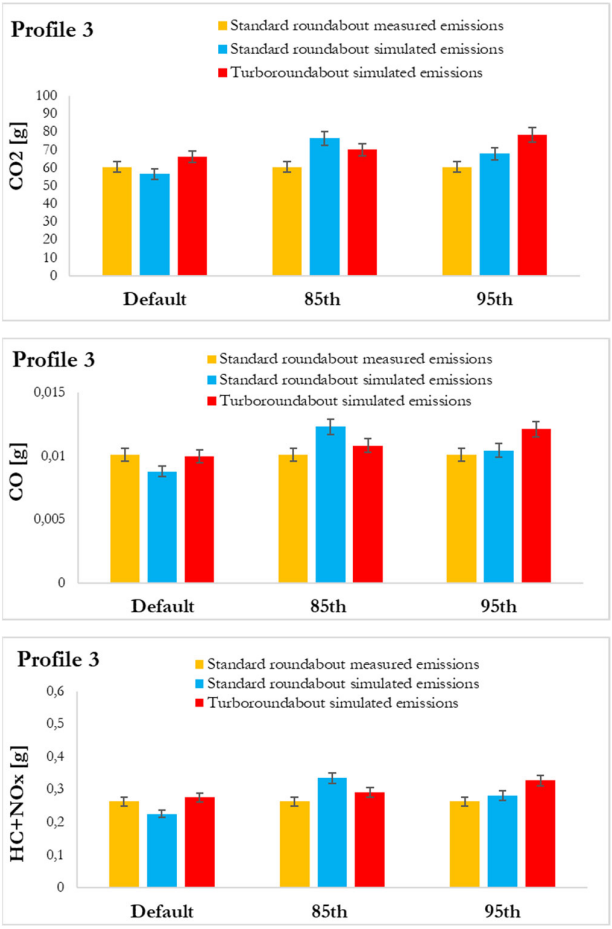

Fig. 5.23: Roundabout vs turbo roundabout emissions (profile 3)

According to literature (13) the turbo-roundabout accentuates the tendency to traffic calming compared to the traditional layout of two-lane roundabout distinguishing itself for slightly lower speeds and instantaneous speed profiles that have one or more stops with more frequency during the generic user travel. This aspect also denotes a more regular distribution of VSP Mode, which results in the distance of vehicles less subject to sharp variations in acceleration and deceleration.

The results in above figures just represent a first exam of AIMSUN to simulate second-by-second speed profiles used to estimate emissions. More experience under different traffic conditions is needed to obtain more generalizable results since significant differences still can be returned when each single trajectory is considered. Despite this, 95th percentile parameters calibration is more robust than the 85th one in most of cases to be effective in producing a VSP distribution more consistent with the VSP distribution from field-collected vehicle activity and in reducing the errors in emissions estimates.

Conclusions

It should be noted that the case study shows the first results aimed at addressing the feasibility of converting existing roundabouts into turbo-roundabouts and their impacts from an environmental perspective. Further examples could improve their generalization. However, major efforts consisted in the use of the Vehicle Specific Power (VSP) methodology which employs speed trajectories to estimate the second-by-second emissions generated from vehicles and the AIMSUN software to simulate speed-travel time profiles through the roundabouts. For a first characterization of the emissive phenomenon reference was made to an existing two-lane roundabout in Palermo, Italy, where vehicle trajectory data along with traffic volumes were collected. model calibration was also made based on the comparison between the individual GPS trajectories on-field collected and second-by-second speed profiles derived from AIMSUN.

In order to quantify the emission impacts and compare the emissions from vehicles moving through the two-lane roundabout and the turbo-roundabout, pollutant emissions were estimated from the VSP modal emission rates, and the distribution of time spent in each VSP mode from the speed profiles that were simulated in AIMSUN. Although the travel times spent in acceleration were on average higher through the turbo-roundabout than the two-lane roundabout, the conversion of a two-lane roundabout to a turbo-roundabout resulted in a comparable amount of emissions, primarily due to the low volume conditions observed in the field where the two-lane roundabout would still be the more appropriate solution. The main finding provided from this pilot study is referred to the positive potential of a novel attitude in the conceptualization and performance evaluation of road units in order to align urban infrastructural projects with the worldwide shared long-term ambitions for a low-emission mobility.

References

1. Fortuijn, L. G. H. (2009). Turbo Roundabouts: Design Principles and Safety Performance. *Transportation Research Record* 2096(1), pp. 16-24
2. Tollazzi, T. (2015). Alternative Types of Roundabouts: An Informational Guide. *Springer*, New York
3. Macioszek, E. (2015) The road safety at turbo roundabouts in Poland. *Archives of Transport* 33(1), pp. 57-67
4. Mauro, R., Branco, F. (2010) Comparative analysis of compact multilane roundabouts and turbo-roundabouts. J. *Transp. Eng.* 136, pp. 316–322
5. Giuffrè O., Guerrieri, M., Granà A. (2009). Evaluating capacity and efficiency of turbo-roundabouts. *Transportation Research Board 88th Annual Meeting*, Washington DC, United States, January 11-15, 2009
6. Guerrieri, M., Corriere, F., Lo Casto, B., Rizzo, G.: A model for evaluating the environmental and functional benefits of "innovative" roundabouts. Transportation Research. Part D, *Transport and Environment* 39, pp. 1-16, doi: 10.1016/j.trd.2015.05.004 (2015)
7. Andrighettoni, C. and R., Mauro. Un nuovo tipo di incrocio a rotatoria [A new type of roundabout] – *Le Strade, Ed. La Fiaccola*, Milano, vol. 1/2, N.1434, 2008, pp. 17-23. ISSN: 0373-2916.
8. Andrighettoni, C. and R., Mauro. Un nuovo tipo di incrocio a rotatoria [A new type of roundabout] – *Le Strade, Ed. La Fiaccola*, Milano, vol. 1/2, N.1434, 2008, pp. 17-23. ISSN: 0373-2916.
9. Džambas T., Ahac S., Dragčević V. (2017) Geometric design of turbo roundabouts. *Tehnicki Vjesnik* 24(1): 309-318 DOI: 10.17559/TV-20151012162141
10. Salamati, K., Coelho, M., Fernandes, P., Rouphail, N. M., Frey, H.C., Bandeira, J. (2014) Emission Estimation at Multilane Roundabouts: Effect of Movement and Approach Lane, *Transportation Research Record* 2389, pp. 12-21
11. Coelho, M. C., Farias, T. L., Rouphail, N. M. (2006) Effect of roundabout operations on pollutant emissions. *Transportation Research Part D: Transport and Environment* 11(5), 333–343

12. Vasconcelos, L., Silva, A.B., Seco, Á.M., Fernandes, P., Coelho M.C. (2014) Turbo roundabouts Multicriterion Assessment of Intersection Capacity, Safety, and Emissions. *Transportation Research Record* 2402, pp. 28-37
13. Fernandes, P., Pereira, S. R., Bandeira, J. M., Vasconcelos, L., Bastos Silva, A., Coelho, M.C. (2016) Driving around turbo-roundabouts vs. conventional roundabouts: Are there advantages regarding pollutant emissions? *International Journal of Sustainable Transportation*, 10:9, pp. 847-860
14. Dodi, D. (2019). Il concetto di turbo rotatoria. Un'applicazione progettuale [The turbo roundabout concept. a design application] *Bachelor's Thesis in Urbanistic and City Science*, University of Palermo, Italy
15. AIMSUN Dynamic Simulator User Manual 8, *Transport Simulation System (TSS)* (2011).
16. Anya, A.R., Rouphail, N., Frey, H. C., Schroeder, B.J. (2014) Application of AIMSUN Microsimulation Model to Estimate Emissions on Signalized Arterial Corridors. *Transportation Research Record Journal of the Transportation Research Board* 2428(2428), 75-86.
17. Jiménez-Palacios, J.L. (1999) Understanding and Quantifying Motor Vehicle Emissions with Vehicle Specific Power and TILDAS Remote Sensing. Ph.D. Thesis, Massachusetts *Institute of Technology, Department of Mechanical Engineering.*
18. Barceló J. (2010) Fundamentals of Traffic Simulation, *Springer*: London.
19. Giuffrè, O., Granà, A., Tumminello, M.L., Sferlazza, A. (2018) Capacity-based calculation of passenger car equivalents using traffic simulation at double-lane roundabouts. *Simulation Modelling Practice and Theory* 81, 11-30.

Chapter 6

On-road emission monitoring in rural roundabouts. A case study in Aveiro, Portugal

The background

The research activity highlighted in this work was focused on traffic pollutant emissions in urban roundabouts. In order to further explore these topics, a cooperation with the Centre for Mechanical Technology and Automation at University of Aveiro, Portugal, was carried out in 2019 and 2021.

The main goal of this period of study abroad was to compare different rural roundabouts in terms of traffic performance, pollutant emissions and noise based on an integrated empirical approach aimed at testing the impact caused by carbon dioxide and nitrogen oxides (NO_x) measured by a PEMS, and noise through equivalent continuous A-weighted sound level (L_{eq}); differences in traffic volumes (approaching, conflicting, and exiting traffic flows), volume-to-capacity ratio (V/C) and the specific roundabout layouts were considered. About this last aspect, a compact two-lane, a single-lane and a multi-lane roundabout were selected outside the urban area of Aveiro as case studies.

Methodology overview

The research team collected experimental data on noise, vehicle exhaust emissions, dynamic and engine, as well as overall congestion levels through three roundabouts in Aveiro, Portugal. Input data such as approaching (Q_{in}), conflicting (Q_{conf}) and exiting (Q_{out}) traffic volumes, and queue length were collected by video cameras installed at the studied locations. At the same time, a sound level meter was installed at the approach area of each roundabout to measure the equivalent noise sound level. On-road measurements of a light duty diesel vehicle included PEMS[1] components for volumetric fractions of CO_2 and NO_X, and an OBD interface for vehicle activity and engine data. The relationship between congestion level of the roundabouts and the probability of occurrence of each speed profile was established using discrete choice models (1); then, the emissions, noise and V/C ratio in Single-Lane roundabout (SL), Compact-

[1] Portable emission measurement system.

Two-Lane roundabout (CTL), and Multi-Lane (ML) roundabout were compared. Note that the acronyms introduced above will be used hereinafter to denote the roundabouts here examined.

The case study

Three roundabouts located on the N-235 (SL) and N-109 (CTL and ML) national roads near Aveiro (Portugal) exhibiting high traffic volumes were selected. The through movements from the East to West approach in the SL, and South to North approach both for CTL and ML layouts were examined. The major road approaching the ML is a two-lane entry from 120 m to the yield lane (see Figure 6.1). Concerning slope, all layouts are located in flat areas and for this reason a 0% value was considered. The speed limit in CTL and ML is 50 km/h, while in SL is 60 km/h.

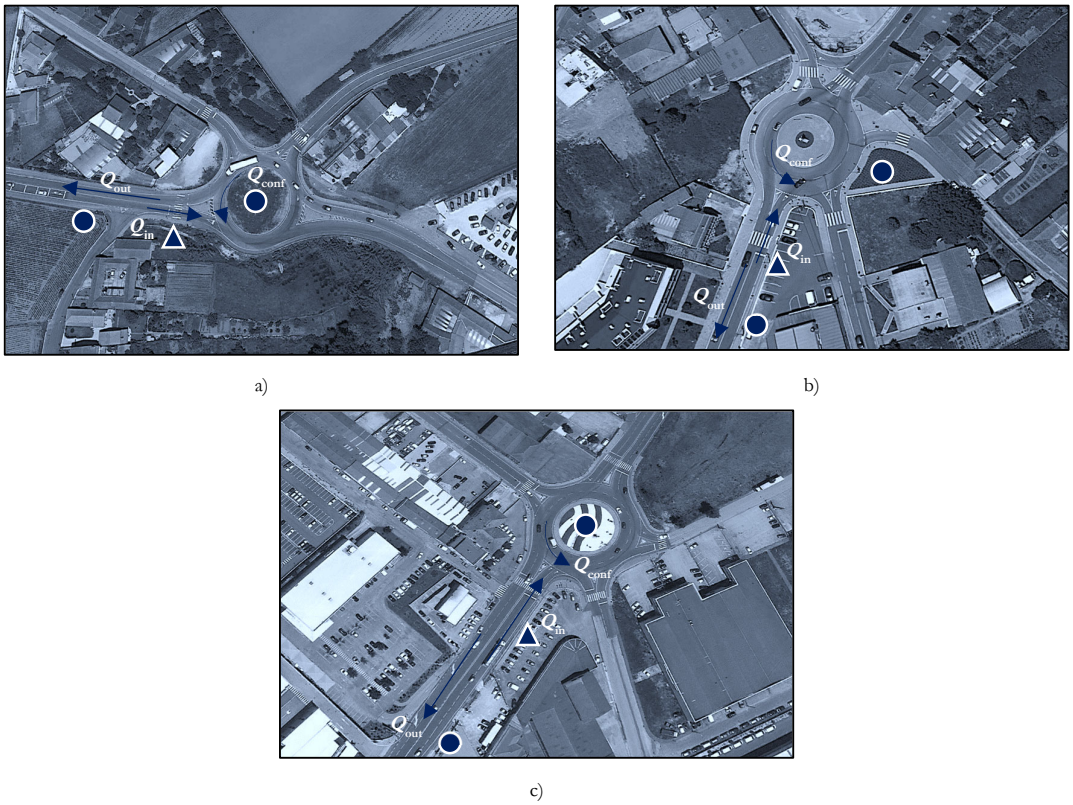

Figure 6.1: Aerial View of the three roundabouts, Aveiro, Portugal: a) Single-Lane; b) Compact-Two-Lane; and c) Multi-Lane.

In the following Table 6.1 the geometric and operational characteristics of the examined roundabouts are presented.

Table 6.1: Geometric and operational features of the three surveyed roundabouts

	Entering Speed (km/h)	Circulating Speed (km/h)	Circulating Width (m)	Inscribed Diameter (m)	Central Island (m)	$Q_{in} + Q_{out}$ (vph)	Heavy Duty Vehicles (%)
SL	58.6	28.8	6	44	32	700 – 1,700	~10%
CTL	44.5	24.2	9.5	36	18	300 – 1,400	~2%
ML	40.1	29.2	10	55	35	700 – 2,200	~5%

Data collection

On-road emissions

The measured instantaneous engine and speed profiles were calculated from experimental data on vehicle dynamics using a light duty diesel vehicle (LDDV) as test vehicle complying with Euro VI emission standard and equipped with a GPS Travel Recorder and OBD-II ELM327 Bluetooth.

The 3DATX ParSYNC integrated PEMS (2)was used to record on-road emissions. The device used a single unheated sample line which directs the sample flow through a chiller to remove water vapor before entering the unit here considered. This lightweight PEMS measures both CO_2 (in volume fraction with a range of 0 – 20%), and NO/NO_2 (with a range of 0 – 5,000 ppm) at a frequency of 1 Hz by using a replaceable GasMOD™ Sensor Cartridges for both cases. Previous studies have confirmed the goodness of integrated PEMS as a tool for collecting emission data from LDV (3).

To ensure the accuracy of PEMS measurements, routine calibrations of pollutant analyzers (controlling for zero and span drift once per trip) were conducted using the UN 1956 gas mixture. Emissions were measured only in hot conditions, after a 30-minute preconditioning period to let PEMS reach all the set-points.

A Bluetooth OBD-II was connected to the car's OBD socket to collect - with 1 Hz frequency parameters such as the OBD speed - the mass air flow (MAF), the fuel flow rate (FFR), the revolutions per minute (RPM), the manifold absolute pressure (MAP), the intake air temperature (IAT), the engine load, the barometric pressure, and the engine volumetric efficiency. At the same time, a temperature/pressure sensor monitored ambient temperature and humidity, and a QSTARZ GPS Travel Recorder logged vehicle position and elevation.

Data collections were conducted during three weeks between June and July 2019 in weekdays (Monday to Friday). Test sessions included several time slots from 7:00AM to 10:00PM. The test drivers respected the national law concerning the roundabout driving. A total of 200 travel runs for each through movement were performed for this study (approximately 140 km of road

coverage over the course of 5 h). These series of measurements were sufficient to enable the estimation of a 95% confidence interval (4). The average temperatures observed for the studied locations were from 18ºC to 22ºC, while humidity range was 60% and 90%. All driving sessions took place in dry and windless (< 5 m/s) weather. Exhaust emissions were measured over a roundabout influence area of 680 m, consisting of 350 m upstream the yield line.

Noise and traffic data

Entry, exit and conflicting traffic volumes, queue length, and number of vehicle stops were gathered from videotapes installed at the surveyed intersections (Figure 6.1). The first camera captured all the vehicle paths through the roundabouts, while the second camera recorded the queue lengths and idle time at the selected movements. The values of approaching (Q_{in}), conflicting (Q_{conf}) and exiting (Q_{out}) traffic volumes were obtained for slots of 15 min, as well as the number of drivers that experienced no stop, one stop, and multiple stops speed profiles through the roundabouts (5). Noise data were collected using a sound level meter (Class 1 instrument) RION-NL-52. Before each recording, the instrument was balanced using a sound calibrator RION -NC-74 that gives an output noise signal with a sound level pressure equal to 94 dB, frequency equal to 1,000 Hz. Taking into account possible ground reflection effects, sound level in each location was equipped by a tripod 1.5 m high. The distance between sound level meter and road axis for SL, CTL and ML was 1.9 m, 1.9 m and 1.7 m, respectively. More than 27 hours of video and noise data were collected from three roundabouts (106 data slots of 15-min).

Experimental data analysis

Before data processing as done by (6) (7), all the signals from PEMS, OBD and GNSS data were aligned and data errors were removed. Typical errors included OBD speed, and engine RPM values that were no longer being updated, negative NO and NO_2 values from PEMS and strange events detected during noise measurements.

The measured speed profiles at all roundabouts were extracted and then separated in order to assess their specific characteristics as collected in field (8). For a driving style characterization of the PEMS runs, the relative positive acceleration (RPA) was used (9). This acceleration-based metric is recognized to be a good measure of different driving behaviors, and it is computed using positive acceleration from each trip by means of the following equations (9).

$$a_i = \frac{v_{i+1} - v_{i-1}}{2 \times 3.6} \quad (6.1)$$

where:

- a_i - acceleration in the second of travel i (m.s^{-2})
- v_{i+1} - vehicle instantaneous speed in the second of travel i +1 (km/h);
- v_{i-1} - vehicle instantaneous speed in the second of travel i -1 (km/h).

$$RPA = \frac{\sum_i \frac{v_i}{3.6} \times a_i^+}{d} \quad (6.2)$$

where:

- RPA - Relative Positive Acceleration (m/s^2);
- a_i^+ - positive values of the acceleration for the second of travel i (m/s^2);
- d - Total distance of the trip (m).

To assign one of three speed profiles (no stop, one stop and multiple stops), a process of discrete choice was used; it was based on stochastic processes where the decision maker makes a choice that optimizes the speed profiles distribution (1). A multinomial logistic regression model (MLRM) was applied to predict the probability of occurrence of each speed profile at SL, CTL and ML based on the collected data set. The expressions for the probability of occurrence of different speed profiles are below presented; see also (1) (5). The β parameters were estimated from measured data and calibrated to optimize the utility function for each roundabout with the collected traffic conditions.

$$P_n(Y = P_I) = \frac{1}{1 + e^{\beta 2,0 + \beta 2,1Q} + e^{\beta 3,0 + \beta 3,1Q}} \quad (6.3)$$

$$P_n(Y = P_{II}) = \frac{e^{\beta 2,0 + \beta 2,1Q}}{1 + e^{\beta 2,0 + \beta 2,1Q} + e^{\beta 3,0 + \beta 3,1Q}} \quad (6.4)$$

$$P_n(Y = P_{III}) = \frac{e^{\beta 3,0 + \beta 3,1 Q}}{1 + e^{\beta 2,0 + \beta 2,1Q} + e^{\beta 3,0 + \beta 3,1Q}} \quad (6.5)$$

where:

P_I – Proportion of vehicles that experienced no stop speed profile;

$\beta_{2,0}$ – Intercept for the outcome of one stop speed profile;

$\beta_{2,1}$ – Coefficient for outcome of multiple stop speed profile;

$\beta_{3,0}$ – Intercept for outcome of multiple stops speed profile;

$\beta_{3,1}$ – Coefficient for outcome of multiple stops speed profile;

P_{II} – Proportion of vehicles that experienced one stop speed profile;
P_{III} – Proportion of vehicles that experienced multiple stops speed profile.

The method suggested by the Regulatory Information 40 CFR 86.144 for exhaust emissions was used to calculate the pollutant mass at each second (10). Starting from exhaust flow rates and exhaust gas concentrations, the emission rates of NO, NO_2 and CO_2 (mass per time unit) were estimated.
Since the mass air flow (MAF) was not reported by electronic control unit (ECU), it was obtained from the revolution per minute (RPM), the manifold absolute pressure (MAP), and the intake air temperature (IAT) by means of the speed density method expressed as follows:

$$M_{\text{air}} = MW_{\text{air}} \frac{P_{\text{MAP}} - \frac{P_B}{C_{\text{engine}}} \times V_{\text{engine}} \left(\frac{S_{\text{engine}}}{120}\right)}{R(T_{\text{intake}} + 273.15)} \eta_{\text{engine}} \qquad (6.6)$$

where:

- M_{air} – Mass air flow rate (g/s);
- MW_{air} – Molecular weight of the air (28.9 g/mol);
- P_{MAP} – MAP (kPa);
- P_B – Barometric pressure (kPa);
- C_{engine} – Engine compression ratio (dimensionless);
- V_{engine} – Engine size (L);
- S_{engine} – Engine speed in revolutions per minute (rpm);
- η_{engine} – Engine volumetric efficiency (dimensionless);
- R – Universal gas constant (8.314 J/mol/K);
- T_{intake} – IAT (ºC).

The generic form of Equation 6.6 can be used to obtain the exhaust the mass flow rate using the available data displayed by the electronic control unit:

$$\dot{m}_{\text{exhaust}} = \dot{m}_{\text{air}} + \dot{m}_{\text{fuel}} \qquad (6.7)$$

where:

- $\dot{m}_{\text{exhaust}}$ - exhaust mass flow rate (g/s);
- $\dot{m}_{\text{air}}$ - mass air flow rate (g/s);

- $\dot{m}_{\text{fuel}}$ - fuel flow rate (g/s).

According to (10), CO_2 and NO^2_X mass emission rates were estimated by using the following expressions:

$$m_{CO_2} = \dot{V}_{\text{exhaust}}\, \rho_{CO_2} X_{CO_2} \quad (6.8)$$

$$m_{NO_X} = \dot{V}_{\text{ex}}\, \rho_{NO_X} X_{NO_X} \frac{1}{1-0.0047(H-75)} \quad (6.9)$$

where:

- $\dot{V}_{\text{exhaust}}$ - exhaust volumetric flow rate (corrected to standard conditions) (m^3/s);
- ϱ_{CO2} - density of CO_2 at the standard conditions (1.830 kg/m^3);
- X_{CO2} - volume fraction of CO_2 measured by PEMS (%).
- ρ_{NOX} - Density of NO_X at the standard conditions (1.913 kg/m^3);
- X_{NOX} - Volume fraction of NO_X measured by PEMS (ppm);
- H – Humidity (%).

The hourly emissions generated by vehicles entering a generic roundabout is expressed by the following equation (1) (5):

$$E_j = Q_{\text{in}}\left(E_{\text{I,j}} \times P_I + E_{\text{II,j}} \times P_{\text{II}} + E_{\text{III,j}} \times P_{\text{III}}\right) \quad (6.10)$$

where:

- E_j - predicted emissions $j \in J$, $J = \{CO_2, NO_X\}$ (g);
- Q_{in} - number of approaching vehicles (vph);
- $E_{\text{I, j}}$ - predicted emissions per vehicle associated with no stop speed profile (g);
- P_{I} - proportion of vehicles that experienced no stop speed profile;
- $E_{\text{II, j}}$ - predicted emissions per vehicle associated with one stop speed profile (g);
- P_{II} - proportion of vehicles that experienced one stop speed profile;
- $E_{\text{III, j}}$ - predicted emissions per vehicle associated with multiple stops speed profile (g);

[2] NOx corresponds to the sum of concentration signals for NO and NO_2.

- P_{III} - proportion of vehicles that experienced multiple stops speed profile.

To conduct noise measurements with a sound level meter, the semi-dynamical model of Quartieri et. al. (11) was used. This model was calibrated to estimate the equivalent continuous A-weighted sound level for a specific lane by the traffic volumes and the vehicle average speed.

$$L_{eq}^{1h} = 10\log[V_{LDV} + n_V \times V_{HDV}] + L_{w,i} - 20\log(d) - 46.563 \qquad (6.11)$$

Where:

- V_{LDV} - hourly LDV[3] volumes (vph);
- n_V - equivalent acoustic factor that represents the number of LDV that produce the same sound energy of one HDV[4];
- V_{HDV} - hourly HDV volumes (vph);
- $L_{w,i}$ - source power level of LDV (dBA);
- d - Distance between the observation point and the road axis (m).

The equivalent acoustic factor depends on the vehicle speed and HDV driving state such as cruising, acceleration, and deceleration. The source power level ($L_{w,i}$) was obtained by using the following expression (11):

$$L_{w,i} = \begin{cases} 82, \text{ if } v < 11.5\,, \\ \alpha_L + \beta_L\, log(v)\,, \text{ otherwise} \end{cases} \qquad (6.12)$$

where:

- v - average vehicle speed (km/h);
- a_L - 53.6 ± 0.3 dBA (11);
- β_L - 26.8 ± 0.2 dBA (11).

The final step was to compute the total hourly equivalent continuous A-weighted sound level in order to take into consideration the effect of all approaching and exiting lanes at the sampled roundabouts:

[3] Light Duty Vehicle
[4] Heavy Duty Vehicle.

$$L_{eq,tot}^{1h} = 10\,log\left(\sum_{i=1}^{t} 10^{\frac{L_{eq,i}^{1h}}{10}}\right) \quad (6.13)$$

where:

- $L_{eq,tot}^{1h}$ - total hourly equivalent continuous A-weighted sound level (dBA)
- t - number of the approaching and exiting lanes[5] (CTL/SL – 1+1; ML – 2+2);
- $L_{eq,i}^{1h}$- hourly equivalent continuous A-weighted sound level for the lane i (dBA).

Table 6.2: Traffic performance and emissions by speed profile and roundabout layout (with standard deviation values).

	Speed Profile	RPA (m/s²)	Travel Time (s)	Idle Time (s)	CO_2 (g/km)	NOx (g/km)
SL	I	0.15 (0.05)	58 (7)	N/A[6]	92 (14)	1.56 (0.96)
	II	0.22 (0.05)	67 (6)	3.4 (2.4)	103 (20)	1.28 (0.56)
	III	0.23 (0.03)	78 (9)	5.7 (1.9)	122 (5)	2.44 (0.72)
	Average	0.20 (0.04)	68 (7)	4.5 (2.1)	105 (13)	1.76 (0.75)
CTL	I	0.14 (0.03)	61 (5)	N/A	114 (11)	2.35 (0.68)
	II	0.18 (0.03)	67 (5)	2.9 (1.3)	123 (23)	2.67 (1.13)
	III	0.23 (0.03)	112 (36)	14.8 (9.8)	171 (35)	3.54 (1.42)
	Average	0.18 (0.03)	80 (15)	8.8 (5.5)	136 (23)	2.85 (1.07)
ML	I	0.15 (0.03)	67 (10	N/A	90 (14)	1.23 (0.48)
	II	0.19 (0.02)	71 (7)	3.1 (1.7)	110 (14)	1.75 (0.48)
	III	0.20 (0.03)	97 (17)	21.0 (12.5)	129 (21)	1.95 (0.70)
	Average	0.18 (0.03)	78 (11)	12.1 (7.1)	110 (16)	1.64 (0.55)

•

[5] Concerning the compact-two-lane and the single-lane roundabouts, one approaching lane and one exiting lane were considered, while two approaching and exiting lane were accounted for the multi-lane layout.
[6] N/A = Not Applicable

Results

The results showed in Table 6.2 indicated that SL had on average lower travel (15% and 13%) and idle (40% and 60%) times, and CO_2 per kilometer (20% and 5%) compared to the other layouts. Drivers in the SL experienced 7% more NO_X per kilometer than in the ML. This aspect is probably due to a more aggressive driving behavior that resulted in sharp acceleration episodes (10% more RPA than CTL and ML did). The coefficient of variability of NO_X reselted equal to 0.43, 0.38 and 0.34 for SL, CTL and ML, respectively. Another interesting aspect is that the acceleration rate of vehicles tended to increase as Q_{conf} decreases (1), as the case of SL where the conflicting traffic is low (Q_{conf} < 150 vph). CTL, even if achieved similar performance levels to ML, presented the highest emission levels. For no stop speed profiles, vehicles at the ML produced less pollutant emissions (CO_2 –21%; NO_X – 48%) than vehicles in the CTL. This layout also had 21% lower NO_X compared with SL. As expected, vehicles spent lower travel times crossing SL due to high approaching speeds that were obseverd in the field.

Figure 6.2 shows the CO_2 and NO_X emission rates, acceleration, and vehicular jerk[7] distributions in each 20 m segment length. In these graphs the average of all runs performed per roundabout are exhibited. The impacts in downstream regarded NO_X compared to CO_2. For instance, vehicles generated in the first 150 m (22% of travelling distance) after exiting the roundabout 29%, 30%, 41% of CO_2, and 32%, 35%, 51% of NOx for SL, CTL, and ML, respectively. Emission rates at downstream were higher at CTL compared to other layouts.

Measured acceleration was higher in both circulating and downstream areas, but some differences were identified among the layouts. The average acceleration was 0.50 $m.s^{-2}$ at the downstream of CTL, which was 65% and 45% higher than the values observed at SL and ML, respectively. Since vehicles experienced multiple stops, some acceleration peaks were observed upstream of the SL. Circulating areas were mainly affected by vehicular jerk (used as an indicator of driving volatility), especially in SL (2.5 times higher than the SL average) and CTL (9 times higher than the CTL average). During this step, taking into account the number of examined roundabouts equal to 3, it was not possible to investigate about the correlation between pollutant emissions, noise, and traffic with the geometric characteristics of the considered layout. This aspect has not been addressed as the spirit of the research focused more on the measured emissive characterization.

[7] Indicator of driving volatility (12).

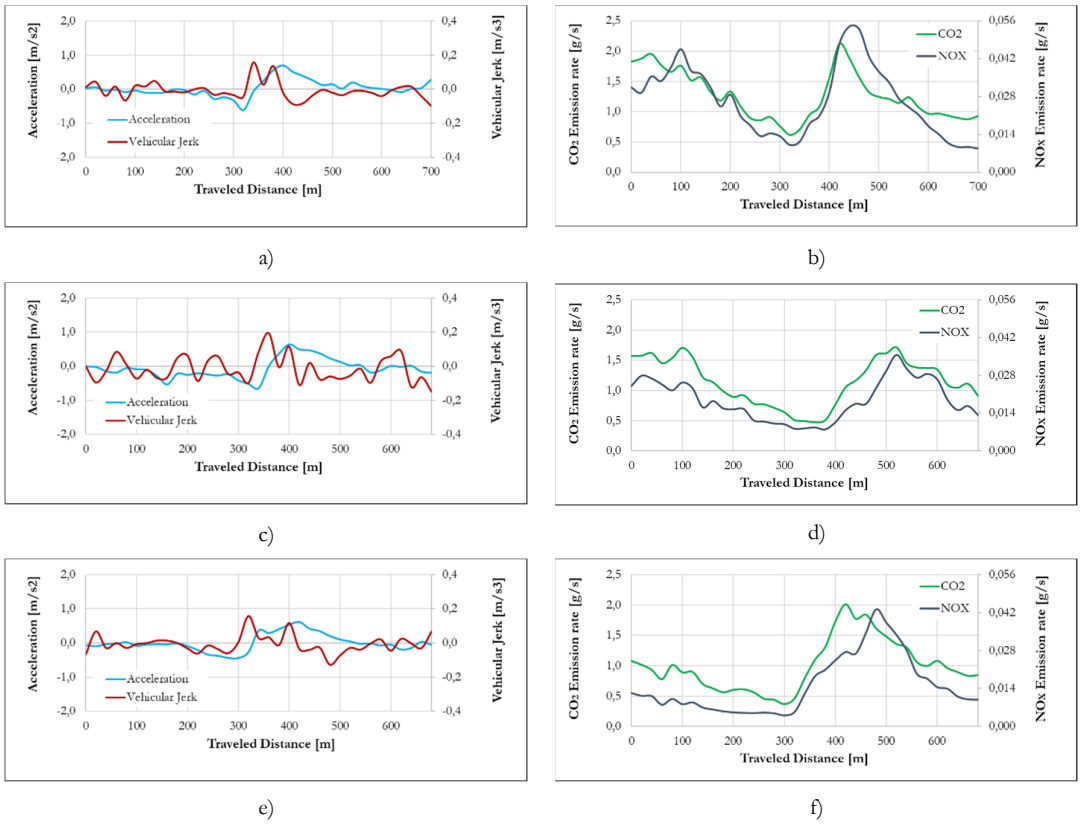

Figure 6.2: Recorded parameters compared by distance and by layout: a) CTL - CO_2/NO_X; b) CTL – acceleration/vehicular jerk; c) SL - CO_2/NO_X; d) SL – acceleration/vehicular jerk; e) ML - CO_2/NO_X; f) ML – acceleration/vehicular jerk.

Speed profiles predictive models were computed by means of multinomial logistic regression model (MLRM) for each sampled roundabout layout. The parameters of each regression were calibrated through maximum likelihood using SPSS software. The samples were gathered in a database with three fields: roundabout layout (SL, CTL and ML), speed profile (SPI: no stop speed profile; SPII: one stop speed profile; SPIII: multiple stops speed profile) and Q_{total} - Q_{in} + Q_{conf} (15-min time slot).

For the ML layout, the calibrated β parameters did not correlate well the data sample at 5% significance level (p-value > 0.05) as the other layouts.

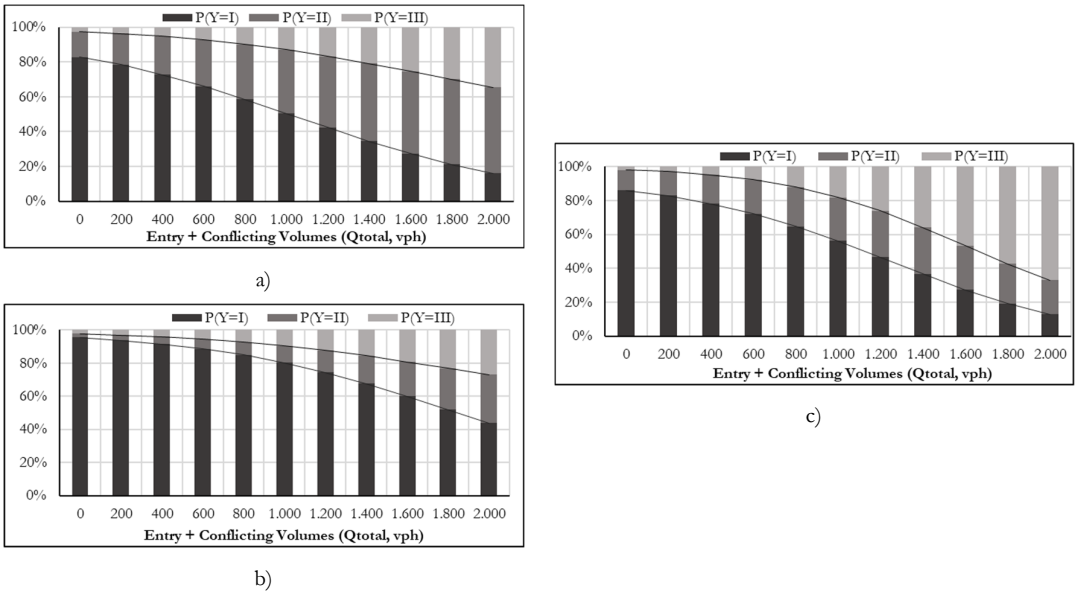

Figure 6.3: Predictive models for the relative occurrence of profiles I, II and III by layout: a) CTL; b); SL and c) ML

Previous diagrams in Figure 6.3 exhibite that the probability of the driver to enter the roundabout without stopping (SPI) decreases as the traffic flow increases. More than 50% of vehicles enter the SL without stopping for Q_{total} lower than 1,800 vph, while this occurred for lower values at CTL and ML. SL could handle more traffic, this impression is misleading. In fact, SL has lower conflicting traffic compared to the other layouts. For traffic flows higher than 1,800 vph, approximately 30% of vehicles at SL and CTL, and 70% at ML, experience multiple stops.

In Figure 6.4 the V/C ratio is shown to better highlight the role of conflicting traffic volumes, for each roundabout layout, in relative occurrence of the three speed profiles here considered.

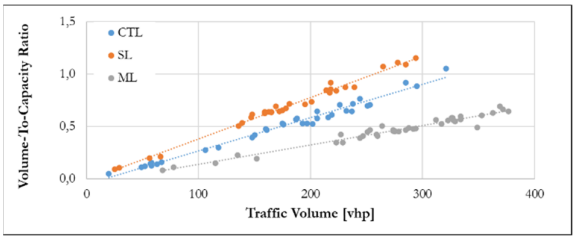

Figure 6.4: Volume-to-Capacity ratio for the three sampled roundabouts[8]

[8] Each point corresponds to 15min time slots of traffic observation.

Concerning traffic noise aspects, the field measurements showed higher values of LA_{eq} at SL because of high approaching speeds and high percentage of HDV and motorcycles. Quartieri et al. model (11) was applied to the surveyed sample, and the results presented a goodness of fit compared with the recorded ones (see Figure 6.5). The percentage error between the estimated and observed LA_{eq} was from 0.1% and 6%., with a maximum difference around 3.5 dBA. This model does not consider the contribution of the vehicles acceleration, so it tends to underestimate LA_{eq} under high traffic volumes. This is noticeable into the differences that were obtained in the ML, where idle time was higher than in the other sampled roundabouts (see Table 6.2).

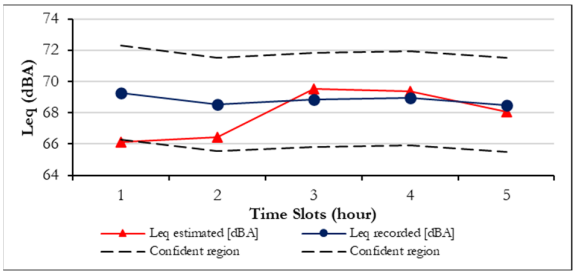

a)

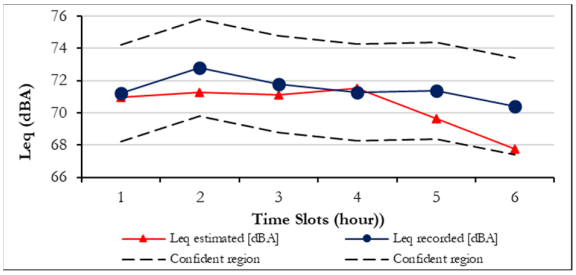

b)

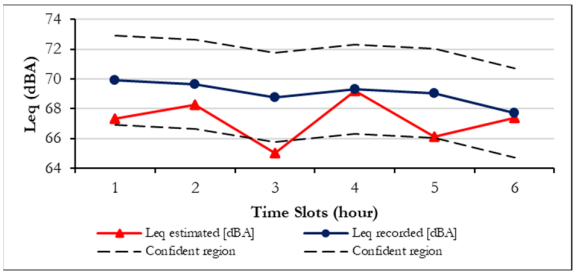

c)

Figure 6.5: Comparison between the estimated and recorded noise for each sampled roundabout: a) CTL; b) SL; c) ML

Conclusions

In this chapter the impact of SL, CTL and ML rural roundabouts on traffic performance, pollutant emissions, noise and capacity were explored. Empirical data of vehicle activity and emissions by using a portable emission measurement system (PEMS) were collected; traffic volumes and noise to assess traffic performance, L_{eq} and V/C ratios were surveyed to support the proposed methodology.

Field measurements showed that SL generated lower travel time and CO_2 emissions per unit of distance travelled (5% -20%) than ML and CTL roundabouts. At the same time, SL roundabout yielded higher relative accelerations (10% higher on average) and NO_X emissions per unit of distance travelled than the ML layout. The implementation of predictive discrete models pointed out that SL yielded the lowest CO_2 per vehicle, since vehicles spent less time driving in the roundabout. However, its implementation can result in higher L_{eq} at low traffic volumes because vehicles drove at higher speeds in the approach compared to the other roundabouts.

References

1. *Effect of roundabout operations on pollutant emissions.* Coelho, M. C., T. L. Farias, and N. M. Rouphail. 5, 2006, Transportation Research Part D: Transport and Environment, Vol. 11, p. 333-343.

2. 3DATX. *In 3-dimensional data analysis (3DATX) Corporation.* 2018.

3. *A comparison of a mini-PEMS and a 1065 compliant PEMS for on-road gaseous and particulate emissions from a light duty diesel truck.* Yang, J., T. D. Durbin, Y. Jiang, T. Tange, G. Karavalakis, D. R. Cocker, and K. C. Johnson. 2018, Science of The Total Environment, Vol. 640-641, p. 364-376.

4. *How many times should I run the Model? Performance Measure. Specific Findings from VISSIM models in Missouri.* Fries, R., Y. Qi, and S. Leight. Washington, DC : s.n., 2017. 96th Annual Meeting of the Transportation Research Board.

5. *Driving around turbo-roundabouts vs. conventional roundabouts: Are there advantages regarding pollutant emissions?* Fernandes, P., S. R. Pereira, J. M. Bandeira, L. Vasconcelos, A. B. Silva, and M. C. Coelho. 9, 2016, International Journal of Sustainable Transportation, Vol. 10, p. 847-860.

6. *Real-world fuel use and gaseous emission rates for flex fuel vehicles operated on E85 versus gasoline.* Delavarrafiee, M., and H. C. Frey. 3, 2018, Journal of the Air & Waste Management Association, Vol. 68, p. 235-254.

7. *Effects of Errors on Vehicle Emission Rates from Portable Emissions Measurement Systems.* Sandhu, G., and H. Frey. 2013, Journal of the Transportation Research Board, Vol. 2340, p. 10-19.

8. *Road grade quantification based on global positioning system data obtained from real-world vehicle fuel use and emissions measurements.* Yazdani Boroujeni, B., and H. C. Frey. 2014, Atmospheric Environment, Vol. 85, p. 179-186.

9. *Impact of driving style and road grade on gaseous exhaust emissions of passenger vehicles measured by a Portable Emission Measurement System (PEMS).* Gallus, J., U. Kirchner, R. Vogt, and T. Benter. 2017, Transportation Research Part D: Transport and Environment, Vol. 52, p. 215-226.

10. *EPA.* [Online] https://www.govinfo.gov/content/pkg/CFR-2012-title40-vol19/xml/CFR-2012-title40-vol19-sec86-144-94.xml.

11. *On the Improvement of Statistical Traffic Noise Prediction Tools.* Quartieri, J., G. Iannone, and C. Guarnaccia. Iasi, Romania : s.n., June 13-15, 2010. 11th WSEAS Int. Conf. on Acoustics & Music: Theory & Applications. p. 201-207.

12. *What is the level of volatility in instantaneous driving decisions?* Xin Wanga, Asad J. Khattak, Jun Liu, Golnush Masghati-Amoli, Sanghoon Son. 58, 2015, Transportation Research Part C, p. 413-427.

Conclusions

Based on the objectives and scope of the thesis, two main aspects have been explored:
(1) the use of measures of kinematic parameters from the vehicle trajectories collected in the field through a sample of urban roundabouts to calibrate the modelling parameters in AIMSUN;
(2) the estimation of pollutant emissions from VSP modal emission rates and the distribution of time spent in each VSP mode obtained from the speed profiles gathered in the field and simulated in AIMSUN.
The main finding provided from this study is referred to the feasibility of the methodological approach that employs in an integrated way vehicle trajectory data collected in the field using a smartphone app, the VSP methodology, and a microscopic traffic simulation model in order to estimate emissions at urban roundabouts. With the trajectory data collected from a smartphone app, speed, and acceleration (deceleration), indeed, can be obtained directly.
The versatility of the micro-simulation model for a calibration aimed at improving accuracy of the emissions estimates was tested in order to ensure that second-by-second trajectories experienced in the field by a test vehicle through the sampled roundabouts properly reflected the speed profiles simulated from a micro-simulation model. Thus, it was possible to explore the driving performance at the roundabouts under examination from an environmental point of view.
In this view, the calibration process here done could be considered a sustainable alternative to the established methods of calibration based on behavioral parameters as already available in literature and used in practice. It is also feasible the use of smartphone for vehicle activity data collection and the subsequent data analysis, which will enable to reduce the cost of on-field surveys and to significantly increase the data volume that can be collected and shared through the interested digital community.
A not secondary objective was to assess the environmental performance where an existing roundabout is converted into another roundabout with an alternative design. The results also confirmed the feasibility of the smart approach that integrates the use of field-observed and simulated data to estimate and to compare emissions at urban roundabouts. The main finding provided from this specific research activity may be referred to the positive potential of a novel attitude in the conceptualization and performance evaluation of road units in order to align urban infrastructural projects with the worldwide shared long-term ambitions for a low-emission mobility.
However, the results have to be seen in relation to the selected case studies and the test vehicle which was used to collect on-field data. Given the need for new solutions supporting data collection and analysis of environmental impact in road transport, the results from this thesis necessarily lead to further research to identify driving behaviors and road performance not limited to the application of the VSP methodology, and environment considerations. This must be related to the need of transportation engineers to consider the trade-off among different factors as traffic emissions, delays and queue lengths, road safety, and so on. In this view the period of study abroad also

allowed to experience on models and approaches that should be used in any integrated assessment of environmental performance of road units.

Future and possible developments can include:

- gathering data on a great number of intersections of roundabouts, particularly, where a greater variability in terms of approaching, entering or circulating speeds, geometric features, and traffic flows occur;

- assessment of further infrastructural and traffic situations also through microsimulation;

- development of models to relate the speed profile to the entry capacity, simulation of traffic operations in presence of CAVs and evaluation of their effects on the amount of pollutant emissions.

Given the need to ensure smart tools supporting the reduction of environmental impacts in road transport, the study can be considered as a starting point for future assessment of infrastructural options when decision makers require to assess changes in the design or operation of urban transportation systems to support their choices.